Universidad Autónoma de Madrid

Department of Biochemistry

The role of telomeres and telomerase during zebrafish heart regeneration

Dorota Bednarek

Madrid, 2015

Departamento de Bioquímica
Facultad de Medicina
Universidad Autónoma de Madrid

Tesis Doctoral

The role of telomeres and telomerase during zebrafish heart regeneration

Dorota Bednarek

Master in Life Sciences

Director: Dr. Ignacio Flores Hernández

Fundacion CNIC Carlos III

Madrid 2015

Dr. **Ignacio Flores Hernández**, Principal Investigator at the National Center for Cardiovascular Research (CNIC-ISCIII), warrants that this work was performed in his Laboratory in the Cardiovascular Development and Repair Department and supports the defense of the thesis entitled:

"The role of telomeres and telomerase during zebrafish heart regeneration".

During this period Dorota Bednarek was supported by a PhD Fellowship from the Ministerio de Economía y Competitividad BES-2010-033554/ SAF2009-10480).

Madrid, October 2015,

Ignacio Flores Hernández

Fundación Centro Nacional de Investigaciones Cardiovasculares Carlos III
C/Melchor Fernández Almagro, 3 28029 Madrid
Telf. 00 34 91-4531200 Fax: 00 34 91-4531245 www.cnic.es

SUMMARY

Telomeres are specialized nucleoprotein structures that protect the ends of chromosomes from DNA repair and degradation activities. The maintenance of telomeres is essential for chromosome stability. Without new synthesis, telomeres (TTAGGG repeats) undergo progressive shortening with each cell division. Telomere shortening can lead to the appearance of critically short telomeres triggering the activation of a persistent DNA damage response and the subsequent induction of cellular senescence or apoptosis. Telomerase is a reverse transcriptase that elongates telomeres, efficiently compensating telomere attrition during cell division. A common feature of the telomerase-positive cells is their highly regenerative capability.

Zebrafish (Danio rerio) has emerged as an excellent model to study tissue regeneration due to its remarkable capacity to fully repair several organs, including the heart. In contrast to mammals, this lower vertebrate is able to replace damaged cardiac muscle after an insult with newly formed fully functional myocardium. During the regeneration process of the zebrafish heart, differentiated cardiac myocytes dedifferentiate and robustly proliferate. Telomerase activity can be detected in the zebrafish model not only in young animals, but also in old ones. Here we demonstrate that after cardiac injury in zebrafish, telomerase become hyperactivated and telomeres transiently elongate, preceding a peak of cardiomyocyte proliferation and full organ recovery. We have used *tert*$^{-/-}$ animals to analyze the role of telomerase in zebrafish heart regeneration. We show that under the high demands imposed by heart injury telomere reserves cannot be maintained without telomerase. Absence of telomerase decouples dedifferentiation from proliferation, drastically impairing proliferation and leading to accumulation of DNA damage. Instead of regenerating myocardial tissue and regressing cardiac fibrosis *tert*$^{-/-}$ hearts increment the percentage of cells that present DNA damage and senescence characteristics, leading to blockade in the regeneration process.

Our results provide direct evidence for the essential role of telomerase during the zebrafish heart regeneration and reveal a role of this enzyme in cardiac cell protection from the injury-induced elevated levels of DNA damage.

RESUMEN

Los telómeros son estructuras nucleoproteícas que protegen los extremos de los cromosomas de mecanismos de reparación y de degradación del ADN. Pese a que el mantenimiento de los telómeros (repeticiones TTAGGG) es esencial para la estabilidad de los cromosomas, éstos se acortan progresivamente con cada división celular. Los telómeros críticamente cortos desencadenan un daño persistente al ADN conduciendo a la senescencia o la apoptosis de la célula. La telomerasa es una reverso transcriptasa que alarga los telómeros, compensando eficientemente su desgaste. Una característica común de las células en las que la telomerasa está activa es su gran capacidad regenerativa.

El pez cebra (Danio rerio) es un excelente modelo para el estudio de la regeneración tisular debido a su notable capacidad para regenerar órganos, incluyendo el corazón. A diferencia de los mamíferos, el pez cebra es capaz de reemplazar el músculo cardiaco dañado por nuevo miocardio completamente funcional. Durante el proceso de regeneración del corazón los cardiomiocitos diferenciados sufren un proceso de desdiferenciación y proliferan. En el pez cebra la actividad telomerasa es detectable durante toda la vida del animal. Los resultados de esta tesis demuestran que tras la lesión cardiaca en el pez cebra se produce un aumento de la telomerasa, un alargamiento telomérico y un incremento en la proliferación de los cardiomiocitos, conduciendo a la recuperación del órgano. Mediante el uso de animales carentes de telomerasa (*tert*$^{-/-}$) se observó que esta enzima es esencial para el mantenimiento de las reservas teloméricas tras la lesión. La ausencia de telomerasa afecta drásticamente a la proliferación de los cardiomiocitos y conduce a la acumulación de daño en el ADN. En lugar de regenerarse, los corazones *tert*$^{-/-}$ presentan un incremento en el número de células con daño al ADN y características senescentes, bloqueando el proceso de regeneración.

Nuestros resultados demuestran que la telomerasa es esencial para la regeneración del corazón del pez cebra y revelan una nueva función de esta enzima protegiendo a las células cardíacas de los elevados niveles de daño en el ADN tras la lesión.

GLOSSARY:

aldh1a2: aldehyde dehydrogenase 1 family, member A2

At: atrium

a.u.: arbitrary units

BA: bulbus arteriosus

bp: base pair

BrdU: bromodeoxyuridine

CM: cardiomyocyte

CPMRs: count per million repeats

CVD: Cardiovascular diseases

DAPI: 4',6-diamidino-2-phenylindole

DDR: DNA damage response

DNA: deoxyribonucleic acid

dpa: days post amputation

dpi: days postinjury

DSBs: double stranded DNA breaks

dsDNA: double-stranded DNA

FVS: ventricular fractional shortening

G-tail: 3´ single-stranded G-rich DNA

GSEA: Gene Set Enrichment Analysis

hpi: hours postinjury

IA: Infarcted area

IHC: immunohistochemistry

iPS: Induced pluripotent stem cells

ISH: *in situ* hybridization

kb: kilobase

LV: left ventricle

MI: myocardial infarction

mRNA: messenger RNA

mTERT: mouse telomerase reverse transcriptase

PCNA: proliferating cell nuclear antigen

pH3: phospho-histone H3

Q-FISH: Quantitative Fluorescent in situ hybridization

qRT-PCR: quantitative reverse transcription polymerase chain reaction

RA: retinoic acid

raldh2: retinaldehyde dehydrogenase

RFVS: relative fractional volume shortening

RNA: ribonucleic acid

RNA-seq: RNA sequencing

SD: standard deviation

ssDNA: single-stranded DNA

SA-β-gal: senescence-associated β-galactosidase

terc: RNA-component of telomerase

tert: telomerase reverse transcriptase

$tert^{-/-}$: telomerase reverse transcriptase knockout

TIFs: telomere dysfunction-induced foci

TRAP: Telomeric Repeat Amplification Protocol

TUNEL: terminal deoxynucleotidyl dUTP nick end labeling

UI: uninjured

V: ventricle

VV: ventricular volume

vmhc: ventricular myosin heavy chain

WHO: World Health Organization

WT: wildtype

ZFN: zinc-finger nucleases

ZIRC: Zebrafish International Resource Center

β -Gal: beta-galactosidase

γ-H2AX: phospho-histone H2A.X

INTRODUCTION

The heart is a wonder of nature, able to operate without interruption for decades and to respond to a multitude of stimuli. It is the main component of the circulatory system, fulfilling the role of a pump. Thanks to its operation, blood circulates through the blood vessels to all parts of the body, delivering oxygen, nutrients and other essential substances (hormones, etc.) to organs and cells. At the same time, the blood returning to the heart disposes of carbon dioxide and assists in the removal of metabolic waste products.

Diseases of the heart and circulatory system constitute the leading cause of death worldwide, claiming 17.3 million lives each year (Mozaffarian et al., 2015). There are 32.4 million myocardial infarctions (MI) and strokes across the globe every year (WHO). Cardiovascular diseases (CVD) contribute to one-third of all deaths worldwide, most of them (78%) occurring in the low- and middle-income countries. While advances in treatment strategies and pharmacotherapy over the past 15 years have dramatically reduced (39%) mortality among patients with heart disease, the prevalence of CVD is expected to increase further over the next two decades (WHO). Heart disease prevention along with proper screening and treatment for CVD can help reduce the devastating impact of heart disease on global public health.

1. Human myocardial infarction

Myocardial infarction (MI) triggers severely deleterious consequences in the heart at the cellular and structural level. The left ventricle of an adult human heart contains about four billion cardiomyocytes, the main cellular component of the heart that ensures its pumping function. Physiological aging is associated with death of cardiac cells, and in the absence of a specific pathology the healthy heart loses about 1g of myocardium (about 20 million cardiomyocytes) per year (Olivetti et al., 1990; Laflamme & Murry, 2011). A medium intensity MI over a few hours can destroy up to 25% of the heart muscle, equivalent of 50 years of normal aging (Caulfield et al., 1976; Murry et al., 2006). The term *myocardial infarction* denotes the local death of cardiomyocytes due to extended ischemia, which may be caused by an increase in perfusion demand or a decrease in blood flow. The main cause of myocardial infarction is the occlusion of a coronary artery due to atherosclerosis. Necrotic myocardium provokes an inflammatory response that causes infiltration of neutrophils, lymphocytes and monocytes, which eliminate dead cells and damaged tissue debris (Jennings et al., 1990, reviewed Frangogiannis, 2012). The

damaged cardiac muscle is replaced over the next few weeks by fibrotic tissue. Myofibroblasts that accumulate in the area of the lesion secrete large amounts of collagen and other extracellular matrix proteins (reviewed in Fan et al, 2012; reviewed Frangogiannis, 2006). The fibrotic response increases the rigidity of the ventricular wall, providing mechanical support to the infarcted heart. However, scar development is irreversible and prevents the reestablishment of proper heart contraction and relaxation, resulting in a reduced cardiac output (Díez et al., 2002). Permanent scarring thus decreases the heart's pumping efficiency and weakens the organ, and this increases the heart's susceptibility to further MI events, aneurism, heart decompensation pathology, and organ failure (reviewed in Kikuchi & Poss, 2012).

2. The heart in model organisms

Animal models give us the possibility to devise the optimal intervention to reduce the risk of CVD and improve the diagnosis and treatment of these pathologies (reviewed in Zaragoza et al., 2011). However, given the implication of genetic and environmental factors in cardiovascular pathophysiology it is extremely difficult to reproduce the human disease in a single experimental model organism. Different evolutionary histories have generated different forms of the cardiovascular system, with different levels of efficiency, but they all perform the same basic function.

2.1. The mammalian heart

The hearts of humans and other mammals contain four chambers. The two upper chambers are the right and the left atria, and the two lower chambers are the right and the left ventricles. The four-chambered, double-circulation mammalian heart works at high pressure. Deoxygenated blood returns from the systemic circulation to the right atrium via the superior and inferior vena cava and passes through the tricuspid valve to the right ventricle. From here, it is ejected through the pulmonary valve into the pulmonary artery, and passes to the lungs. Oxygenated blood returns from the lungs via the pulmonary vein and enters the left atrium. The blood then passes

through the mitral valve to the left ventricle, from where it is pumped through the aortic valve to the aorta and the systemic circulation (**Figure I 1)**.

The histological composition of the mature heart in all vertebrates is similar. The wall of the heart comprises three layers: epicardium, myocardium and endocardium. The epicardium is the outermost layer of the heart wall and is composed of mesothelial cells. The myocardium constitutes the muscular middle layer making up the majority of the thickness and mass of the heart wall. It is composed of contractile striated muscle tissue. The endocardium is the innermost thin endothelial layer that faces the lumen of the heart. The heart is located in the anterior part of the body chest. It is encased by a double-walled sac, called pericardium, and is nourished by the coronary vasculature.

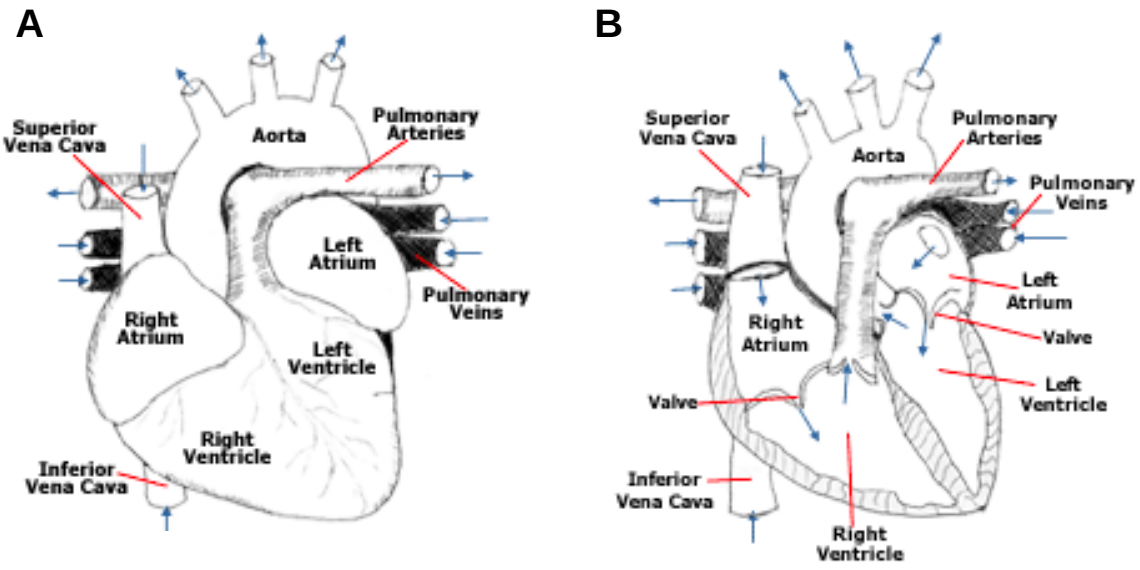

Figure I 1. Mammalian heart structure and function. (A) External view of a four chambered heart, as found in human. Blue arrows indicate the blood flow direction. (B) Internal view of a four chambered heart, as found in human. Blue arrows indicate the blood flow direction.

2.2. The zebrafish heart

The two-chambered, single-circulation fish heart is anatomically distinct from the adult mammalian heart, but similar to the embryonic heart in mammals. The heart of the zebrafish

(ZF) is composed of one thin-walled atrium (A), equivalent to the mammalian atria, and one thick-walled muscular ventricle (V). The atrium and ventricle are not septated. A rudimentary valve is located between the two chambers. The atrium receives the deoxygenated blood from the body via the sinus venous. The blood is pumped through the atrioventricular canal to the ventricle and next from the ventricle to the bulbus arteriosus (BA) - an elastic compartment, which has the ability to stretch and squeeze, and constitutes the base of the aorta (Hu et al., 2001). From the BA the blood is sent to the gills, where it takes in oxygen and releases carbon dioxide. From the gills, the blood moves to the brain and other important body structures (**Figure I 2)**.

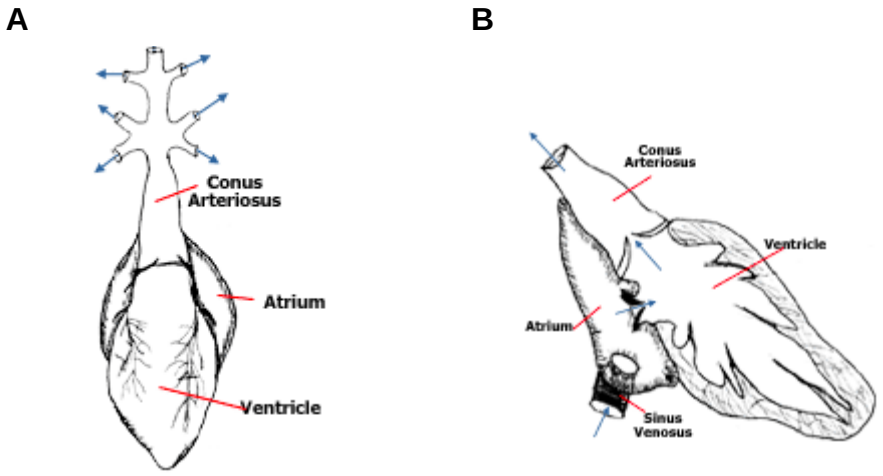

Figure I 2. Zebrafish heart structure and function. (A) External view of a two chambered heart, as found in zebrafish. Blue arrows indicate the blood flow direction. (B) Internal view of a two chambered heart, as found in zebrafish. Blue arrows indicate the blood flow direction.

In the young zebrafish heart, the myocardial wall is divided into two layers, a compact layer (one or two cells thick) and a highly developed trabecular layer, which extends into the ventricle. However, the trabecular layer regresses and is not present in the adult heart.

There are numerous differences between mammalian and fish cardiac biology, most of which are due to adaptation to the different conditions in their natural habitats. Zebrafish heart is much smaller than the mouse or the human heart, and it supports a very low blood pressure, 50 times lower than the human left ventricle (LV) (Hu et al., 2001). Most of the cardiomyocytes in adult

zebrafish are small, mononuclear and diploid (Wills et al., 2008), contrasting with the situation in humans and mice, in which cardiomyocytes quickly undergo hypertrophy.

3. Tissue regenerative capacity

Coronary heart disease and MI constitute one of the biggest health care concerns across the globe. Therapeutic approaches allowing the regenerative replacement of damaged cardiac muscle are essential for the development of effective treatments for cardiovascular diseases. An attractive approach to design strategies for the regeneration of the cardiovascular system is to dissect the cellular and molecular basis of natural regeneration in mammals. Regeneration is the replacement of tissues and organs lost by amputation, disease, injury or even normal aging. Regenerative capacity varies substantially between organs and organisms. Identifying the key players in the regeneration process requires the study of a spectrum of model systems. Many mammalian tissues, including cardiac muscle, spinal cord, and limbs, have a strikingly low regenerative capacity, however, tissue regeneration can be evaluated in several vertebrate models such as salamander, newts, amphibians or teleost fish, in which the regenerative capacity is much higher (**Figure I 3)**. Since fundamental processes and mechanisms are conserved among vertebrates, studies performed in these regenerative models might provide the keys to promoting regeneration in mammals.

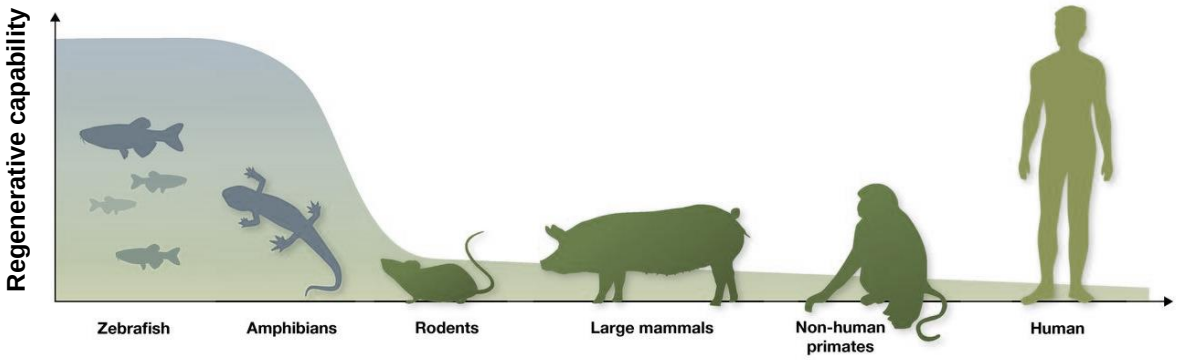

Figure I 3. Regeneration in various model organisms. Schematic representation indicates regenerative capabilities of various model organism from lower vertebrates (zebrafish and amphibians) to human. Adapted from Sahara et al., 2015.

3.1. The zebrafish model of regeneration

The zebrafish (*Danio rerio*) is a small tropical fresh-water fish originally from Southeast Asia. It lives in rivers of northern India and Pakistan as well as in Nepal and Bhutan. Zebrafish belong to the Cyprinidae family, which also include carps and catfish. Zebrafish are small (adult individuals measure between 2.5-5 cm), cheap to maintain, easy to breed, produce large clutches, develop rapidly, and have transparent embryos and larvae. Due to these features, the zebrafish has become the favored model organism for developmental biologists. The zebrafish model has been exploited in an exceptional manner in the field of cardiovascular development. One of the reasons for its extensive use is the prolonged survival of its larvae in the absence of active circulation, which allows the identification of a large number of mutants in genetic screenings (Staudt & Stainier, 2012). Mutants with defects in atrial or ventricular contractility, rhythm, beat rate, conduction or retrograde flow have been isolated using chemical mutagenesis (Stainier et al., 1996). Zebrafish embryos are also ideal for drug and small molecule screening (Bakkers, 2011). Combination of chemical screenings with transgenic zebrafish lines has led to the identification of factors that regulate hematopoiesis (North et al., 2007) or that influence gluconeogenesis (Gut et al., 2013). The adult zebrafish is able to regenerate several organs, including fins (Johnson & Weston, 1995; Poss et al., 2003), kidney (Diep et al., 2011), liver (Sadler et al., 2007), pancreas (Moss et al., 2009), retinal neurons (Vihtelic and Hyde, 2000), optic nerves (Bernhardt et al., 1996), brain (Kroehne et al., 2011), hair cells in the inner ear and lateral line (Harris et al., 2003), spinal cord (Becker et al., 1997), and heart muscle (Poss et al., 2002a). However, the zebrafish model also has major limitations. Although they are vertebrates, fish are phylogenetically distant from humans, so findings in this model do not have direct clinical application. Moreover, during evolution, the genome of teleost fish underwent at least one duplication, generating a degree of gene redundancy that hinders functional analysis. A common criticism of this model is the inability to manipulate their genome in a targeted manner in order to replace or remove specific sequences. However, this limitation has been overcome with the advent of techniques for efficient genome manipulation. These approaches involve the use of nucleases targeted to specific sequences, including the ZFN (zinc-finger nucleases; Urnov et al., 2010), the TALEN system (transcription activator-like effector

nucleases; Joung & Sander, 2013), and the CRISPR-Cas RGEN system (RNA guided endonucleases; Hwang et al., 2013).

3.2. Cardiac regeneration

The design of rational therapeutic strategies for heart failure first requires a full characterization of the ability of mammalian cardiomyocytes (CMs) to divide in response to heart damage (reviewed in Steinhauser & Lee, 2011). If the heart has a robust intrinsic regenerative capacity, like the zebrafish heart, therapeutic approaches should focus on ensuring the survival, maintenance and functional integration of the newly generated cardiomyocytes with preexisting cardiac tissue. Alternatively, if the capacity of renewal is low—as seems to be the case in mammals—the goal should be to replace lost or dysfunctional cardiomyocytes, either by stimulating this low renewal capacity or by finding other cell sources possessing the ability to differentiate into cardiomyocytes. Data obtained from different species and triggered by different pathological conditions suggest three possible ways for myocardial renewal: the direct division of preexisting adult mature cardiomyocytes, the dedifferentiation of preexisting cardiac myocytes followed by their proliferation and differentiation, and the differentiation of progenitor cells (Senyo et al. 2013; Jopling et al., 2010; Kikuchi et al., 2010; Lepilina et al., 2006; Hsieh et al., 2007; Loffredo et al., 2011;).

The cardiac regenerative response in zebrafish involves a substantial amount of cardiomyocyte proliferation, and zebrafish cardiomyocytes have a much higher degree of cell cycle activity than their mammalian counterparts. Even in uninjured adult zebrafish hearts, approximately 3% of cardiac myocytes incorporate the thymidine analogue bromodeoxyuridine (BrdU) during a continuous 7-day injection. Following amputation of the ventricular apex, CMs hyperplasia vigorously renews the myocardium. The fraction of BrdU-positive cardiomyocytes is 10-fold higher at 14 days post amputation (dpa) comparing with uninjured hearts (Poss et al., 2002a). This contrasts with the situation in mammals. Although several studies indicate some endogenous capacity of adult mammalian cardiomyocytes to divide, this is still considered a very rare event (Beltrami et al., 2001; Kajstura et al, 2010, b; Soonpaa & Field, 1997). An accurate estimate of myocardial cell division was obtained with a transgenic mouse line expressing a nuclear-localized beta-galactosidase (beta-Gal) reporter gene exclusively in cardiomyocytes,

allowing determination of ^{3}H-thymidine incorporation in the myocardium (Soonpaa & Field, 1997). Examination of DNA synthesis in 10000 cardiomyocytes in healthy adult mouse hearts revealed a maximum labeling index of 0.0006%, while after heart injury this increases to 0.0083%. In contrast to adult CMs, mammalian cardiomyocytes do proliferate during fetal development. Shortly after birth, these cardiac myocytes down-regulate cell cycle factors (cyclin A, cdk2) and loose the proliferative capacity. It coincides with increases levels of the cell cycle inhibitors, p21 and p27 (reviewed in Pasumarthi & Field, 2002). At this time of development, hyperplastic fetal cardiac growth undergoes transition and since now is mediated by cardiomyocyte hypertrophy.

3.3. Heart regeneration in zebrafish

The first solid evidence for the regenerative ability of a vertebrate heart after an injury was obtained in the zebrafish model a decade ago. After amputation of the ventricular apex (approximately 20% of the ventricle), adult zebrafish survived and completely recovered the histological organization and morphological characteristics of the adult heart within 30 to 60 days (Poss et al., 2002a; Raya et al., 2003). Unlike MI in mammals, accumulation of connective tissue after amputation was minimal; fully regenerated hearts showed no detectable remains of fibrotic tissue of any kind and no consequent remodeling typical of post-infarcted tissue in humans (Poss et al., 2002a; Raya et al., 2003). Although these early studies did not describe the recovery of heart function, visual inspection of these hearts revealed no heartbeat abnormality. However, heart amputation does not reproduce the damage triggered by ischemia-induced MI; for example, physical removal of the part of the ventricle provokes a weaker inflammatory response, with no need for debris removal. There was therefore intense interest in the development of an injury model that more closely reflected the pathophysiological processes observed in the human heart after MI. In mouse and rat models, a MI-like effect is achieved by occluding a coronary artery; however, an artery-ligation approach is not feasible in zebrafish due to the small size of the ventricle (1mm^3) and the fact that only a proportion of the ventricle muscle is perfused by the coronary vasculature (Choi & Poss, 2012). As an alternative, several groups have used cryoinjury. Cryoinjury causes local damage to all cardiac cell types and leads to a transient fibrotic tissue deposition reminiscent of the fibrotic scar formed in mammals after

MI (Chablais et al., 2011; González-Rosa et al., 2011). Like the resection model, cryoinjury damages about 25% of the ventricle without impacting survival of the animal. The dead tissue is cleared and replaced by newly formed myocardium within 60-130 days post injury (dpi) (Chablais et al., 2011; González-Rosa et al., 2011; Schnabel et al., 2011). The zebrafish can also regenerate after genetic ablation of cardiomyocytes (Wang et al., 2011) and hypoxia-reoxygenation injury (Parente et al., 2013) (**Figure I 4)**. Initial experiments to determine the cell source for newly regenerated tissue in the regenerating zebrafish heart involved a double transgenic line that expresses two fluorescent proteins in the myocardium with different stabilities and folding times. These experiments suggested that undifferentiated progenitors cells were the principal source of regenerating cardiomyocytes (Lepilina et al., 2006). Subsequent genetic fate mapping studies unambiguously demonstrated that dead cardiomyocytes in zebrafish are not replaced by stem cells, but by preexisting cardiomyocytes, which first dedifferentiate and proliferate, and then re-differentiate to replace the injured tissue with newly-formed myocardium (Jopling et al., 2010; Kikuchi et al., 2010).

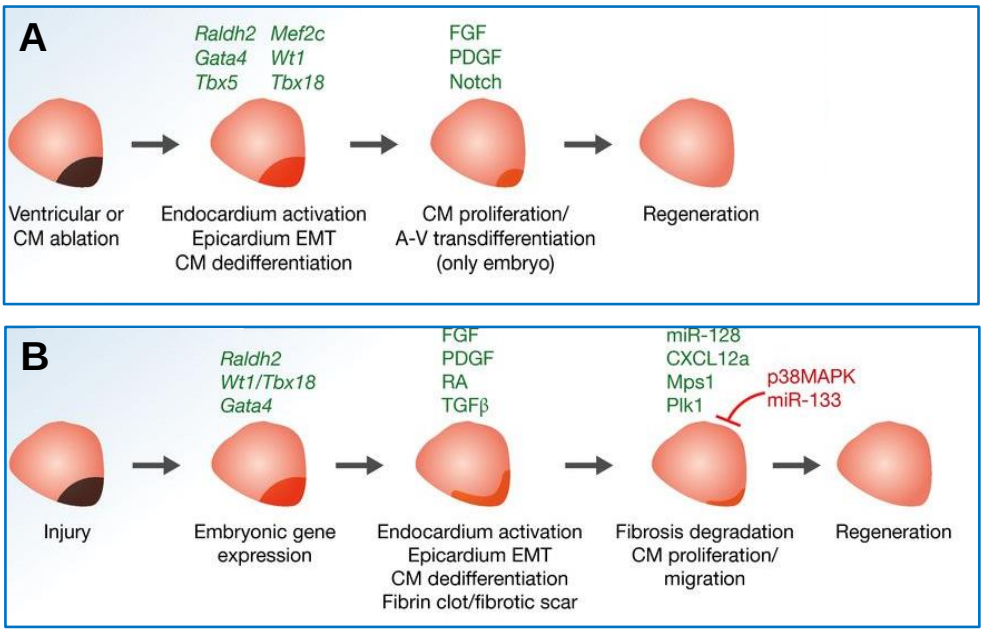

Figure I 4. Zebrafish heart regeneration. (A) Schematic representation of zebrafish heart regeneration after CM ablation model. Genetic ablation allows to specifically ablate up to 60% of cardiomyocytes. Genetic ablation of cardiomyocytes does not induce deposition of collagen matrix but only formation of a blood/fibrin clot. Induced reactivation of genes expressed during embryonic

heart development, such as *Gata4*, *Nkx2-5*, *Raldh2*, *Wt1*, and *Tbx18*, followed by activation of endocardium and epicardium, including EMT of epicardial cells. All ultimately lead to full regeneration of the ablated myocardium. (B) Schematic representation of zebrafish heart regeneration after cryoinjury or apical resection model. Cardiac cryoinjury damage 20–30% of the ventricular myocardium, together with endocardium and epicardium. The cryoinjury model produces massive, but transient, scar-like fibrosis around the injured area. Scar formation is mediated by the TGF-β/Activin signaling pathway. Following scar formation and/or EMT of epicardial cells, which causes FGF- and PDGF-driven revascularization into the myocardium proliferating cardiomyocytes appear around the injured sites. Several paracrine signals, including RA, synthesized by the epicardium and endocardium, and C-X-C motif chemokine 12a expressed in epicardial cells, have been suggested to promote cardiomyocyte proliferation All ultimately lead to full regeneration of the damaged myocardium. A-V, atrial-to-ventricular; CM, cardiomyocyte; EMT, epithelial-to-mesenchymal transition; MI, myocardial infarction. Adapted from Sahara et al., 2015.

A notable feature of mature cardiomyocytes is their sarcomeric contractile apparatus, which occupies a substantial part of the cell body. The sarcomere structure constitutes a physical barrier for cytokinesis, and thus impedes cell proliferation (Jopling et al., 2010; Kikuchi et al., 2010; Wang et al., 2011.). Proliferating cardiomyocytes undergo a limited dedifferentiation featuring disassembly of the sarcomeric structure, detachment from neighbors, expression of positive regulators of cell-cycle progression such as polo-like kinase1 (*plk1*), monopolar spindle1 (*mps1*) and cyclin-dependent kinase1 (*cdc2*), and downregulation of sarcomere genes such as ventricular myosin heavy chain (*vmhc*). Moreover, disassembly of the energy-demanding contractile machinery and reduction of the cellular energy demand enables cardiomyocytes to manage hypoxic stress (Szibor et al., 2014.). Overall the dedifferentiation state of cardiomyocytes during myocardial tissue regeneration increases their plasticity, promotes their survival under hypoxic conditions, and increases their disposition to re-enter the cell cycle.

After heart damage in zebrafish, the epicardium re-expresses the embryonic markers *wt1b*, *tbx18* (a T-box- family transcription factor), and *aldh1a2* (an enzyme involved in the synthesis of retinoic acid; RA). The altered epicardium actively proliferates, even away from the damaged area. Investigators hypothesized that the epicardium might support myocardial regeneration by contributing to revascularization of the amputated area (Lepilina et al., 2006). This makes sense ontogenically because during heart development the epicardium contributes to the coronary vasculature and secretes paracrine factors that stimulate myocardial proliferation (Carmona et al., 2007; Lie-Vemana et al., 2007). In addition, the epicardium releases extracellular matrix

components such as fibronectin, suggested to promote cardiomyocyte regeneration through interaction with integrin beta 3 (*itgb3*) (Wang et al., 2013). Endocardial cells, which line the inside of the cardiac chambers, also play a significant role in myocardium development (reviewed in Choi & Poss, 2012) and might also be important for heart regeneration. After cardiac injury, endocardial cells undergo rapid morphological changes, adopt a rounded shape, and detach from myocardial cells (Gamba et al., 2014; Kikuchi & Poss, 2012). Moreover, within hours of injury, endocardial cells throughout the heart upregulate genes involved in developmental processes, including *aldh1a2* (Kikuchi et al., 2011; Lepilina et al., 2006). The endocardium also activates the expression of *il11a*, which triggers jak1/stat3 signaling in cardiomyocytes in order to promote their proliferation (Fang et al., 2013). These observations suggest that cardiomyocyte proliferation and remodeling might require paracrine-like contributions from the endocardium and epicardium.

However, little is known about the molecular factors involved in the restoration of heart muscle. Although many transcriptional changes have been identified after heart amputation (Lien et al., 2006), few candidate factors have been validated functionally, and no studies have been performed with tissue-specific models. There are thus many aspects that we do not understand about the regeneration of the zebrafish heart. Characterization of the mechanisms that drive heart repair in zebrafish is likely to have subsequent applications in the design of new therapies to improve the practically nonexistent cardiac regenerative capacity in adult mammals.

3.4. Heart regeneration in mammals

While lacking the remarkable regenerative capacity of the zebrafish heart, postnatal mammalian hearts do undergo a degree of cardiomyocyte renewal during normal aging and disease. Motivated by the discovery of cardiac regeneration in zebrafish, investigators turned their attention to the response of mouse hearts to ventricular damage in the neonatal period, when myocardial growth is still hyperplastic, not hypertrophic, and cardiomyocytes are structurally similar to those of fish. After apical amputation, neonate hearts recover completely with no trace of fibrosis if the procedure is performed before the seventh day of life (Porrello et al., 2011) (**Figure I 5)**. The same result is obtained in a model of coronary ligation (Porrello et al., 2013).

In neonate mice, positive markers for cardiomyocyte proliferation also reveal partial disassembly of the sarcomere apparatus (Porrello et al., 2011). In addition, recent work suggests that a population of resident c-kit+ progenitors contributes to the restoration of the myocardium and coronary vasculature in the newborn heart but not in the adult (Jesty et al., 2012). Although amputation in neonates is an emerging model for the study regeneration in mammals, some authors remain skeptical about these results. While the undamaged adult zebrafish heart exhibits minimal proliferation, the neonatal mouse heart has a high proliferation rate during the first 7 days of life, when the organ is still growing. The restoration of the ventricle therefore might be the result of a global compensatory proliferative response rather than a local regenerative response (reviewed in Choi & Poss, 2012).

Understanding why adult mammalian cardiomyocytes lose their ability to proliferate may hold the key to new therapeutic strategies for increasing survival and facilitating regenerative replacement of damaged myocardium. Such therapies would be of enormous social and economic impact.

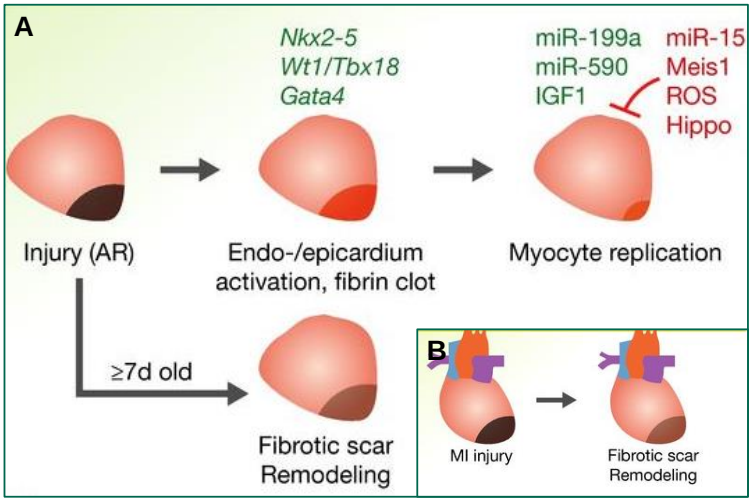

Figure I 5. Heart regeneration in mammals. (A) Schematic representation of mouse heart regenerative/replicative processes following injury. Similar to zebrafish regenerative processes are seen post-injury in hearts of 1-day-old mice, but not after 7 days nor in humans (B), where fibrotic scar formation and pathological remodeling occur. Regeneration enhancers are indicated in green, inhibitors in red. MI, myocardial infarction. Adapted from Sahara et al., 2015.

4. Telomeres and telomerase

The prevailing mechanism of zebrafish heart regeneration is cardiomyocyte proliferation after partial dedifferentiation. Given that successful DNA replication and extensive cell division require the presence of functional telomeres, we investigated the role of telomeres and telomerase during zebrafish heart regeneration.

4.1. Telomere structure

Telomeres (from the Greek words "*telos*" – end; "*meros*" – part) are dynamic nucleoprotein structures that cap and stabilize the ends of linear chromosomes (**Figure I 6**). In all vertebrates the DNA component of telomeres consists of tandemly repeated guanine-rich hexanucleotide sequence $(TTAGGG/CCCTAA)_n$. Telomeric DNA shows huge interspecies heterogeneity in size, ranging from 2-100 kb (Sfeir, 2012). Telomere length also varies with tissue and cell type, chromosome number, and organismal age. Differences in the length of telomeric motifs have been detected between non-homologous and even homologous chromosomes within individual cells in humans and mice (Kipling & Cook, 1990; Starling et al., 1990; Londoño-Vallejo et al., 2001; Bekaert et al., 2004).

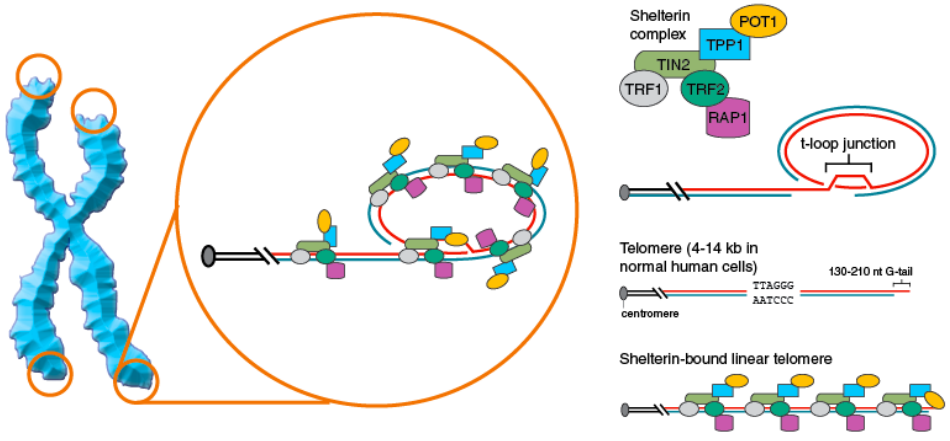

Figure I 6. Telomere structure. Eukaryotic double-stranded telomeric DNA (dsDNA) is followed by 3´ enriched G content single-stranded overhang (G-tail). In humans telomeric 3´ G-tails sequences range 130 to 200 bases in size and they have been shown to fold back and form higher order DNA structure (T-loop) in order not to being recognized as a DNA double-stranded break. In mammals,

telomere DNA component is accompanied by a specialized six-protein complex, also known as shelterin, that binds either to specific sequences within single- or double-stranded telomeric region or eventually to the other telomeric proteins. Two proteins of the shelterin complex, TRF1 (telomeric repeat binding factor 1) and TRF2 (telomeric repeat binding factor 2) bind directly double stranded DNA whereas POT1 (protection of telomeres1) binds to the 3´single-stranded G-rich DNA (G-tail). RAP1 (repressor activator protein1) interacts with TRF2, while TIN2 (TRF1-interacting nuclear factor 2) bridges TRF1 and TRF2 protein (dsDNA binding complex) with POT1\TPP1 (TIN2 and POT1-interacting protein) component (ssDNA binding complex). Adapted from Cessare & Reddel, 2010.

4.2. Telomere function

Telomeres were first described in 1938, when *Drosophila* geneticist Hermann Muller used X-rays to fragment chromosomes. He proposed that

> *…the terminal gene must have a special function, that of sealing the ends of the chromosome, so to speak, and that for some reason, a chromosome cannot persist indefinitely without having its ends thusly "sealed". This gene may accordingly be distinguished by a special term, the "telomere"…* (Muller, 1938)

Around the same time, Barbara McClintock's independent experiments with maize led her to the same proposal. She proposed that a functional chromosome end structure is essential for genome stability, being necessary to prevent chromosome shortening, fusion of chromosomal termini with other pieces of genomic DNA, and degradation by the DNA repair machinery (McClintock, 1941).

4.2.1. The end replication problem

In 1972, James Watson noticed that

*"While 5' to 3' oriented growth should proceed smoothly to the end of its template, I see no simple way for 3' to 5' growth to reach the 3' end of its template" (*Watson, 1972.*)*

Watson therefore surmised that semi-conservative replication machinery would not be able to fully replicate the lagging strand of linear chromosomes. The following year, Alexey

Matveyevich Olovnikov presented his independent studies reaching the same conclusion. Olovnikov proposed that chromosome termini are stochastically shortened during each mitotic cycle. This is now referred to as the end-replication problem. In the standard replication model, DNA synthesis requires a primer—a RNA template with free 3´-OH group—to initiate nucleotide incorporation. Because DNA polymerases replicate DNA only in the 5′ to 3′ direction, removal of the terminal RNA primer at the 5′ end of the lagging-strand leaves a small gap, a short single-stranded region that cannot be filled in by the canonical DNA replication machinery. This region is extremely vulnerable to enzymes that degrade ssDNA. As a result, in the absence of an appropriate compensatory mechanism, telomeric DNA sequences become shorter with each round of DNA replication (Watson, 1972; Olovnikov, 1973). Attrition of telomeric DNA repeats provokes telomere deprotection, and this activates a DNA damage checkpoint response that successively leads to cell-cycle arrest and senescence. Normal mammalian somatic cells proliferate a limited number of times in vitro, with the maximum number being referred to as the Hayflick limit. Each mitosis thus slightly shortens telomeres, and the chromosome ends eventually reach a critical length and uncapping occurs, limiting cellular lifespan. Short telomeres are associated with organ dysfunction, human aging disorders, and age-associated diseases such as coronary artery disease, heart failure and cancer (Sherr & McCornick, 2002; Ogami et al., 2004; Starr, 2007; Donate & Blasco, 2011).

4.3. DNA damage and senescence in the context of telomere biology

The number of DNA damage events taking place in each cell of the human body is estimated at > 20000 every day (reviewed in Loeb, 2011). Double stranded DNA breaks (DSBs) are considered one of the most dangerous DNA injuries for genome stability, since DSBs generate new chromosome ends at internal sites in chromosomes. DSBs must be repaired in order for cell proliferation to proceed. Repair can occur by either non-homologous end joining (NHEJ), which results in ligation of the broken ends, or homologous recombination (HR), which uses a homologous DNA sequence to restore the genetic information lost at the break site (reviewed in Caldecott, 2008; reviewed in Ciccia & Elledge, 2010). Chromosome ends are highly dynamic entities that must adjust telomere accessibility depending on the stage of the cell cycle. This is achieved by switching telomere structure between protected (closed) and deprotected (replication-competent) states during the replication process (**Figure I 7**). Telomere deprotection

can be induced by depletion of shelterin or by telomeric DNA degradation, which occurs spontaneously within each cell division in the absence of compensatory mechanisms. Telomere uncapping, whether by depletion of the protein component TRF2 or by telomere shortening, activates the same DNA damage response as DSBs (Passos et al., 2007; Galati et al., 2013).

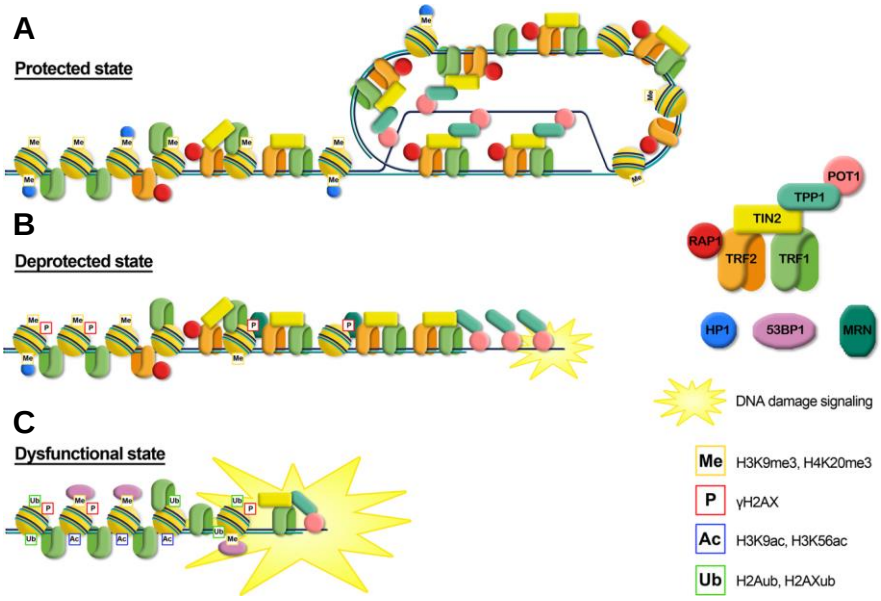

Figure I 7. Graphical representation of the different telomere states, characterized by different levels of telomeric proteins and post-translational modifications. (A) Protected state: telomere is in a closed form, probably the t-loop, maintained by the binding with the shelterin proteins This state inhibits the DNA damage response. (B) Deprotected state: telomere shortening could disrupt the closed structure leading to an open state, characterized by a decrease of heterochromatic marks. Telomeres are recognized as DNA damage, signaled by phosphorylation of H2AX, but retain enough shelterin proteins (mainly TRF2) to prevent NHEJ and thus telomeric fusion. DNA damage signaling leads to replicative senescence. (C) Dysfunctional state: if growth arrest checkpoint is inactivated, telomeres continue to shorten leading to a fully uncapped form, deriving from the depletion of shelterin proteins such as TRF2 or POT1. Telomere dysfunctions are signaled by phosphorylation of H2AX and the ubiquitylation of H2A and H2AX. Telomeres are not protected from the DNA damage response machinery, giving rise to extensive telomere fusions. Adapted from Galati et al., 2013.

The replication-competent telomere state not only triggers tremendous changes in the epigenetic pattern and nucleosome organization; it also activates the DNA damage checkpoint response that

leads to cell-cycle arrest (Galati et al., 2013). Depletion of shelterins leads to telomere end-to-end fusions, promoting genome instability. The checkpoint induced by critical-length telomeric repeats initiates replicative senescence, during which telomeres do not undergo fusion events but instead accumulate gamma-H2A and 53BP1. Human telomeres shorten at a rate of approximately 50-200 bp per population doubling (Ambrus et al., 2006; Anchelin et al., 2011). Critically short telomeres interfere with normal cell-cycle progression, leading to cell senescence or cell death (apoptosis) under normal conditions (reviewed in Armanios & Blackburn, 2012; reviewed in Nelson & Bertuch, 2011; Prescott et al., 2012; Lin et al., 2012). Moreover it is possible that loss of proliferative competition itself promotes cancer formation in response to telomere shortening. Telomere dysfunction can promote tumor formation by inducing environmental alterations (Jiang et al., 2007). Cells can develop a secretory phenotype in response to telomere dysfunction and senescence (Parrinello et al., 2005). Environmental alterations related with senescence associated secreting phenotype (SASP) can influence the selective outgrowth of (pre-) malignant cell clones in ageing organs and tissues (Bilousova et al., 2005). Interestingly, senescence in mammals is determined not by average telomere length, but by the presence of short telomeres that trigger the DDR. Critical shortening of a single telomere is thus sufficient to accelerate the onset of senescence in cells that lack telomerase activity (reviewed in Maicher et al., 2012; reviewed in Gobbini et al., 2014). Furthermore, telomeres might contribute to senescence independently of their length or dysfunction (Grimes & Chandra, 2009). Thus, cellular senescence can be induced as a response to persistent DSB (telomere-independent or stress-induced premature senescence) or uncapped telomeres (replicative senescence). Intense, acute stress will generate DSBs at higher frequency and might alter broken DNA ends to make them more resistant to repair, leading to DSB persistence and therefore induction of senescence via the non-telomeric DNA damage response in non-proliferating tissues (Passos et al., 2007).

4.4. Telomerase

Telomerase is an enzyme that counteracts the loss of the telomeres by catalyzing the addition of *de novo* telomeric DNA to the ends of linear chromosomes. The activity of this enzyme is restricted in multicellular organisms to varying degrees. In humans a strong repression is found in somatic tissue during development. However, telomerase activity is found in humans until

adulthood in proliferative tissues, including germ cells (ovaries and testis) and cells of the hematopoietic and immune systems (Wright et al., 1996; Morrison et al., 1996). In the mouse, the catalytic subunit mTERT is widely expressed at low levels in adult tissues, with highest expression in thymus and intestine (Greenberg et al., 1998). In adult zebrafish, telomerase activity is found throughout the lifespan of the animal. Adult zebrafish express the *tert* gene in most tissues, and zebrafish telomeres are of a similar size to those found in normal human cells and tissues.

4.4.1. Telomerase structure

Telomerase is a DNA polymerase, homologous to other reverse transcriptases in being composed of a catalytic subunit, telomerase reverse transcriptase (TERT), and an RNA component (TERC) (Greider & Blackburn, 1985) (**Figure I 8**).

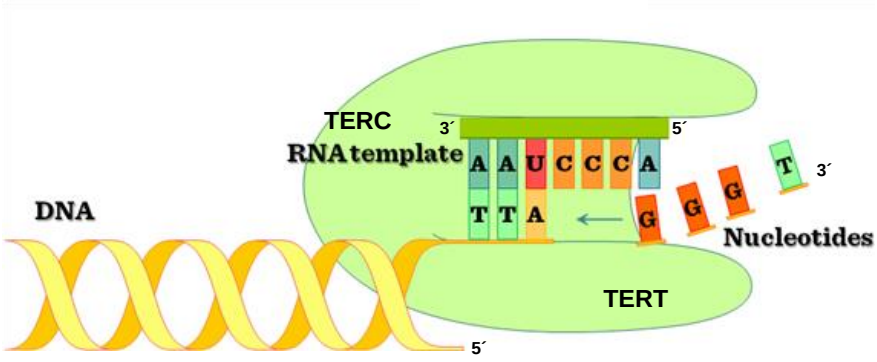

Figure I 8. Telomerase structure in mammals. Schematic image of telomerase components: catalytic subunit, telomerase reverse transcriptase (TERT) and RNA template (TERC). Adapted from Kvel et al., 2011.

A short template sequence in the TERC is copied by the TERT to synthesize new telomere repeats that are added to chromosome ends. In addition to the template, other conserved RNA structural elements play important roles in catalysis and in telomerase localization, maturation, and assembly (Chen & Greider, 2004). Telomerase RNA is mutated in the autosomal dominant form of congenital dyskeratosis (Vulliamy et al., 2001). Recent studies of telomerase RNA

function and telomerase biogenesis provide a basis for understanding the role of telomerase in this disease (Chen & Greider, 2004; Vulliamy et al., 2001).

4.4.2. Telomerase function

In almost all eukaryotic cells, the task of solving the end-replication problem and counteracting telomere attrition is assigned to the active telomerase holoenzyme complex (Sfeir & Lange, 2012). The mechanism underlying the access of telomerase to chromosome ends and the regulation of its activity in mammalian cells is not fully understood. A crucial step in telomerase action during cellular proliferation is its recruitment to chromosome ends in a timely manner to ensure that the ends of lagging strands are replicated correctly. Telomere elongation by telomerase is a multistep process. First, the nucleotides at the 3´ flanking end of the telomere are hybridized to the complementary end of the TERC, within the RNA domain of the telomerase complex. The template sequence consists of 11 nucleotides. TERT then fills up the gap in the termini of the telomerase template with triphosphate nucleotides, resulting in the assembly of a complete hexanucleotidic repeat on the template. Telomerase then relocates, the telomere is extended in the 3´ direction, and the cell cycle is repeated. Finally, the DNA polymerase can synthesize the lagging strand, and chromosome end is thus faithfully replicated. This process can maintain telomere length or result in telomere lengthening (reviewed in Cong et al., 2002).

5. Zebrafish telomere biology

Zebrafish have heterogeneous telomeres of a length similar to those of humans (15-20 kb) and that undergo progressive shortening with age. Unlike the situation in mammals, zebrafish telomerase is constitutively active from embryonic stages to adulthood and throughout life. However, as in humans, telomerase expression in zebrafish somatic cells is not sufficient to counteract telomere attrition, establishing telomere length as an internal clock for cell division (Anchelin et al., 2011). The prominent regenerative ability of zebrafish throughout life may be related to the detectable telomerase activity that maintains telomeres during the robust cell proliferation associated with tissue renewal. Telomerase-deficient mice require several generations of inbreeding, before the telomere shortening become evident. In contrast, first

generation zebrafish telomerase mutants, although they are born and develop normally (**Figure I 9**), progressively develop a degenerative phenotype and die prematurely (Henriques et al., 2013). Notable aging features of telomerase-deficient zebrafish are loss of body mass, spinal curvature as a consequence of muscle degeneration, gastrointestinal atrophy, liver and retina degeneration, and increased inflammation at later stages (Henriques et al., 2013). Telomerase deficiency in zebrafish also leads to premature infertility. Embryos derived from interbreeding of first generation zebrafish telomerase mutants die at early developmental stages.

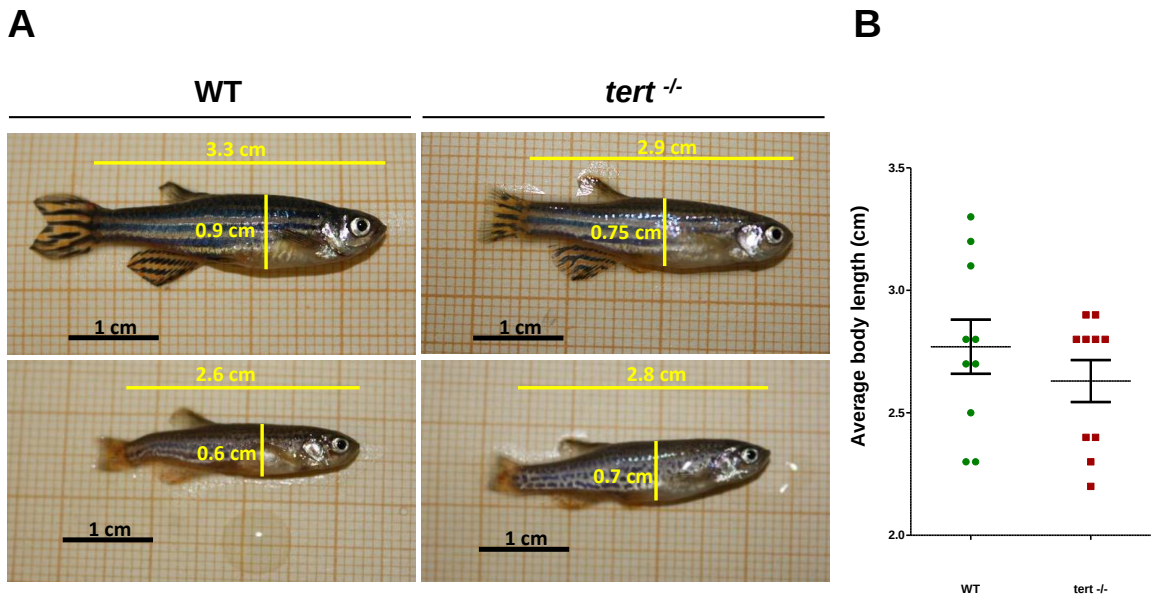

Figure I 9. Mutation in *tert* gene does not affect phenotype of adult zebrafish. (A) Representative siblings of young adult zebrafish WT and *tert* mutant (*tert*$^{-/-}$) do not present significant alterations in the body size. (B) Quantification of body length for both genotypes in centimeters (cm).

OBJECTIVES

The objectives of this thesis were:

1. To determine the role of telomerase during cardiac regeneration in zebrafish.
2. To analyze zebrafish heart regenerative capacities in the absence of telomerase.
3. To explore downstream consequences due to absence of telomerase activity.
4. To explore the importance of telomeres length during heart regeneration by telomapping analysis within zebrafish uninjured and injured hearts.
5. To find possible implications for understanding disease and developing therapies.

MATERIAL AND METHODS

Animal husbandry

All the experiments during this work were performed followed the Guidelines of the European Union Council 86/609/EUC in accordance with directive 2007/526/EC – on the protection of animals used for scientific purposes, governed by Royal Decree 1201/2005. All animal procedures were approved by Spanish Bioethical Committee. Animals were maintained in recirculating tanks (Westerfield, 2000) and experiments were conducted with adult zebrafish between 6 and 9 months of age, raised at a standard density of 3 fish/l. Adult fish were maintained at 26-28 ºC, with a light:dark cycle of 14:10 hours and were fed twice daily with dry food (Sera) and arthemia. For this work we have used AB wild type line (ZIRC, Eugene, OR, USA) and the telomerase mutant line *tert* $^{AB/hu343}$, which is available at the ZFIN repository (ZFIN ID: ZDB-GENO-100412-50) from the Zebrafish International Resource Center (ZIRC). The *tert* $^{AB/hu3430}$ mutants were generated at Utrecht University (Netherlands) by target-selected ENU (N-ethyl-N-nitrosourea) mutagenesis. This telomerase mutant line carries a nonsense T to A transition in the second exon of the *tert* gene, leading to premature stop codon and a truncated protein with only the first 156 of the 1088 amino acids and an absence of the RNA-binding and reverse transcriptase domains (Anchelin et al., 2013; Henriques et al., 2013).Genotyping was performed by PCR of the *tert* gene (*tert* primers: forward 5'GACGACCAGTTCGGATCCCTTC 3'; reverse - 5' CTTTACCCTCCGCCGCTTTACC 3'). Characterization of *tert*$^{-/-}$ zebrafish was performed in F1 and F2 animals produced by *tert*$^{+/-}$ incrossing.

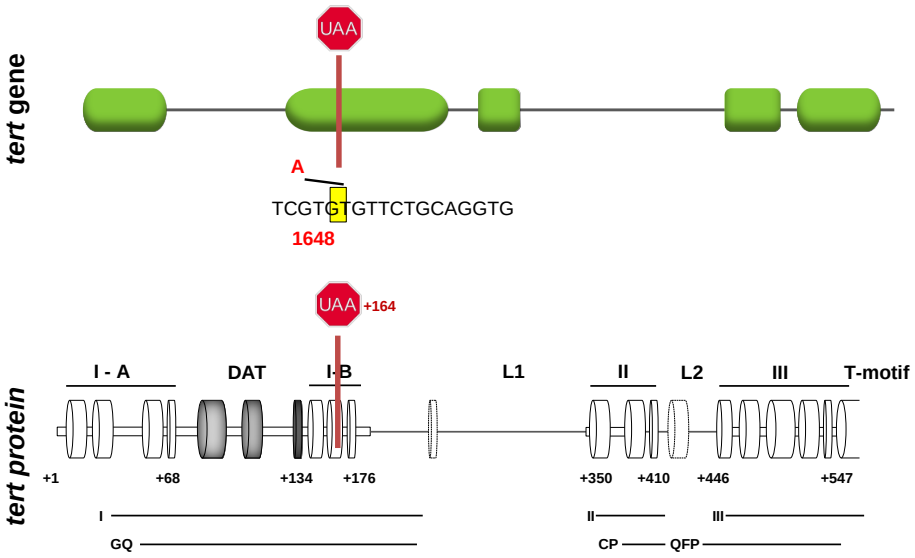

Figure MM 1. Nonsense terthu3430 mutation leads to a nonfunctional product. Scheme of T to A point mutation in the second exon of *tert* gene, leding to codon STOP and non-functional truncated protein

Ventricular cryoinjury

Preparation of cryoprobe and cryoinjury was performed as previously described (González-Rosa and Mercader, 2012). To induce ventricular cryoinjury in adult zebrafish, the animals were anesthetized in a Petri dish with solution of 0.032% tricaine dissolved in a aquarium water. When the animal did not respond to the pinch of the caudal fin, was moved then and placed in a moistened sponge in such a way that the ventral part was accessible for manipulation. Using a binocular microscope, the animal's heart was located using as reference the silver pigmentation of the pericardial sac. The scales of this area were removed with the help of forceps. Afterwards a small incision was made through the body wall and the pericardial sac, but without damaging the heart. After opening the pericardial sac, in order to expose the ventricle, abdomen of the animal was gently compressed using two fingers. Previously cooled in liquid nitrogen cryoprobe was placed on the ventricular surface until thaw. The complete surgical procedure takes 3-5 minutes per fish. Next, the animals were placed in a tank of fresh water at the standard density. As a control for this procedure sham operation was performed, based on opening the pericardial wall and applying a probe that has not been pre-cooled.

BrdU labeling

To perform the pulse-chase experiments for BrdU, the animals were anesthetized using tricaine and injected intraperitoneally at 3 and 7 dpi with 0.05 ml of a solution of 2.5 mg · ml-1 of BrdU (Sigma) in PBS. Animals were then left to continue healing until 7 or 14 dpi.

Zebrafish heart dissection

For dissection of the heart of adult zebrafish, the animals were sacrificed at different time points after cryoinjury by immersion in 0.16% (weight-volume · 1) Tricaine for 10 minutes. The dissection was performed in PBS supplemented with 0.1 M KCl and 2 U ml -1 heparin, in order to stop the heart in diastole evenly and respectively prevent the formation of blood clots. The body wall was removed by three sequential sections. A first deep cut, took place between the gills severing the aorta. This step is important in order to avoid excessive accumulation of blood

within the ventricle. The second incision, perpendicular to the main axis of the body, is made from the base of the right pectoral fin to the base of the left one. Through a third incision from the base of the right pectoral fin to the first incision, the body wall was removed, thereby leaving exposed the heart. Finally, to release the heart, the aorta was clamped and the binding of the atrium and sinus venous was cut. Before fixation, the samples were washed in dissection buffer to remove excess blood.

Histological analysis

For analysis by conventional and immunofluorescence or in situ hybridization on histological sections, the hearts of adult zebrafish were fixed in paraformaldehyde (PFA, Merck) to 4% in phosphate-buffered saline (PBS) overnight at 4 °C in gentle agitation. Samples were then washed in PBS + 0.1% Tween20, dehydrated using ethanol series of increasing gradation and embedded in paraffin wax. All histology was performed on sections of 5-7 µm using a semiautomatic Leica RM2245 microtome. These sections were mounted serially on five Superfrost Plus slides (Fisher Scientific) – each slide contained consecutive sections of the heart - and dried overnight at 37 ° C. Until use, the samples were stored at 4 ° C.

Histological detection of connective tissue and collagen deposition

Sections were deparaffinized in xylene (Merck) and rehydrated using alcohols of decreasing gradation up to distilled water. To differentiate the connective tissue of the heart muscle Masson's trichrome-Goldern was performed, following the manufacturer (Merck). As a result of this technique, the cardiac muscle is dyed red and the connective tissue – both the cellular components as well as extracellular- is dyed green.

Immunofluorescence on paraffin sections

For detecting proteins in tissues by immunofluorescence, sections were deparaffinized in xylene, rehydrated and washed in distilled water. Epitopes were retrieved by heating slides for 15 minutes in citrate buffer (10 mM sodium citrate, pH 6.0) in the microwave at full power and then permeabilized with Triton X-100 to 0, 5% in PBS for 10 minutes at room temperature. Non-specific binding sites were saturated by incubation for 1 hour in blocking solution (3% BSA, 5% goat serum, 0.3% Tween-20). All washes were performed in PBSTw (Tween-20 0.1% in PBS).

Endogenous biotin was blocked with the avidin-biotin blocking kit (Vector, Burlingame, CA, USA). Slides were then incubated overnight with primary antibodies at 4°C. Primary antibodies used were anti-myosin heavy chain (MF20, DSHB; diluted 1:20), anti-tropomyosin (CH1, DSHB; diluted 1:20), anti-L-plastin (kindly provided by P. Martin, University of Bristol, (Evans et al., 2013)), anti-erg1 (Abcam, diluted 1:100) anti-proliferating cell nuclear antigen (PCNA, Santa Cruz Biotechnology; diluted 1:100), anti-bromodeoxyuridine (BrdU, BD Biosciences; diluted 1:30), anti-phospho-histone H3 (PH3, Millipore; diluted 1:100), and anti-phospho-histone H2A.X (γ-H2AX, GeneTex; diluted 1:300). Primary antibody signal was revealed after incubation for 1 hour at room temperature with biotin- or Alexa (488, 568, 633)-conjugated secondary antibodies (Invitrogen; each diluted 1:200) and streptavidin-Cy5 (Vector). Nuclei were stained with DAPI (1:1000) and slides were mounted in Vectashield (Vector, Burlingame, CA, USA). For tyramide amplification, endogenous peroxidase was blocked immediately after hydration of the samples, incubating the slides in a hydrogen peroxide solution 3% in 100% methanol for 15 minutes at room temperature, protecting samples from the light.

Detection of apoptotic cells

Apoptosis was detected by TUNEL – Terminal deoxynucleotidyl dUTP nick end labeling - staining using the “In situ cell death detection” kit from Roche (Mannheim, Germany), following the supplier´s instructions. This procedure was performed in combination with immunofluorescence to determine the death of a particular cell type. The samples were processed following the protocol for immunofluorescence, with some modifications. After dewaxing, hydrated, and permeabilization antigen retrieval, endogenous avidins and biotin were blocked and samples were equilibrated in TdT buffer supplemented with 1 mM CoCl. The reaction of the 2 terminal transferase was performed for 1 h at 37 ° C. This enzyme, incorporating biotin-16-dUTP in the fragmented DNA, can detect a late stage of cell death. After the reaction, the sections were washed in PBSTw and incubated overnight at 4 ° C with the proper primary antibodies.

Immunofluorescence on Q-FISH staining

For combined analysis of Q-FISH and immunostaining for proliferation an additional step was performed with the Vectastain Elite ABC Standard Kit (Vector Laboratories) and the Cy5-

conjugated Tyramide Signal Amplification Plus Kit (TSA Plus, PerkinElmer). Endogenous peroxidase activities were quenched in 3%H_2O_2 in PBS for 10 minutes at room temperature. Before applying secondary antibodies, sections were incubated for 30 minutes with VECTASTAIN®Elite ABC Reagent at room temperature. After 3 washes of 5 minutes each in PBS, slides were incubated for 4 minutes in tyramide-Cy5 conjugate diluted 1:100 in 1XPlus Amplification Diluent (PerkinElmer). After 3 additional 5 minute washes secondary antibodies were applied and slides were processed according to the immunofluorescence and Q-FISH procedure described above.

In situ hybridization on sections

To detect the presence of the messenger RNA of a gene in paraffin sections we performed in situ hybridization. Riboprobes were designed to detect the expression of aldh1a2. The synthesis of digoxigenin-labeled probes, were performed according to the manufacturer's recommendations (Roche). In situ hybridization on sections was performed following established protocols (Mallo et al., 2000), with some modifications. Samples were deparaffinized in xylene (2 x 10 min), washed in ethanol 100 (2 x 10 min) and rehydrated in a series of alcohols of decreasing gradation (every step for 5 min using ethanol 95, 90, 70, 50 and 30%). After washing in PBS (5 min), the tissue was postfixed using 4% PFA for 20 min. Then slides were washed in PBS (2 x 5 min) and digested with proteinase K (10 mg · ml-1) at 37 ° C for 10 min. To stop digestion, the samples were treated with 0.2% glycine in PBS (10 min), washed in PBS (5 min), were postfixed with 4% PFA for 5 min and washed again in PBS. For a better permeabilization of the tissue, proteins were denatured by treatment with 0.2 N HCl (15 min under gentle stirring). After washing (2 x 5 min in PBS), the amino groups of the proteins were acetylated by treatment with acetic anhydride in triethanolamine 0.25% 0.1 M pH 8, with gentle agitation for 10 min. After washing in PBS and water, the sections were incubated in preheated prehybridization solution (50% formamide, 5X SSC pH 5.5, 1X Denhardt's, 0.1% Tween-20, 0.1% Chaps and 50 mg · ml- 1 of tRNA) for 2 h at 65 ° C. After this time, the prehybridization solution was replaced by hybridization solution (same composition as above, but with addition of RNA probe labeled with digoxigenin at a concentration of 1.3 mg · ml-1). Samples were covered with coverslip and hybridized at 65 ° C overnight. To prevent sections from drying, incubations were performed in a humidified chamber with 50% formamide, 5X SSC and 5.5 pH. Following incubation, samples

were washed at 65 ° C in posthybridization 1 solution (2 x 30 min, 50% formamide, 5X SSC pH 5.5, 1% SDS) and post-hybridization 2 solution (2 x 30 min, 50% formamide, 2X SSC, 0.2% SDS). Samples were washed with MABT (3 x 5 min, 100 mM maleic acid, 150 mM NaCl, 0.1% Tween-20, pH 7.5) and blocked for 2 h using 1% blocking solution and 10% goat serum in MABT. Then they incubated with anti-DIG-AP (1: 2000 in the same previous solution) overnight at 4 ° C. The next day, the samples were washed in MABT (3 x 10 min, and then 4 x 1 h), equilibrated using developing buffer (3 x 10 min, 0.1M NaCl, 0.05M MgCl2, Tris 0.1M HCl pH 9.5 and 0.1% Tween-20) and the signal was developed with BM Purple AP substrate (Roche) in darkness. Once signal revealed, the samples were washed in PBS (2 x 5 min), postfixed with 4% PFA for 15 min, dehydrated in alcohols increasing gradation, washed in xylene and mounted using DPX.

Image acquisition and analysis

Images of dissected hearts were obtained using a Leica MZ16FA fluorescence stereo microscope fitted with a Leica DFC310FX camera. Masson's trichrome-Goldern staining images, immunohistochemistry and in situ hybridizations revealed with DAB were acquired on a microscope Nikon Eclipse 90i. Immunofluorescence in sections images were acquired using a confocal microscope Nikon A1R. Quantitative images were analyzed (channels separation, proliferating cells count or measuring area) using NIS-Element software. For the final preparation of the figures – some images were adjusted using Adobe Photoshop CS5. If there were applied any modification of the characteristics of the image, this procedure equally affected the entire image, without addition, alteration or elimination of any features.

Cardiac imaging by echocardiography in adult zebrafish heart

For the echocardiographic image acquisition, the animals were anesthetized by immersion in a mixture of tricaine (130 ppm) and isoflurane (200 ppm) in aquarium water (Huang et al., 2010). The level of sedation was determined by clamping the tail fin using two fingers. Anesthetized animals were placed with the ventral side up on a custom-made sponge soaked in anesthetic solution. Two-dimensional (2D) high-resolution real-time in vivo images were obtained with the VEVO 770 (VisualSonic) Imaging System through a RMV708 (22-83 MHz) scanhead (VisualSonic, Toronto, Canada). For a finer manipulation, the probe was placed in

a mechanical arm, which plunged into the anesthetic about 3 mm from the skin of the fish, scanning an area of 4 mm x 4 mm. Acquisition was set to 200 second-1 per image. This high frequency acquisition allowed visualization of the heart and limits movement of the valve and improved accuracy of measurements. For the 2D image, the frequency was adjusted to 50 MHz, the depth to 10 mm and 60 dB dynamic range and several cardiac cycles were acquired per animal for further appropriate measurements. Additionally, a color Doppler sequence with a frequency of 40 MHz, a depth of 10 mm and a Doppler gain of 33 dB was obtained. A modification of the Simpson method (Schiller et al., 1979) was applied, considering as reference the epicardial edge and not the endocardial border to determine the fraction of systolic shortening (FAS).

Statistical analysis

The statistical significance of the mean difference in experimental groups was analyzed by one-way ANOVA followed by Tukey´s honest significant test and student´s t-test were used when normal distributions can be assumed. Mann-Whitney test was used when the normality assumption cannot be verified with a reliable method. Model assumptions of normality and homogeneity were checked with conventional residual plots. To control the false-discovery rate of RNA-seq data p-values were corrected for multiple-testing using the Benjamini_Hochberg´s method (Benjamini and Hochberg, 1995) obtaining adjusted p-values. Microsoft Excel version 14.4.9 and Prism version 5.0 were used for calculations. *"Mann-Whitney two tailed t-test"* was used to calculate statistical significance of differences in L-plastin signal at 3 and 60 days post injury between WT and *tert*$^{-/-}$ hearts (Fig. S1D,G). Mann-Whitney is a nonparametric test with greater efficiency than the student´s t-test on non-normal distributions. We chose the Mann-Whitney test over the student´s t-test in small data sets when the normality assumption cannot be verified with a reliable method. *"one-way ANOVA followed by Tukey's honest significant difference test"* was used to calculate statistical significance of differences in fractional volume shortening of WT and *tert*$^{-/-}$ zebrafish hearts in the basal condition (sham operated animals) and after injury at 7 days, 30 days and 60 days post-operation (Fig. 2D). It was used since it compares all possible pairs of means in a single step. It was used over multiple two-samples t-test, since the latter would result in an increased chance of committing a statistical type I error. Model assumptions of normality and homogeneity of variance were checked with conventional

residual plots. We did not observe any strong deviation from normality or heterogeneity of variance that justify the use of non-parametric tests. *"unpaired t-test"* was used to calculate statistical significance of differences in those cases in which only two independent groups (e.g. WT and *tert*$^{-/-}$ groups) were compared. The cases were it was used is indicated in the main text or figure legends. *"adjusted p-value"* was used to calculate statistical significance of differences in mRNA expression levels obtained from RNA-seq data. p-values were corrected for multiple-testing using the Benjamini-Hochberg's method (Benjamini and Hochberg, 1995) to control the false-discovery rate in RNA-seq statistical analyses obtaining adjusted p-values.

Telomeric Repeats Amplification Protocol (TRAP)

Telomerase activity was measured with a modified fluorescence telomere repeat amplification protocol as described (Herbert et al., 2006). Pools of two whole hearts were aseptically removed immediately after death and using heparin, cleaned of blood cells and washed with hanks balanced salt solution. Fresh excised heart pools were homogenized immediately, without prior freezing, in 200 ul of CHAPS lysis buffer (10 mM Tris HCl pH 7,5 , 1 mM $MgCl_2$, 1 mM EGTA, 10 % glycerol (v/v), 0,5 % CHAPS (w/v), 0,1 mM PMSF, 1X protease cocktail inhibitor (Roche), β-mercaptoethanol using a motorized disposable pestle (Sigma). iPS cells were resuspended in 200 ul of CHAPS lysis. After 30 min incubation on ice and centrifugation for 20 min at 14000 r.p.m. at 4 ºC, the supernatants were collected and frozen at -80 ºC. Aliquots (10 µl) of WT control extracts (0,2 µg/µl) were treated with 3µl of RNase (10mg/ml) at 37ºC for 20 minutes. Protein concentrations were determined by the method of Bradford (DC TM Protein Assay, BIO-RAD). Telomerase activity was measured in tissue and cell extracts according to (Brittney-Shea et al., 2006) by a fluorescent method. The telomerase reactions were started by adding 2-µl aliquiots of the extracts (containing 0,01 or 0,01 µg protein from iPS cells and 0,4 µg protein from zebrafish heart extracts) to 46,6 µl TRAP reaction mixture containing 20 mM Tris-HCl ph 8,3; 1,5mM $MgCl_2$; 63 mM KCl, 0,05 % Tween 20; 1 mM EGTA, 0,05 mM dNTP, DEPC water (Sigma) and 2 ng ul^{-1} Cy5-TS primer (5'-AATCCGTCGAGCAGAGTT-3'). Then the reaction was incubated at 30ºC for 30 min to allow telomerase to add telomeric repeats to the Cy5-TS primer. After that, 2 U Taq Polymerase (5 U ul-1) and a specific TRAP primer mix were added to 50 ul final reaction. Primer mix contains 100 ng ul^{-1} Ancor primer (5'- GCGCGGCTAACCCTAACCCTAACC-3'), 100 ng ul^{-1} OG

primer (5'-ATGGCATCACCGGCTTAT-3') and 0,01 attamol ul^{-1} TSOG primers (5'-AATCCGTCGAGCAGAGTTATAAGCCGGTGATGCCAT-3'). The reaction mixtures were heated at 95ºC for 5 min to inactivate telomerase, and then subjected to 30 amplification cycles of 95 ºC for 30 s, 55 ºC for 30 s, and 72 ºC for 30s, followed by a single extension cycle at 72 ºC for 7 min. The PCR products were then separated on 10% nondenaturing poliacrylamide gels by electrophoresis at 125 V using 0,5X TBE as running buffer. Finally, fluorescent PCR products were visualized using Typhoon 9400. In order to minimize carry-over contaminations, we performed the three essential steps (preparation of extracts, setting up the telomerase assay reactions and analysis of amplification products) with a separate set of pipettman (with aerosol resistant pipet tips) and in different separated rooms. Moreover, 100X stock of TSOG primer (1 attomol ul^{-1}) was prepared in another entirely separate room from the TRAP room and with another different pipettman.

RNA-seq library production

Total RNA (1 μg) was used with the TruSeq RNA Sample Preparation v2 Kit (Illumina, San Diego, CA) to construct index-tagged cDNA libraries. 4 biological replicates consisting of 3 pooled hearts were used per sample. Quality, quantity and size distribution of the Illumina libraries were determined using the DNA-1000 Kit (Agilent Bioanalyzer). Libraries were sequenced (single-end mode and length 75bp) on the Genome Analyzer IIx System, using the standard RNA sequencing protocol in the TruSeq SBS Kit v5. Fastq files containing reads for each library were extracted and demultiplexed using Casava v1.8.2 pipeline.

RNA-Seq analysis

Sequencing adaptor contaminations were removed from reads using cutadapt software (Martin, 2011) and the resulting reads were mapped and quantified on the transcriptome (Ensembl gene-build 66) using RSEM v1.2.3 (Li and Dewey, 2011). Only genes with at least 2 counts per million in at least 4 samples were considered for statistical analysis. Data were then normalized and differential expression tested using the bioconductor package EdgeR (Robinson et al., 2010). We considered as differentially expressed those genes with a Benjamini-Hochberg adjusted p-value ≤ 0.05.

Electron Microscopy

Transmission Electron Microscopy was performed as described (Willett et al., 1999).

Quantitative fluorescence in situ hybridization (Q-FISH)

Telomere Q-FISH analysis on paraffin-embedded sections was performed as described (Flores et al., 2008). Images were taken using an A1R-A1 Nikon confocal microscope with a 60x objective. Quantitative image analysis was performed on confocal images using Metamorph version 7 (Molecular Devices, Union City, CA) as described (Flores et al., 2008). Briefly, the DAPI image was used to define the nuclear area and the Cy3 image to quantify telomere fluorescence. Telomere fluorescence intensity was measured as "average gray value" (total gray value per nucleus) units. These "average telomere fluorescence" values represent the average Cy3 pixel intensity for the total nuclear area, thereby ruling out any influence of nuclear size on telomere-length measurements. Telomere fluorescence values for each sample were exported to Excel, to generate frequency histograms. A four-color intensity banding was used to generate the map of telomere length. The injury area, determined by the absence of MHC staining was excluded from the analysis.

Western blot analysis

Hearts were dissected and lysed in RIPA buffer (50 mM Tris, pH 8; 150 mM NaCl, 0.1% SDS; 1% NP40 and 0.5% sodium deoxycholate) containing protease inhibitor cocktail (Roche). Total proteins (100 μg) were separated by SDS-PAGE and transferred to a polyvinylidene fluoride (PVDF) membrane. Blots were incubated overnight with primary antibodies. Antibodies to histone γH2AX (GeneTex, GTX127342) were used at 1:1000 dilution, and α-tubulin (Sigma, T8203) at 1:4000. HRP-coupled secondary antibodies (Dako) were used at a 1:5000 dilution. Band intensities were quantified by densitometric analysis using QuantityOne software (BioRad).

Quantification of phosphorylated H2AX foci

Phosphorylated H2AX foci were detected with rabbit polyclonal anti-phospho-histone H2AX antibody (1:300; GeneTex). A cell was considered positive for γ-H2AX when it contained two or more foci. Foci were counted manually.

Senescence-associated β-galactosidase activity

Senescence-associated β-galactosidase (SA-β-gal) activity was detected on freshly prepared cryosections and whole-mounts with the Senescence β-Galactosidase Staining Kit (Cell Signaling), according to the manufacturer's instructions.

RESULTS

1. Ventricular cryoinjury induces telomerase hyperactivation in zebrafish heart

Pre-existing cardiomyocytes proliferation is the primary mechanism for regenerating myocardium in the zebrafish heart (Chablais et al., 2011; González-Rosa et al., 2011; Poss et al., 2002; Raya et al., 2003; Schnabel et al., 2011; Wang et al., 2011). Multiple studies have emphasized the critical role of telomerase in cell proliferation (Flores & Blasco, 2010; Flores et al., 2011). Given that zebrafish tissues have constitutive telomerase activity throughout life (Kishi et al., 2003; Kishi, 2004; Anchelin et al., 2011) we hypothesized that it might prolong the proliferative lifespan of cardiomyocytes upon high demand such as ventricular cryoinjury.

To determine whether telomerase expression is altered during the zebrafish heart regeneration process, we analyzed the expression of *tert* mRNA in homeostatic conditions and 3 days postinjury (dpi). Relative to the control uninjured sample RNAseq analysis showed a significant 2.2-fold increase in *tert* gene expression in hearts at 3 days postinjury (dpi) (**Figure R 1A**). Subsequently we examined the correlation between zebrafish *tert* mRNA transcript levels and telomerase activity. We assayed telomerase activity in zebrafish hearts under homeostatic conditions and during different stages of the regeneration process, by fluorescent Telomeric Repeat Amplification Protocol (TRAP). This PCR-based assay is sufficiently accurate and rapid for the quantification of telomerase activity (Herbert et al., 2006). We observed prominent amplification bands in uninjured heart tissue and in hearts at different stages of regeneration: 1, 3, 4, 7 and 30 days posterior to the cryoinjury (**Figure R 1B, 1C**). Interestingly we found that injury of the ventricular apex (one quarter of the ventricle) provoked an increase in the processivity and intensity of amplification bands three days later, demonstrating that telomerase activity substantially increases in response to heart damage. However, significant upregulation of telomerase activity observed 3dpi was transient and subsequently decreased at later stages to levels similar to those detected in uninjured hearts (**Figure R 1B, 1C**).

Moreover, we confirmed residual detectable telomerase activity in adult hearts at different ages under homeostatic conditions, with no significant differences in activity of this enzyme between the cardiac tissues of 6- and 10-month-old fish (**Figure R 2A, 2B**).

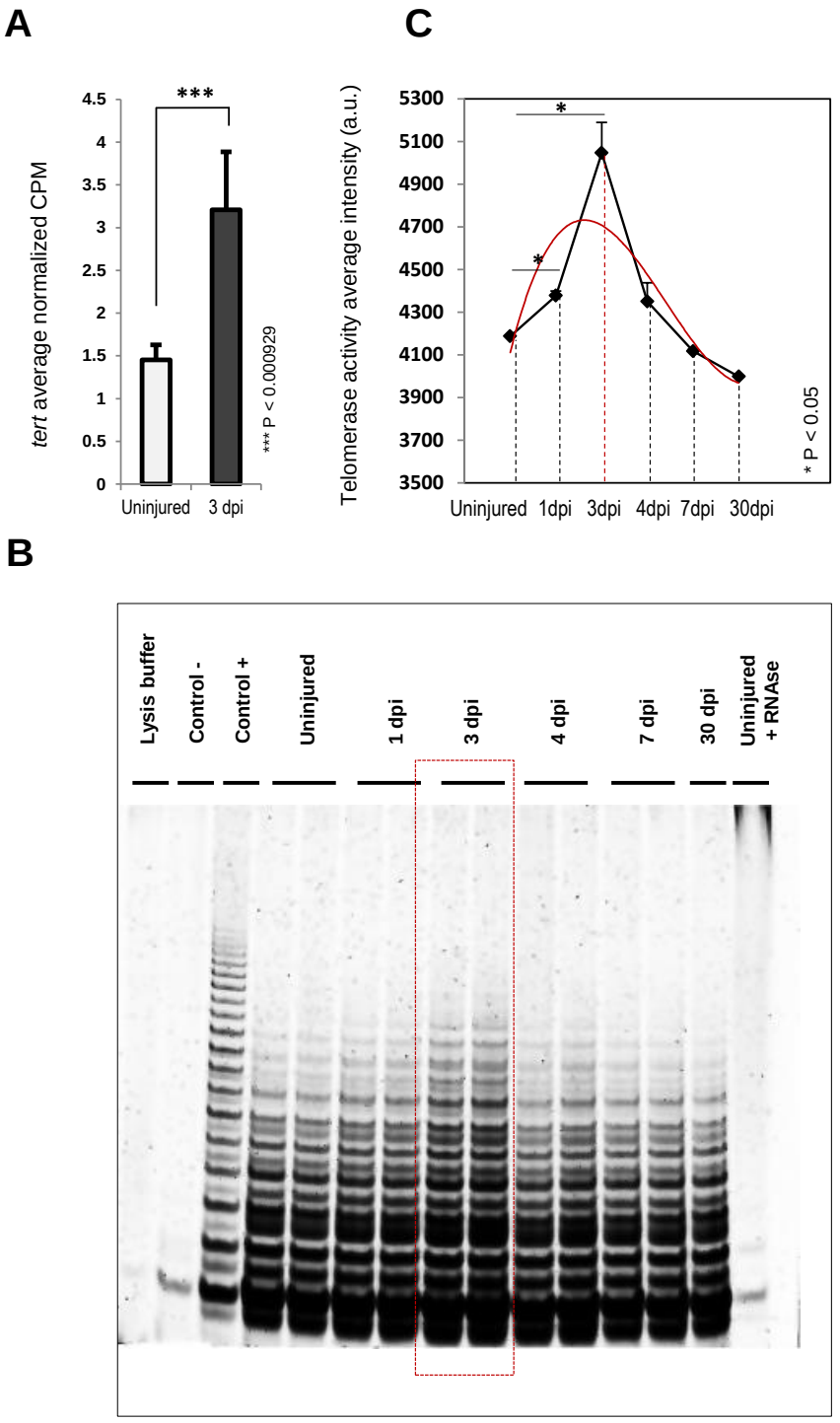

Figure R 1. Heart cryoinjury augments telomerase activity and *tert* expression levels. (A) Zebrafish *tert* mRNA expression levels in homeostasis and during regeneration (3 dpi) (n=4 hearts per condition). CPM, counts per million. Values are means ± SEM *** p<0.001 (B-H adjusted p-value); dpi, days postinjury. (B) Representative TRAP assay in uninjured hearts and hearts at 1, 3, 4, 7 and 30 days after cryoinjury (n=3 per condition and time point). Positive control: iPS (induced pluripotent stem cells). Negative control: *tert*$^{-/-}$ zebrafish heart. Reaction specificity control: uninjured+RNAse. (C) Quantification of intensity of the specific bands for telomerase activity in arbitrary units, in uninjured hearts and hearts at 1, 3, 4, 7 and 30 days after cryoinjury (n=2 pools of 3 hearts per condition; 7 and 30 dpi, 1 pool of 3hearts per condition and time point). Values are means ± SEM;* p<0.05 (B-H adjusted p-value); dpi, days postinjury.

These data suggest that although telomerase activity is present in homeostatic WT zebrafish heart, ventricular injury triggers further increase in the activity of the tert enzyme accompanied by an upregulation of *tert* gene expression.

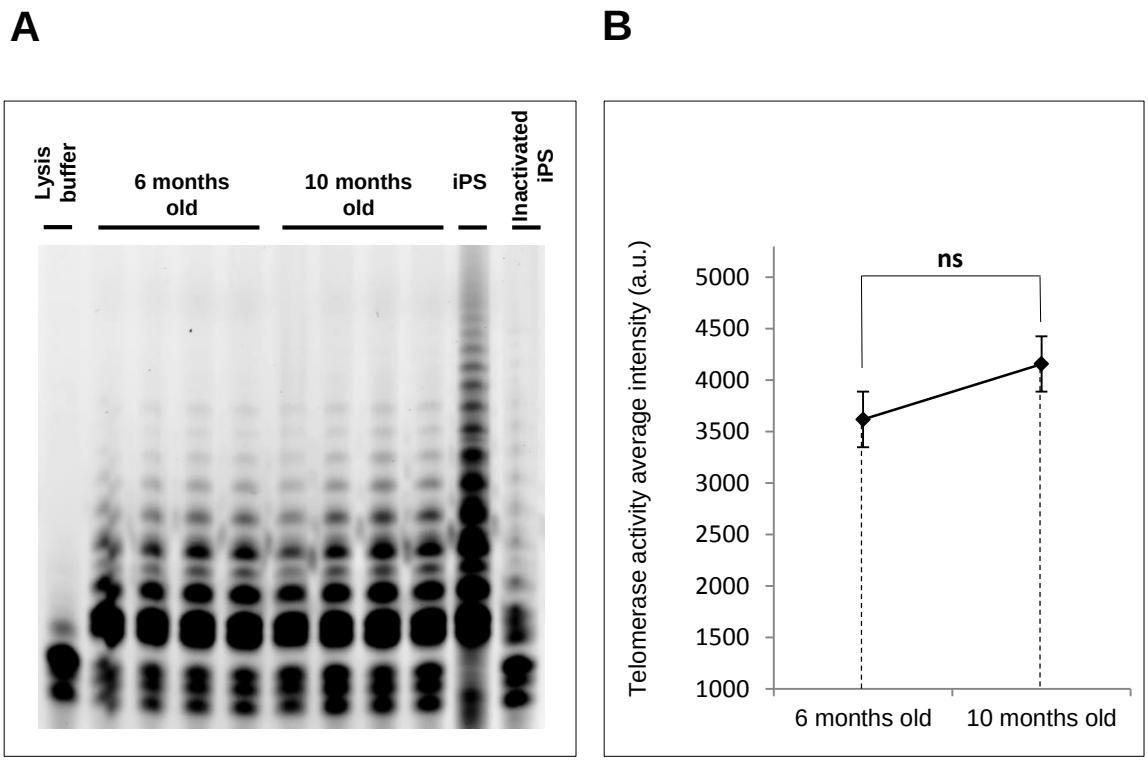

Figure R 2. Detectable telomerase activity in adult zebrafish hearts at different ages. (A) Representative TRAP assay in 6- and 10-month-old zebrafish hearts (n=4 per time point). Positive control: iPS (induced pluripotent stem) cells. Negative control: lysis buffer. Reaction specificity control: inactivated iPS. (B) Quantification of the intesity of the specific bands for telomerase activity in arbitrary units (a.u.), in 6- and 10-month-old zebrafish hearts (n=2 pools of 3 hearts per condition). Values are means ± SEM; ns, non-significant (B-H adjusted p-value); dpi, days postinjury.

2. Nonsense terthu^{3430} mutation leads to a nonfunctional product that does not result in changes of morphology or function of the young zebrafish hearts (6-9 months old)

To determine the effect of lack of telomerase activity on the zebrafish heart, we obtained a commercially available mutant line of the *tert* gene (terthu^{3430}). We confirmed by TRAP assay that the terthu^{3430} mutant completely lacks telomerase activity in the heart and thus constitutes a *tert* knockout model (**Figure R 3A**). Therefore, we refer the terthu^{3430} homozygous mutant strain as *tert*$^{-/-}$. Interestingly, zebrafish *tert* mRNA transcripts were detected in *tert*$^{-/-}$ hearts by RNAseq analysis. Although we observed a high expression of *tert* gene in *tert*$^{-/-}$ uninjured hearts, it did not significantly change at 3dpi (**Figure R 3B**).

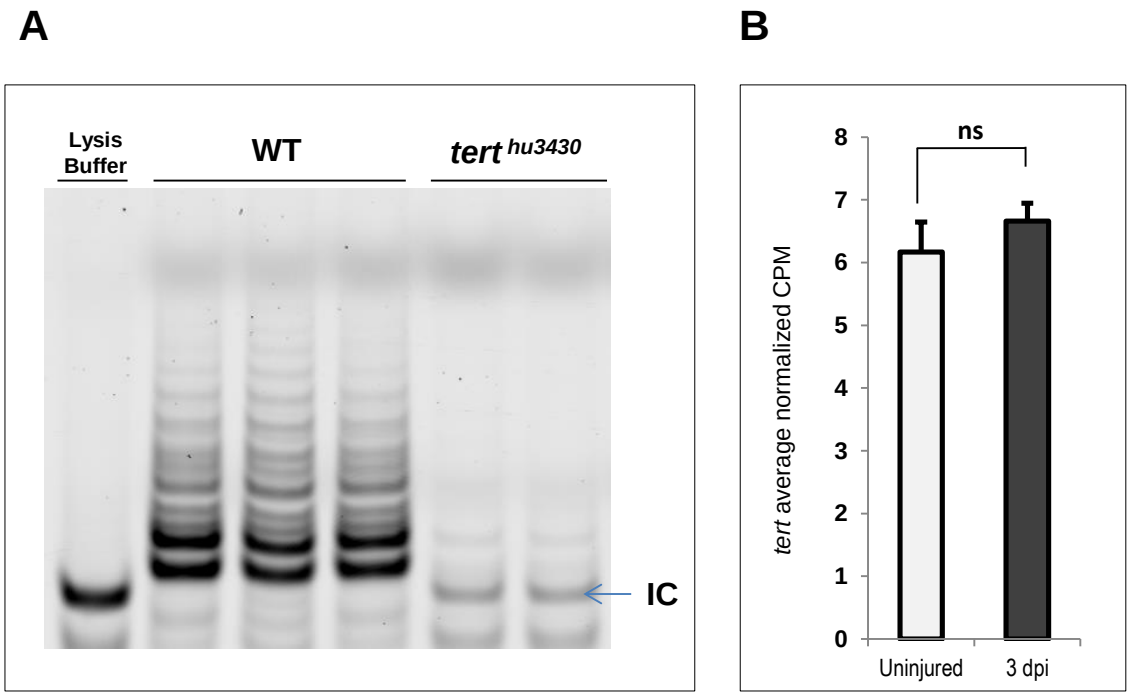

Figure R 3. Nonsense terthu^{3430} mutation in zebrafish heart. (A) Representative TRAP assay in uninjured WT and terthu^{3430} hearts (n=3 pools of 3 hearts for WT and 2 pools of 3 hearts for terthu^{3430}). Negative control: lysis buffer; IC = internal control. (B) Zebrafish *tert* mRNA expression levels in homeostasis and during regeneration (3 dpi) for *tert*$^{-/-}$; CPM, counts per million; Values are means ± SEM; ns, non-significant (B-H adjusted p-value).

We next dissected a pool of 5 uninjured adult wildtype (WT) zebrafish hearts and a pool of 5 hearts from control *tert*$^{-/-}$ siblings and evaluated morphological and histopathological changes between hearts from both groups. Based on whole-mount views and Masson-Goldner trichrome stained sagittal sections we found that despite lacking telomerase enzyme activity, hearts from 6-9-month-old *tert*$^{-/-}$ fish are of normal size and have a normal histology (**Figure R 4A**). Subsequently we evaluated heart size and cardiac function based on standard Doppler echocardiography parameters. We compared ventricular volume in diastole values (VV) to determine heart size and ventricular fractional shortening (FVS) to evaluate cardiac function. Values for either parameter did not differ significantly between genotypes suggesting that lack of telomerase activity is not affecting either heart morphology or heart function in young zebrafish (**Figure R 4**).

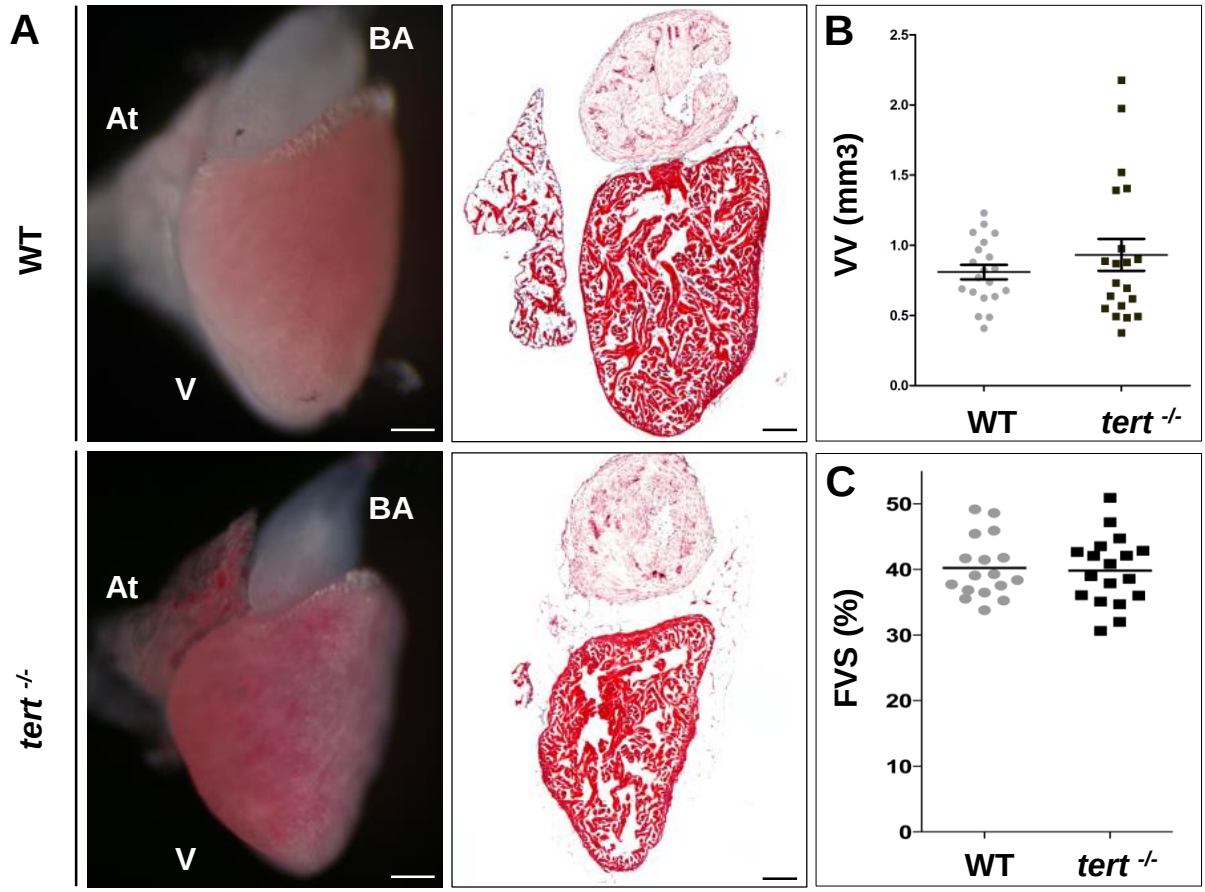

Figure R 4. Lack of telomerase does not affect heart development and function. (A) Normal anatomy in *tert*$^{-/-}$ zebrafish hearts. Whole-mount views of dissected adult wildtype (WT) and *tert*$^{-/-}$ uninjured zebrafish hearts (left) and Masson-Goldner trichrome stained sagittal sections (right). Five animals were analyzed per genotype. V, ventricle; At, atrium; BA, bulbus arteriosus. Scale bars: 100 μm (B) Echocardiographic evaluation of heart size (ventricular volume in diastole; VV). Values did not differ between genotypes. Circles and squares show data for individual animals; horizontal bars represent the mean (unpaired Student's t-test). A total of n=17-20 animals was analyzed per genotype (C) Normal function (ventricular fractional volume shortening; FVS) in *tert*$^{-/-}$ zebrafish hearts. Values did not differ between genotypes. Circles and squares show data for individual animals; horizontal bars represent the mean (unpaired Student's t-test). A total of n=17-20 animals was analyzed per genotype.

3. Ventricular cryoinjury causes substantial heart damage in WT and *tert*$^{-/-}$ zebrafish siblings, but subsequent healing takes place only in WT hearts

To establish the effect of ablating telomerase activity on the regenerative capacity of the zebrafish heart, we performed cryoinjury on the WT and *tert*$^{-/-}$ hearts. In order to determine the

extent of the lesion caused by cryoinjury we sacrificed a group of animals at 3 dpi, when an obvious wound was present, and compared their hearts with hearts of control (uninjured) individuals. The region of damage was detected by local accumulation of blood (**Figure R 5**).

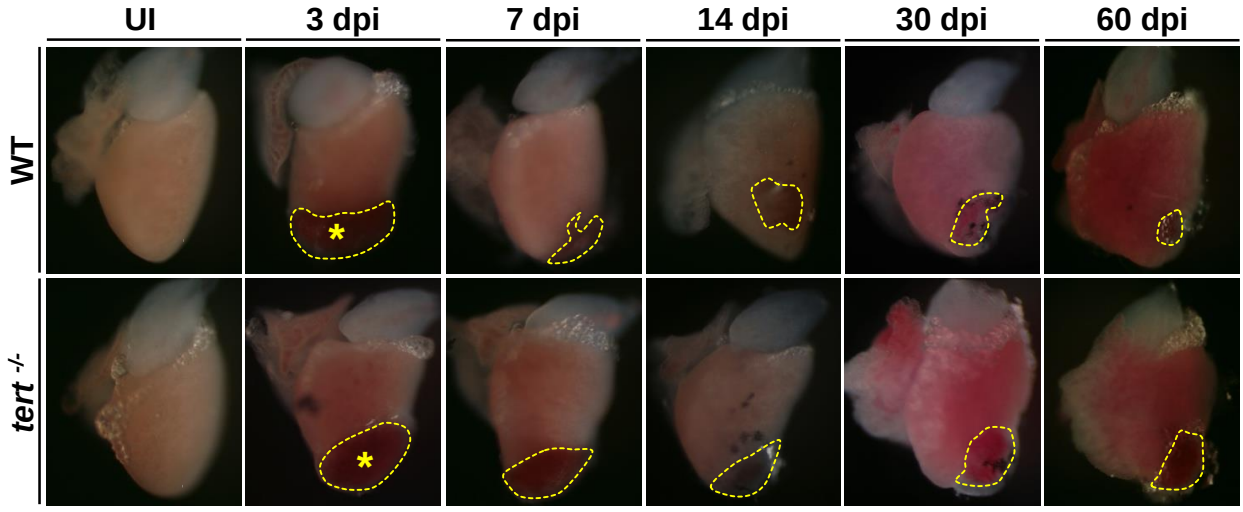

Figure R 5. Heart regeneration is strongly inhibited in *tert*$^{-/-}$ animals. Whole-mount views of uninjured and cryoinjured WT and *tert*$^{-/-}$ zebrafish hearts dissected at the indicated times post-injury. Dotted lines outline the injured area. Asterisks mark the initial injury site. Scale bars: 100 μm; dpi, days postinjury.

Macroscopic observations revealed a variation of the percentage of affected cardiac tissue between animals, but on average it encompassed 20-25% of the ventricular area. We then compared whole-mount general views of injured WT and *tert*$^{-/-}$ zebrafish hearts dissected at the later times post-injury (7, 14, 30 and 60 dpi). We observed that in WT hearts the size of the wound decreased gradually during the regeneration process, whereas a large wound persisted in *tert*$^{-/-}$ hearts at 60 dpi (**Figure R 5**). We performed Masson-Goldner trichrome staining on sagittal sections of uninjured WT and *tert*$^{-/-}$ hearts and at 3, 7, 14, 30 and 60 days after injury. We confirmed the characteristic scar like fibrotic tissue deposition triggered by heart injury in both genotypes (Chablais et al., 2011; González-Rosa et al., 2011) (**Figure R 6**).

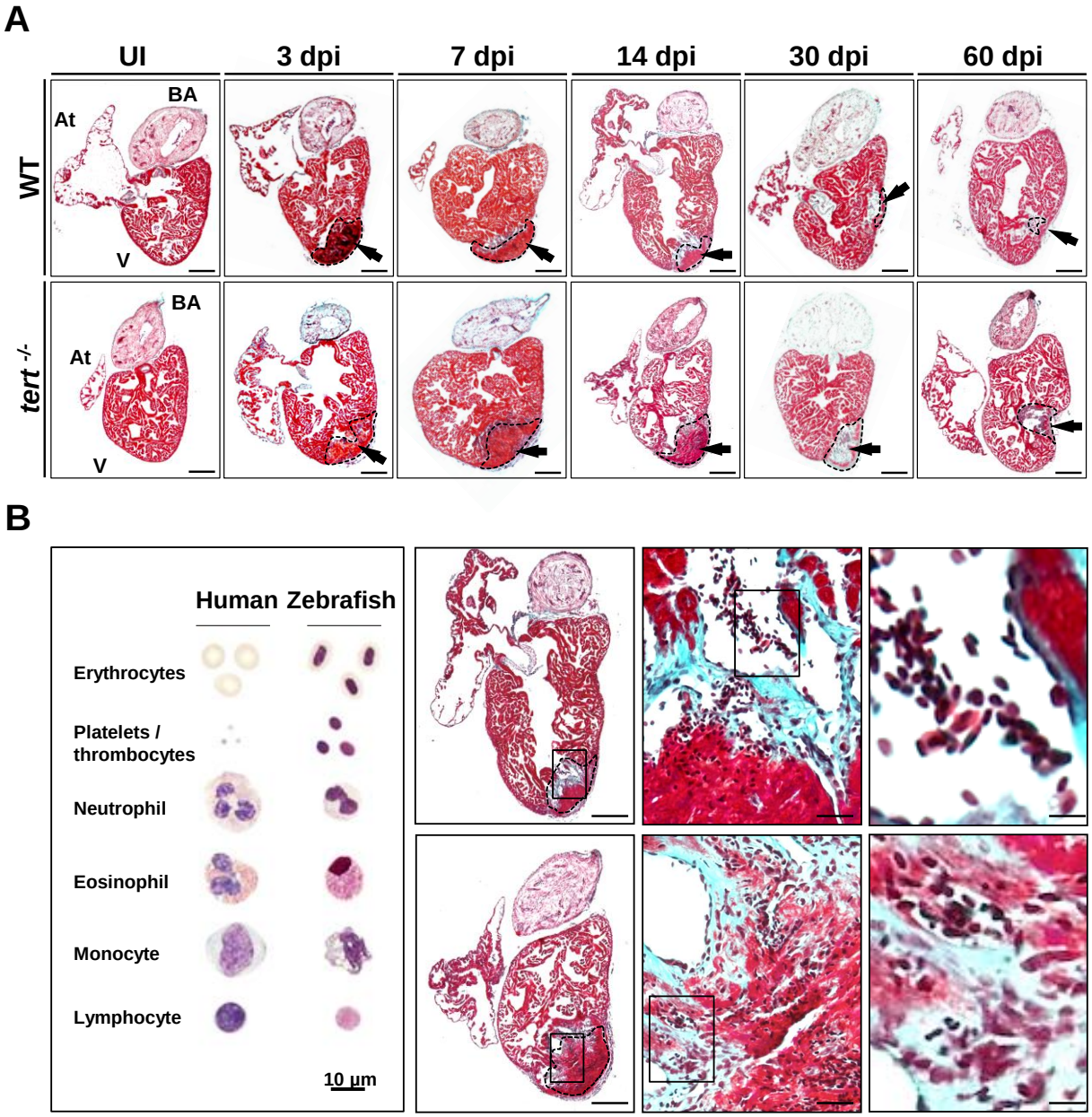

Figure R 6. Histological analysis of regenerative response of WT and *tert*$^{-/-}$ hearts. (A) Masson-Goldner trichrome staining of sagittal sections of uninjured WT and *tert*$^{-/-}$ hearts and at 3, 7, 14, 30 and 60 days after cryoinjury. Cardiac muscle is stained in red and connective tissue is stained in green. Dotted black lines outline the injured area. Black arrows mark the initial injury site. V, ventricle; At, atrium; BA, bulbus arteriosus; Scale bars: 100 µm. (B) Rapid infiltration of the injury site by blood, inflammatory and other circulating cells. Dotted black lines outline the injured area. Scale bars: 100 µm for section view and respectively 50 µm and 10 µm for magnifications.

In WT hearts at 60 dpi we observed an almost complete restoration of the myocardial wall,

although a small region of connective tissue accumulation remained. In contrast *tert*$^{-/-}$ hearts presented a large amount of fibrotic tissue even at 60 dpi and no signs of significant replacement of damaged cardiac muscle with newly formed myocardium (**Figure R 6A**). Moreover, we corroborated that myocardial injury triggers a rapid infiltration of the injury site by blood, inflammatory and other circulating cells as previously reported (reviewed in Frangogiannis, 2014) (**Figure R 6B**).

We next estimated the extent of the ventricular damage caused by cryoinjury (**Figure R 7**). The injured area (IA) occupied similar regions at 3dpi in both genotypes: 20 ± 5% of the total ventricle in WT hearts and 21 ± 6% in *tert*$^{-/-}$ hearts. However at 60 dpi the injured area represented less than 5% of the ventricular region in WT hearts (2.5 ± 0.8%), but was comparable to the injured area at 3 dpi in *tert*$^{-/-}$ hearts (18 ± 2%), suggesting impaired regeneration of damaged cardiac muscle in the zebrafish hearts that lack telomerase.

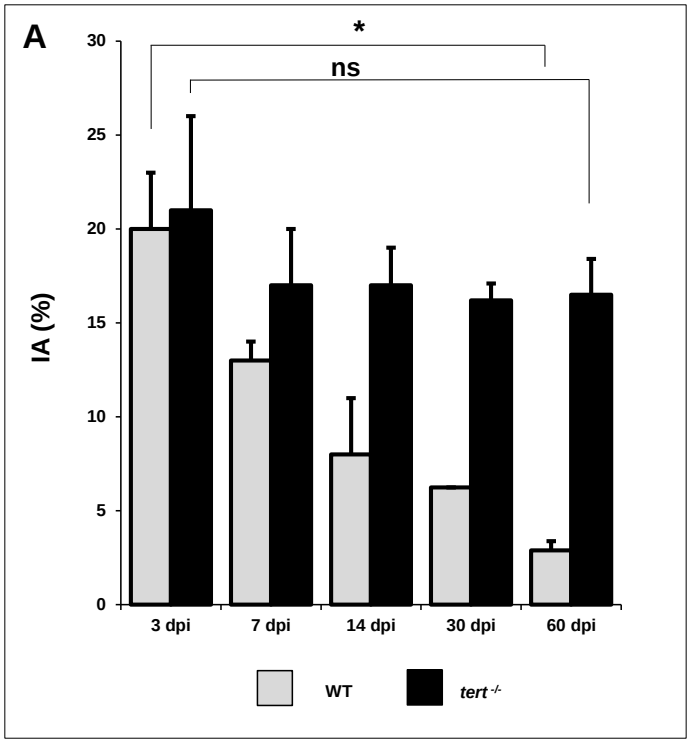

Figure R 7. Heart regeneration is strongly inhibited in *tert*$^{-/-}$ zebrafish. (A) Quantification of the injury size (IA, injured area) on sagittal heart sections at the indicated times post-injury, presented as the percentage of the total ventricular area. Data are means of at least 4 sections per heart from 3-8 hearts per time point, with the exception of WT 30 dpi, where only 1 heart was analyzed. *, $p<0.05$; ns, not significant (Mann-Whitney test). (B) Schematic representation of the regeneration progress for both genotypes. .

4. Cryoinjury leads to a transient functional impairment of cardiac function, with subsequent recovery of ventricular efficiency at 60 dpi in WT hearts

To further substantiate the impaired regeneration response in *tert*$^{-/-}$ hearts, we evaluated cardiac function by 2D echocardiography. This method determines ventricular function in zebrafish *in vivo*. We measured parameters commonly used in clinical practice with some modifications adjusted to the small and hypertrabeculated ventricles of zebrafish (González-Rosa et al., 2014). Cardiac performance was evaluated on the same animals at baseline - prior to injury - and at 7, 30 and 60 days after injury (dpi) for both genotypes. We observed that heart injury triggered a dramatic reduction in systolic function at 7 dpi (measured by fractional volume shortening; FVS) of 47 ± 8% in WT fish and 35 ± 4% in *tert*$^{-/-}$ fish (**Figure R 8A, Figure R 8C**). The FVS value recovered gradually during regeneration in WT fish, indicating that ventricular function was reestablished. Moreover systolic function measured 60 dpi significantly increased and was comparable with the value obtained prior to injury (**Figure R 8A, Figure R 8B**). In contrast, cardiac performance did not recover in *tert*$^{-/-}$ animals even at 60 dpi (**Figure R 8C, Figure R 8D**). Relative fractional volume shortening (RFVS) did not significantly change over time in fish subjected to sham operation from either genotype (**Figure R 8A, Figure R 8C**).

Color flow Doppler echocardiography images of intercardiac blood provided additional information regarding blood flow direction and flow patterns. We observed that blood flow was absent from the site of the injury at 7dpi in both genotypes, but circulating blood was subsequently reestablished at 60 dpi but only in WT hearts (**Figure R 8E; Movie S 1, Movie S 2, Movie S 3, Movie S 4, Movie S 5, Movie S 6**).

These data suggest that the absence of telomerase in zebrafish heart is negatively affecting the injury-induced recovery of heart structure and function.

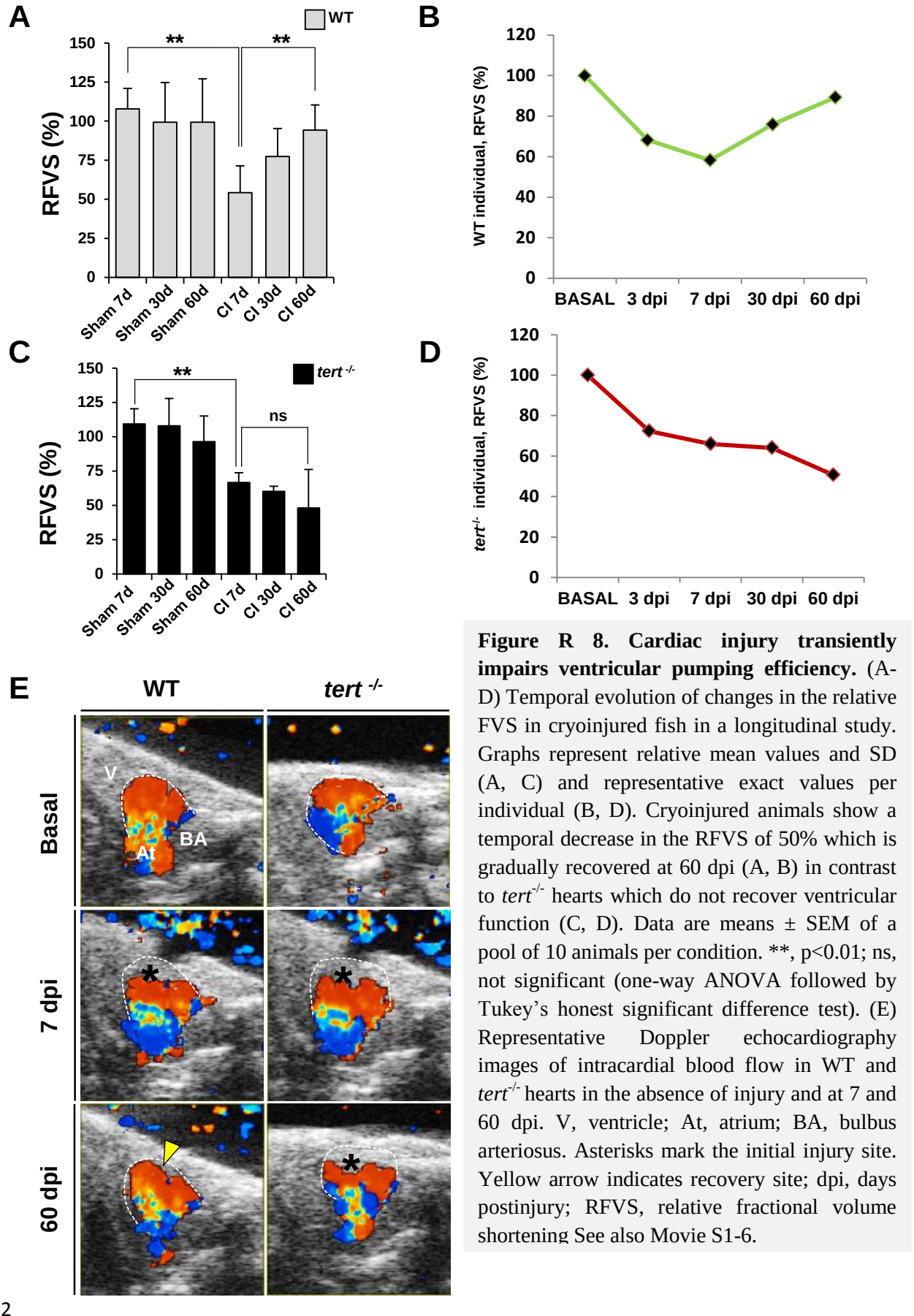

Figure R 8. Cardiac injury transiently impairs ventricular pumping efficiency. (A-D) Temporal evolution of changes in the relative FVS in cryoinjured fish in a longitudinal study. Graphs represent relative mean values and SD (A, C) and representative exact values per individual (B, D). Cryoinjured animals show a temporal decrease in the RFVS of 50% which is gradually recovered at 60 dpi (A, B) in contrast to *tert*$^{-/-}$ hearts which do not recover ventricular function (C, D). Data are means ± SEM of a pool of 10 animals per condition. **, $p<0.01$; ns, not significant (one-way ANOVA followed by Tukey's honest significant difference test). (E) Representative Doppler echocardiography images of intracardial blood flow in WT and *tert*$^{-/-}$ hearts in the absence of injury and at 7 and 60 dpi. V, ventricle; At, atrium; BA, bulbus arteriosus. Asterisks mark the initial injury site. Yellow arrow indicates recovery site; dpi, days postinjury; RFVS, relative fractional volume shortening See also Movie S1-6.

5. The injury-induced inflammatory response is not affected in absence of telomerase

We found that the lack of telomerase impairs zebrafish heart regeneration, but the mechanism leading to successful heart regeneration remains unclear. Immediately after tissue damage, an inflammatory response takes place at the site of injury. Given that gene silencing of the *tert* gene has been shown to impair hematopoiesis (Imamura et al., 2008), we assessed whether *tert*$^{-/-}$ zebrafish show alterations in injury-triggered inflammation. Whole heart RNA-seq analysis detected a strong upregulation of several markers related with inflammatory response in both genotypes at 3 dpi (**Figure R 9**).

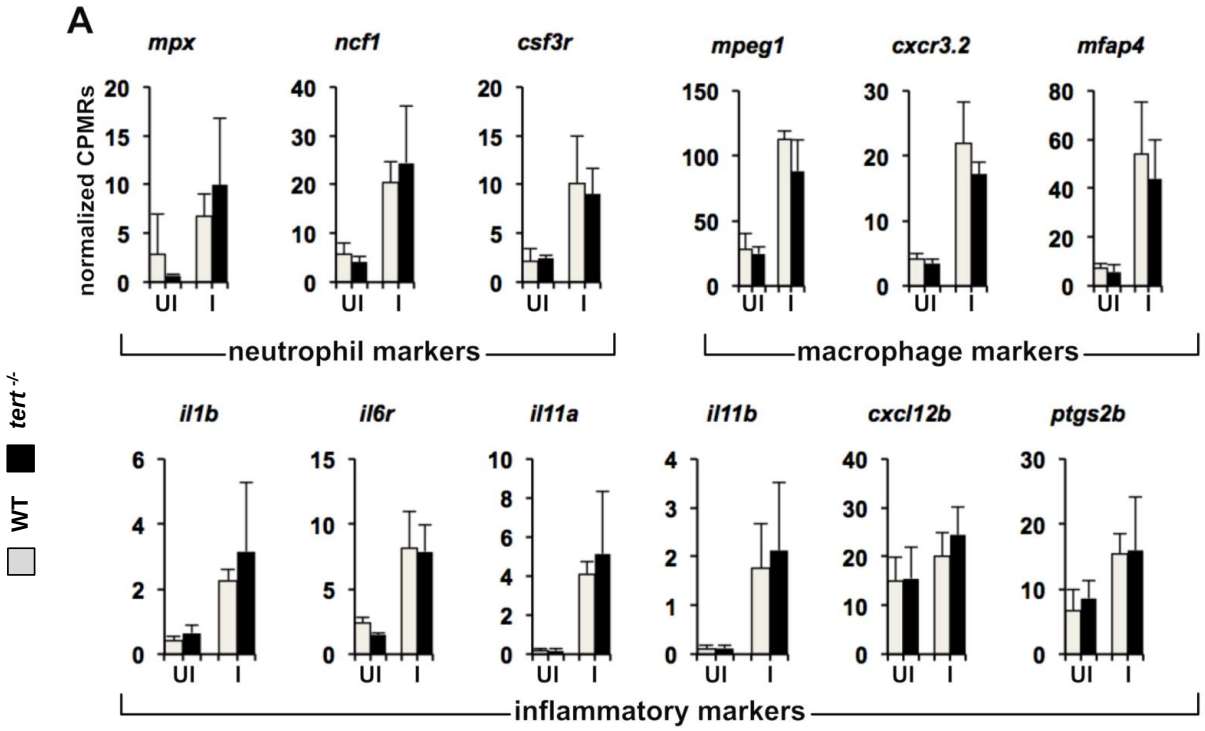

Figure R 9. Inflammatory factors are upregulated during zebrafish heart regeneration. RNA expression of neutrophil, macrophage and inflammatory marker genes in WT and *tert*$^{-/-}$ zebrafish hearts, uninjured or 3 days postinjury (dpi). Injury led to an increase in the expression of the markers analyzed both in WT and *tert*$^{-/-}$ hearts. Differences between WT and *tert*$^{-/-}$ zebrafish hearts are non-significant in all cases (B-H adjusted p-value). CPMRs, counts per million repeats; Data are means ± SEM of values obtained from an RNA-seq experiment of 4 biological replicates, each replicate consisting of 3 pooled hearts. I, injured; UI, uninjured.

We observed striking increases in the expression of inflammatory markers from interleukin family - *il1b, il6r, il11a* or *il11b* as well as the stromal cell-derived factor 1 also known as C-X-C motif chemokine 12 (*cxcl12b)* or prostaglandin-endoperoxide synthase 2b (*ptgs2b*). Neutrophil markers, such as: myeloid-specific peroxidase (*mpx*), neutrophil cytosolic factor 1 (*ncf1*) or granulocyte colony stimulating factor 3 receptor (*csf3r*) and macrophage markers: macrophage expressed *gene* 1 (*mpg1*), C-X-C motif chemokine receptor 3, tandem duplicate 2 (*cxcr3.2*) and microfibrillar-associated protein 4 (*mfap4*) were all upregulated following heart injury. However the expression levels of the genes related with the inflammatory response did not show any significant difference between WT and *tert*$^{-/-}$ zebrafish hearts (**Figure R 9**), suggesting that the injury-induced inflammatory response of WT and *tert*$^{-/-}$ zebrafish is similar.

We compared gene expression profiles by Gene Set Enrichment Analysis (GSEA) to assess the effect of *tert* loss-of-function on a collection of gene sets that represent signaling pathways related to inflammation (Subramanian et al., 2005). Injured heart expression profiles revealed an enrichment of upregulated genes belonging to gene sets related to inflammation, but it was similar in both genotypes (WT, *tert*$^{-/-}$) (**Table R 1**).

customized pathway collection	WT I vs. UI	tert$^{(-/-)}$ I vs. UI	UI tert$^{(-/-)}$vs. WT	I tert$^{(-/-)}$ vs. WT
BioCarta_cytokine_pathway	n.s.	n.s.	n.s.	n.s.
biocarta_inflammation_pathway	n.s.	n.s.	n.s.	n.s.
KEGG_cytokine_cytokine_receptor_ interaction	I	I	n.s.	n.s.
KEGG_jak_stat_signalling_pathway	n.s.	I	n.s.	n.s.
KEGG_t_cell_receptor_signalling pathway	I	I	n.s.	n.s.
Reactome_cytokine_signalling_in_ immune_system	I	I	n.s.	n.s.
Reactome_signaling_by_ils	I	I	n.s.	n.s.

Table R 1. Representative gene sets for signaling pathways related to inflammation in cryoinjured WT and *tert*$^{-/-}$ zebrafish hearts. Bioinformatic analysis of the *tert* loss-of-function zebrafish model on cell inflammation. No significant difference between WT and *tert*$^{-/-}$ hearts in inflammatory response. I, injured; UI, uninjured; n.s., non-significant.

We used L-plastin, a molecular marker of macrophages, to perform immunohistochemistry at 3 dpi (the initial phase of regeneration) and 60 dpi (when the cardiac recovery is in a very

advanced stage) in order to observe injury-induced infiltration of inflammatory macrophages. We found that macrophages were recruited mainly within the wound region, suggesting that these cells represent a population of tissue macrophages that respond to inflammatory stimuli (**Figure R 10A**). However, quantification of L-plastin signal in the injured area and within the border zone did not reveal any significant differences in the level of macrophage infiltration (**Figure R 10B**). These results suggested again that the injury-induced inflammatory response of WT and *tert*$^{-/-}$ zebrafish is similar.

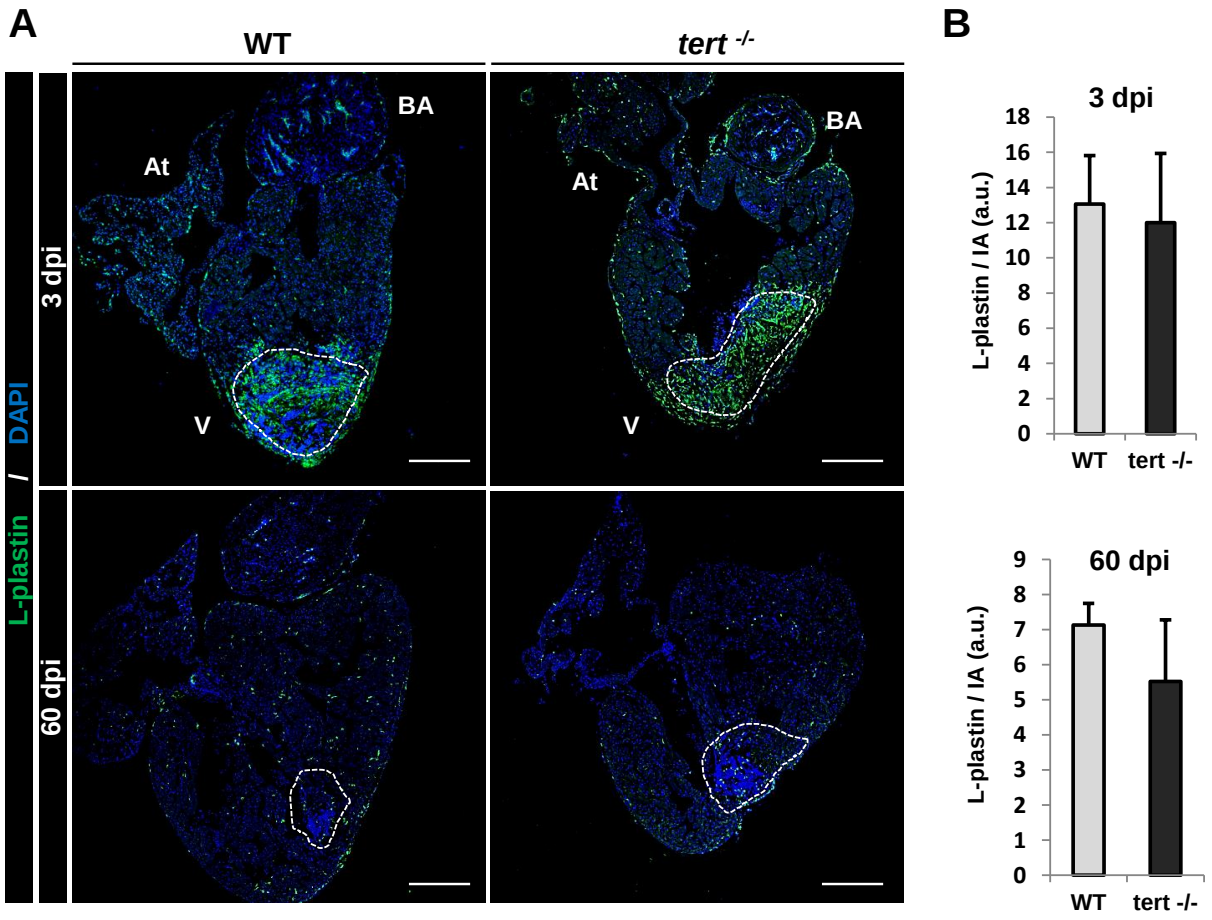

Figure R 10. Injury-induced macrophages infiltration in WT and *tert*$^{-/-}$ zebrafish hearts. (A) Representative immunofluorescence images, showing infiltration of the injured myocardium with macrophages (L-plastin: green signal) on WT and *tert*-/- heart sections. DAPI was used to counterstain nuclei (blue). The injured area is outlined by a dotted line. V, ventricle ; At, atrium; a.u.; BA, bulbus arteriosus; dpi, days postinjury; Scale bars, 100 µm. (B) Quantification of L-plastin positive cells at 3 and 60 dpi show no significant difference between WT and *tert*-/- hearts. Graphs show mean ± SEM L-plastin signal in the injured area (IA) and within 50 µm of the border zone on sections from 3 hearts per condition. dpi, days postinjury; a.u., arbitrary units.

6. The early injury responses of the epicardium and endocardium are not affected by the absence of telomerase.

Responses to injury in zebrafish hearts are initiated in an organ-wide manner before being confined to the wound region (Kikuchi et al., 2011; Lepilina et al., 2006). Injury-induced dedifferentiation and subsequent proliferation of pre-existing cardiomyocytes, that give a rise to a newly regenerated cardiac muscle, is preceded by a rapid and organ-wide activation of the endocardium and epicardium (Kikuchi et al., 2011; Lepilina et al., 2006). Within the first couple of hours of injury, endocardial cells in the whole heart change morphology, adapt a rounded shape, detach from myocardial cells and induce the expression of developmental marker genes, including *aldh1a2* (*aldehyde dehydrogenase 1 family, member A2*) (Kikuchi et al., 2011; Lepilina et al., 2006). Likewise by 3 days post-trauma, the whole epicardium upregulates *aldh1a2* expression. To determine whether the absence of telomerase activity alters the activation of endocardium and epicardium, we analyzed RNA and protein expression of *aldh1a2* (*raldh2*), by *in situ* hybridization (ISH) and immunohistochemistry (IHC) analysis respectively. We found in both, WT and *tert*$^{-/-}$ hearts a similarly strong upregulation of *aldh1a2* RNA and protein in endocardial cells at 6 hours postinjury (hpi) and in endocardial and epicardial cells at 3 dpi (**Figure R 11**).

To confirm these results, we performed RNAseq analysis (**Figure R 12A, B**) and quantitative real-time polymerase chain reaction RT-qPCR (**Figure R 12C**). We observed that *aldh1a2* expression was upregulated by 3 dpi. However no differences of response were observed between WT and *tert*$^{-/-}$ hearts (**Figure R 12A, C**).

We also tested the expression of several other genes inluding, interleukin 11a (*il11a*) in the endocardium and wilms tumor 1b (*wt1b*), T-Box 18 (*tbx18*) *and* fibronectin 1 (*fn1*) in the epicardium. All were upregulated at 3 dpi although differences between WT and *tert*$^{-/-}$ zebrafish hearts were non-significant in all the cases (**Figure R 12A**). In addition, we tested the expression of early embryonic genes encoding activators of the myocardial differentiation program: NK2 Homeobox 5 (*nkx2.5*), GATA binding protein 4 (*gata4*), T-Box 20 (*tbx20*), Heart And Neural Crest Derivatives Expressed 2 (*hand2*) and T-Box 5 (*tbx5*). Interestingly, we found their injury-induced expression to be downregulated although differences were similar in either genotype

(WT, *tert*$^{-/-}$) (**Figure R 12B**). These data were further corroborated by RT-qPCR (**Figure R 12C**).

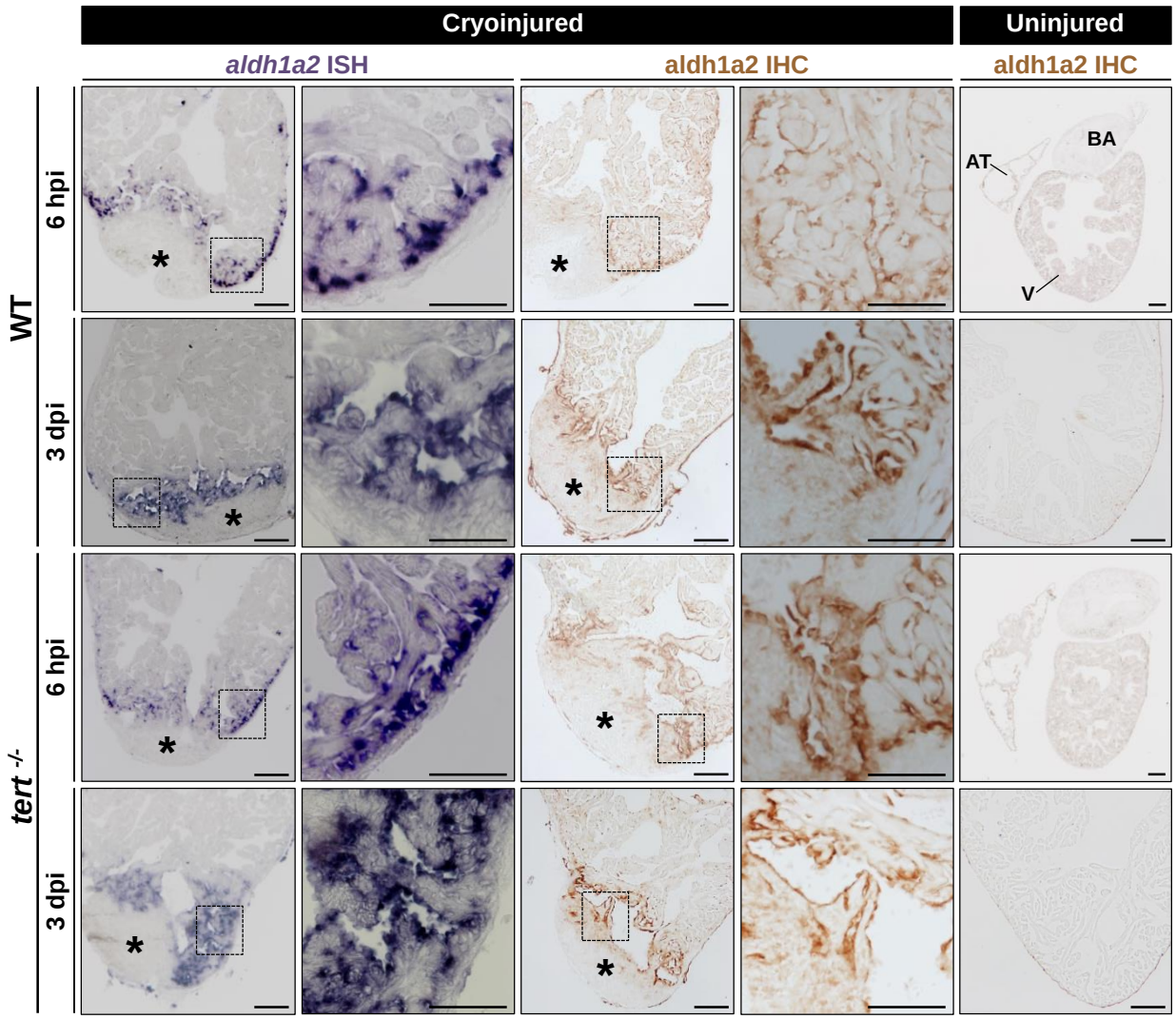

Figure R 11. Early activation of epicardial and endocardial genes is unaffected in the absence of telomerase. Representative images of *aldh1a2* RNA and protein expression detected by *in situ hybridization* (ISH) and immunohistochemistry (IHC) in the endocardium and the epicardium at the indicated times postinjury in WT and *tert*$^{-/-}$zebrafish hearts. IHC on uninjured heart sections are shown for comparison. A total of n=4 hearts were analyzed per condition, with a minimum of 3 analyzed sections per heart. Asterisks mark the injured region. Boxed areas are shown at higher magnification. V, ventricle; At, atrium; BA, bulbus arteriosus; dpi, days postinjury; hpi, hours postinjury. Scale bars: 100 μm for general views and 50 μm for zoomed views.

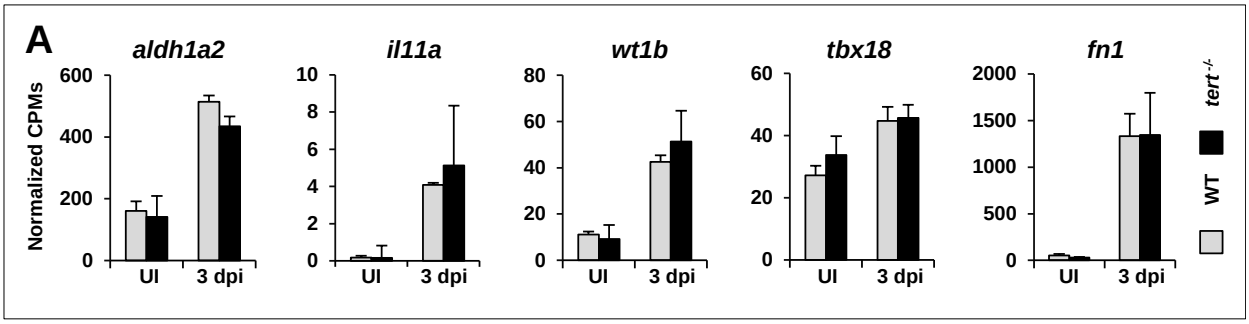
A
aldh1a2
il11a
wt1b
tbx18
fn1
Normalized CPMs
UI
3 dpi
WT
tert -/-

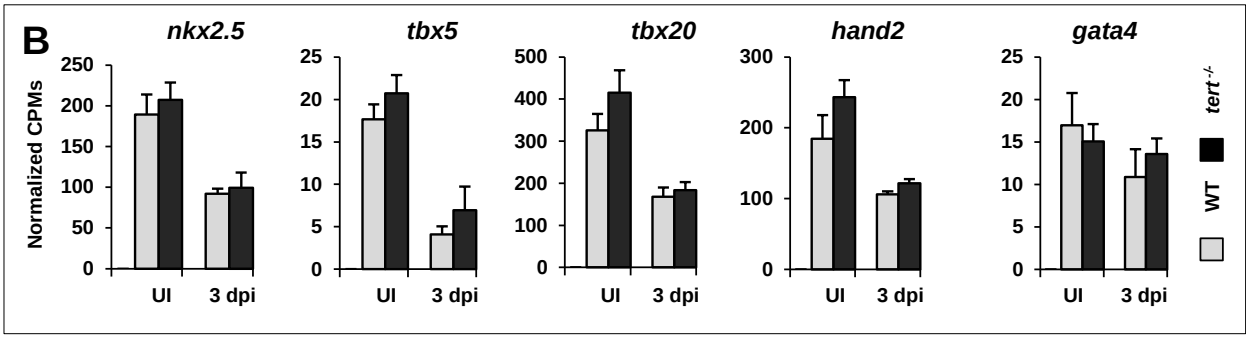
B
nkx2.5
tbx5
tbx20
hand2
gata4
Normalized CPMs
UI
3 dpi
WT
tert -/-

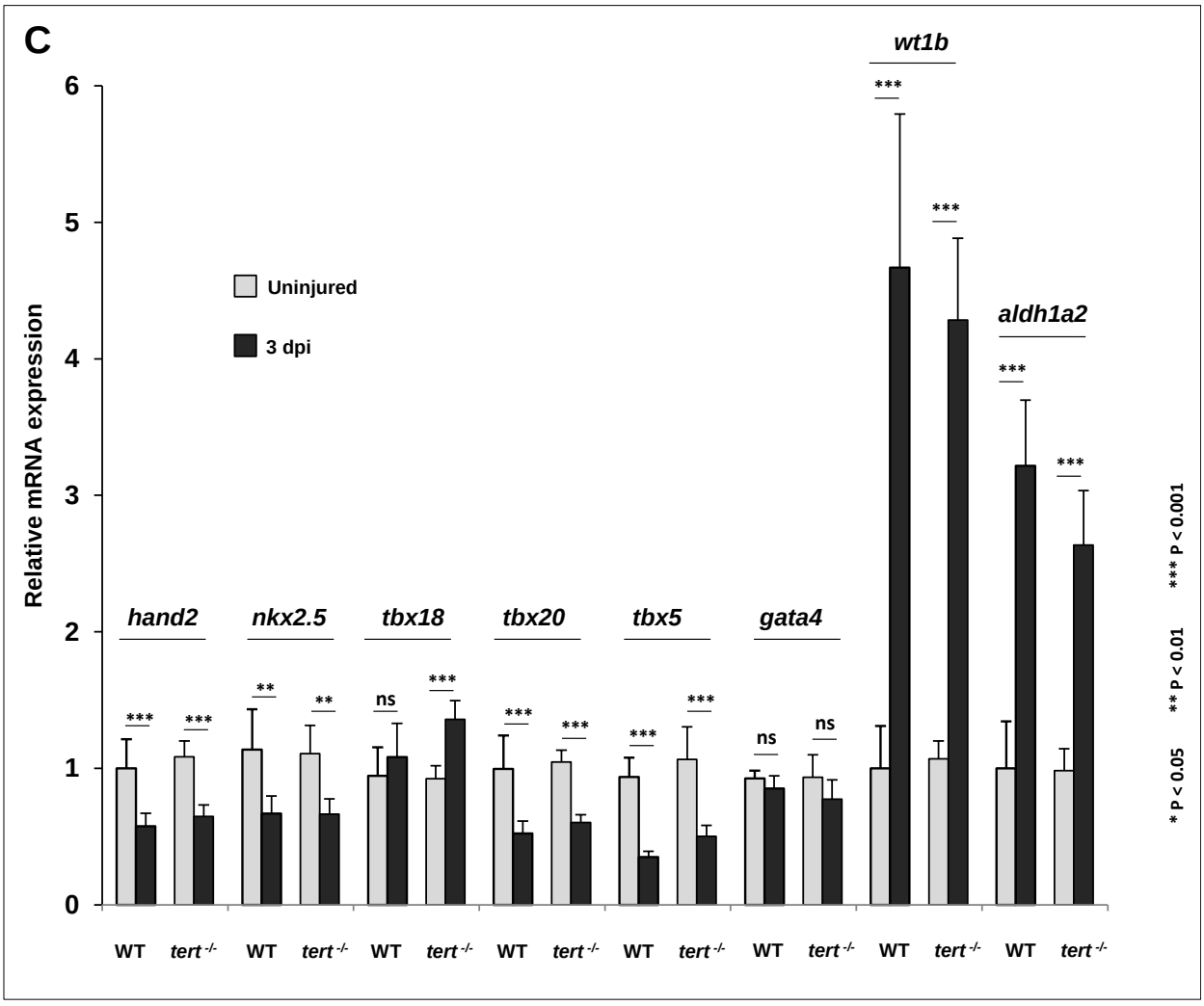
C
Relative mRNA expression
Uninjured
3 dpi
hand2
nkx2.5
tbx18
tbx20
tbx5
gata4
wt1b
aldh1a2
WT
tert -/-
* P < 0.05
** P < 0.01
*** P < 0.001

Figure R 12. Cardiac gene activation induced by heart injury. (A) RNA expression of endocardial genes (*aldh1a2, il11a) and* epicardial genes (*wt1b, tbx18 and* fibronectin) upregulated upon cardiac injury in WT and *tert*$^{-/-}$zebrafish hearts. (B) Injury-induced downregulation of expression of early embryonic myocardial markers (nkx2.5, gata4, tbx20, hand2 or tbx5). Data are means ± SEM of values obtained from an RNA-seq experiment of 4 biological replicates, each replicate consisting of a pool of 3 hearts. Differences between WT and *tert*$^{-/-}$zebrafish hearts are non-significant in all cases *(*B-H adjusted p-value). CPM, counts per million; dpi, days postinjury; UI, uninjured. (C) Quantitative real-time polymerase chain reaction (RT-qPCR) analysis of gene expression in WT and *tert*$^{-/-}$ uninjured hearts and hearts at 3 dpi. The RT-qPCR data for all genes was normalized with *EF1* as reference gene. Data are means ± SEM of values obtained from 4 biological replicates, each replicate consisting of a pool of 3 hearts. *, $p<0.05$; **, $p<0.01$; ***, $p<0.001$; ns, not significant (Mann-Whitney test). dpi, days postinjury.

Our results suggest that a paracrine-like contribution from both the endocardium and epicardium to promote cardiomyocytes proliferation and heart regeneration is not dependent on telomerase activity.

7. Cardiomyocyte dedifferentiation proceeds normally in the absence of telomerase

In response to injury zebrafish cardiomyocytes reduce their contractile state, their sarcomeres disassemble, mitochondria swell and cellular attachments loosen (Jopling et al., 2010; Kikuchi et al., 2010). Dedifferentiation is a cellular process characterized by reversion of specialized, terminally differentiated, mature cells to an earlier developmental stage in response to a stimulus or stress. Dedifferentiation occurs in cardiomyocytes with concomitant re-expression of fetal gene markers and reduction of sarcomere structures, which facilitate cell division. To determine whether these signs of cardiomyocyte dedifferentiation are affected by the loss of telomerase, we analyzed cardiomyocyte ultrastructural features at 3 dpi by transmission electron microscopy. At 3 days post trauma in the injured WT and *tert*$^{-/-}$ zebrafish hearts sarcomeric structure remained organized in the remote area of the heart and mitochondria appeared normal, did not present any dysmorphic features (**Figure R 13, left panel**). In addition, sarcomere disassembly with concomitant mitochondrial swelling and dysmorphia was detected to a similar

extent in both, WT and *tert*$^{-/-}$ cardiomyocytes close to the injury site (**Figure R 13, right panel**), indicating that cardiomyocytes dedifferentiation is unaffected in the absence of telomerase.

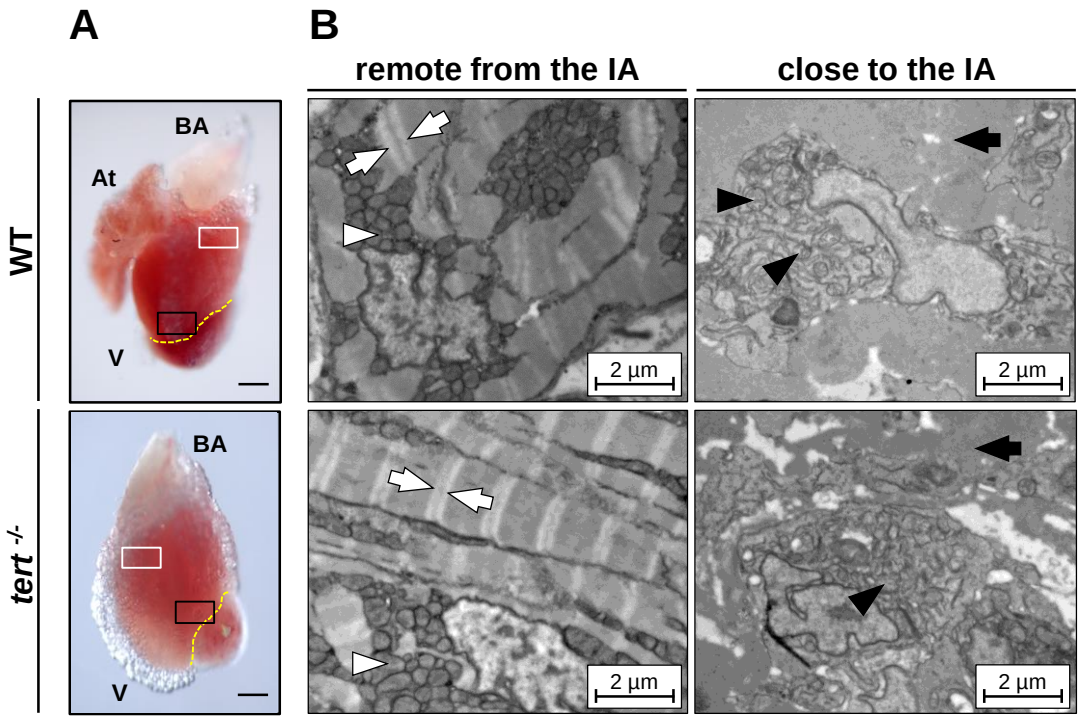

Figure R 13. Cardiomyocytes dedifferentiation is unaffected in the absence of telomerase. (A) Whole-mount views of WT and *tert*$^{-/-}$ zebrafish hearts. Yellow dashed line indicates injury area (IA); black box indicate region close to the IA; white box indicate region remote from the IA. V, ventricle; At, atrium; BA, bulbus arteriosus. Scale bars: 100 µm. (B) Transmission electron micrographs of cardiomyocytes at 3 days post injury. (Left) Representative cardiomyocytes away from the injury site in WT and *tert*$^{-/-}$ hearts, showing ordered sarcomeric fibers with visible Z-lines (white arrows) and perinuclear mitochondria with typical structure (white arrowheads). (Right) Representative cardiomyocytes close to the injury site, showing disorganized sarcomeric structure with loss of Z-lines (black arrows) and dysmorphic mitochondria (black arrowheads). IA, injury area. Scale bars: 2 µm.

8. Impaired proliferation response in the absence of telomerase leads to cardiac regeneration failure

The regenerative process in zebrafish heart is activated by an injury stimulus, inducing cardiomyocytes proliferation that is a primary cellular source for regenerating myocardium. The

prevailing model for myocardial regeneration is that in response to injury, existing cardiomyocytes dedifferentiate to acquire an immature form in which cell division is facilitated (Jopling et al., 2010; Kikuchi et al., 2010). We demonstrated that dedifferentiation of the WT and *tert*$^{-/-}$ cardiomyoytes proceeds normally implying that *tert*$^{-/-}$ cardiac myocytes can proliferate. To study the proliferation response in WT and *tert*$^{-/-}$ animals, we first examined the percentage of cardiac cells positive for proliferating cell nuclear antigen (PCNA), a marker of cells in S-phase (**Figure R 14A**).

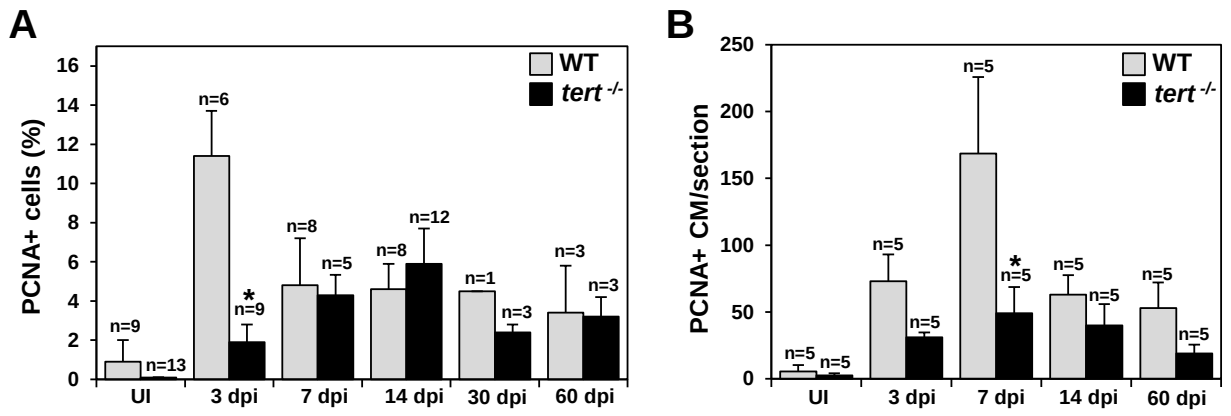

Figure R 14. The absence of telomerase severely reduces proliferation. (A) Cardiac cells positive for proliferative cell nuclear antigen (PCNA) in uninjured (UI) WT and *tert*$^{-/-}$ zebrafish hearts and in hearts at the indicated days after cryoinjury. (A) PCNA+ total cardiac cells. (B) PCNA+ cardiomyocytes. Data are means ± SEM of the percentage of PCNA+ cells (A) or number of PCNA+ cardiomyocytes (B) per cardiac ventricle section (at least 3 sections per animal from the indicated number of animals). *, $p<0.05$ compared with WT samples (Mann- Whitney test). CM, cardiomyocytes; dpi, days postinjury.

A sharp peak in proliferation occurred at 3 dpi in WT hearts, affecting ~11% of total cardiac cells (**Figure R 14A**). We observed a global injury-induced increase in proliferation of epicardial, endocardial and myocardial cells. We found a slow increase in the percentage of proliferating cells in *tert*$^{-/-}$ hearts during the first 14 days after injury, but its maximum was severely reduced compared to the WT hearts. In the absence of telomerase the peak of proliferation reached a maximum of ~6% of cardiac cells and was delayed until 14 dpi (**Figure R**

14A). The impaired proliferative response was even more pronounced for the cardiomyocyte pool, where the proliferation peak at 7 dpi was 3-fold lower in *tert*$^{-/-}$ hearts (**Figure R 14B**).

We indicated a distribution of proliferating cardiac cells within the myocardium, endocardium and epicardium in WT hearts. To determine the location of dividing cardiomyocytes within the ventricle, we immunostained heart sections with anti-MHC (myosin heavy chain), a specific marker for cardiac myocytes (**Figure R 15, Figure R 16**). We differentiated between endocardial and epicardial cells based on their morphology and location in the heart (**Figure R 15**).

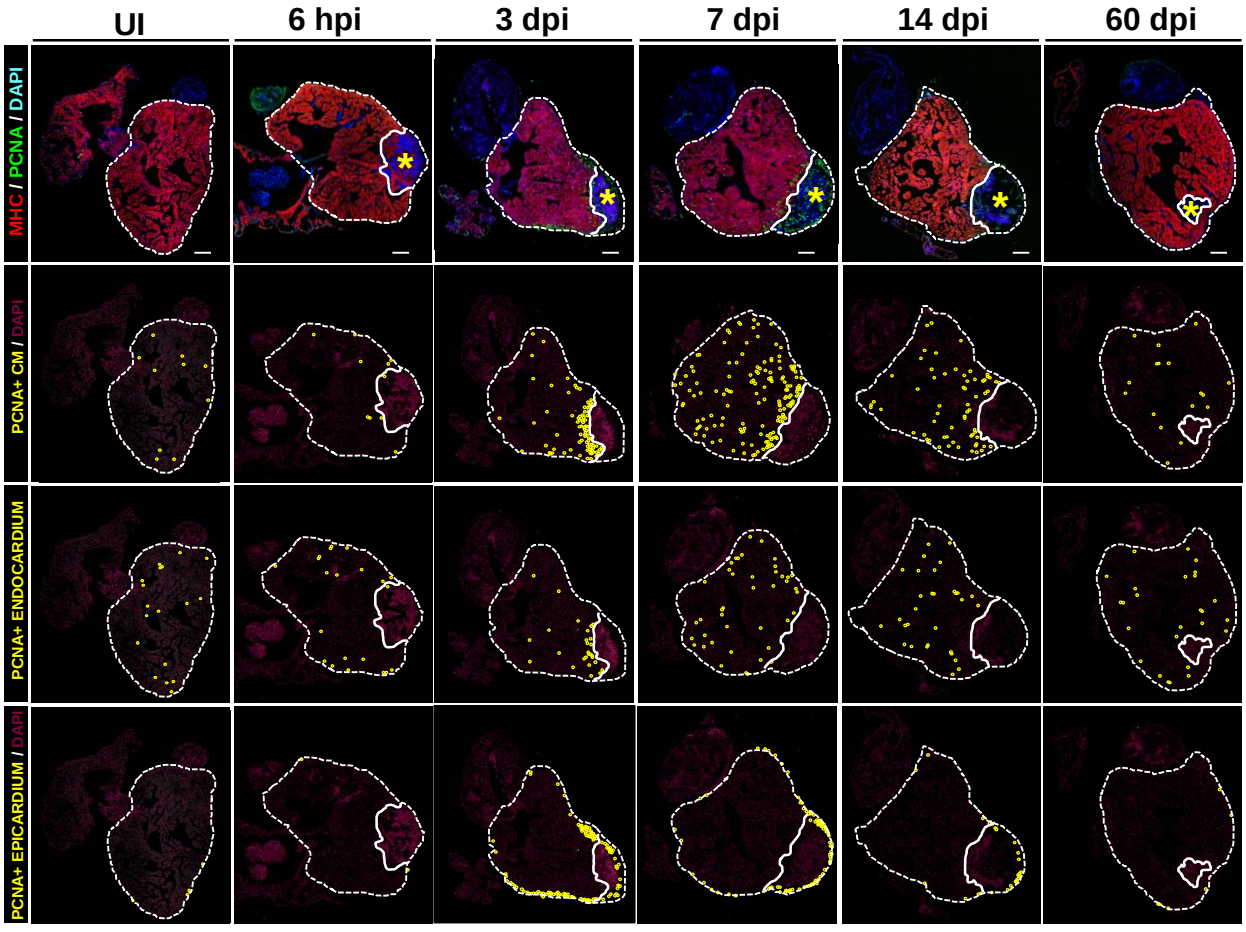

Figure R 15. Injury-induced proliferative response of cardiac cells in WT zebrafish heart. WT heart sections immunostained with anti-myosin heavy chain (MHC) to mark cardiomyocytes (red) and anti-PCNA to mark cells in S-phase (green); nuclei are counterstained with DAPI (blue). The lower rows show the location of PCNA+ cardiomyocytes, endocardial and epicardial cells during regeneration (yellow circles). Nuclear area is shown in magenta. Dotted lines outline the ventricle; white lines indicate injured area; asterisks mark the initial injury site. dpi, days postinjury; hpi; hours postinjury;. Scale bars: 100 μm.

Proliferating cardiomyocytes in WT hearts were found predominantly at the injury borders, but were also detected in the more distal regions. In *tert*$^{-/-}$ hearts, a reduced proliferation response was evident at all stages analyzed both at the injury border zone and within the rest of the ventricle (**Figure R 16**).

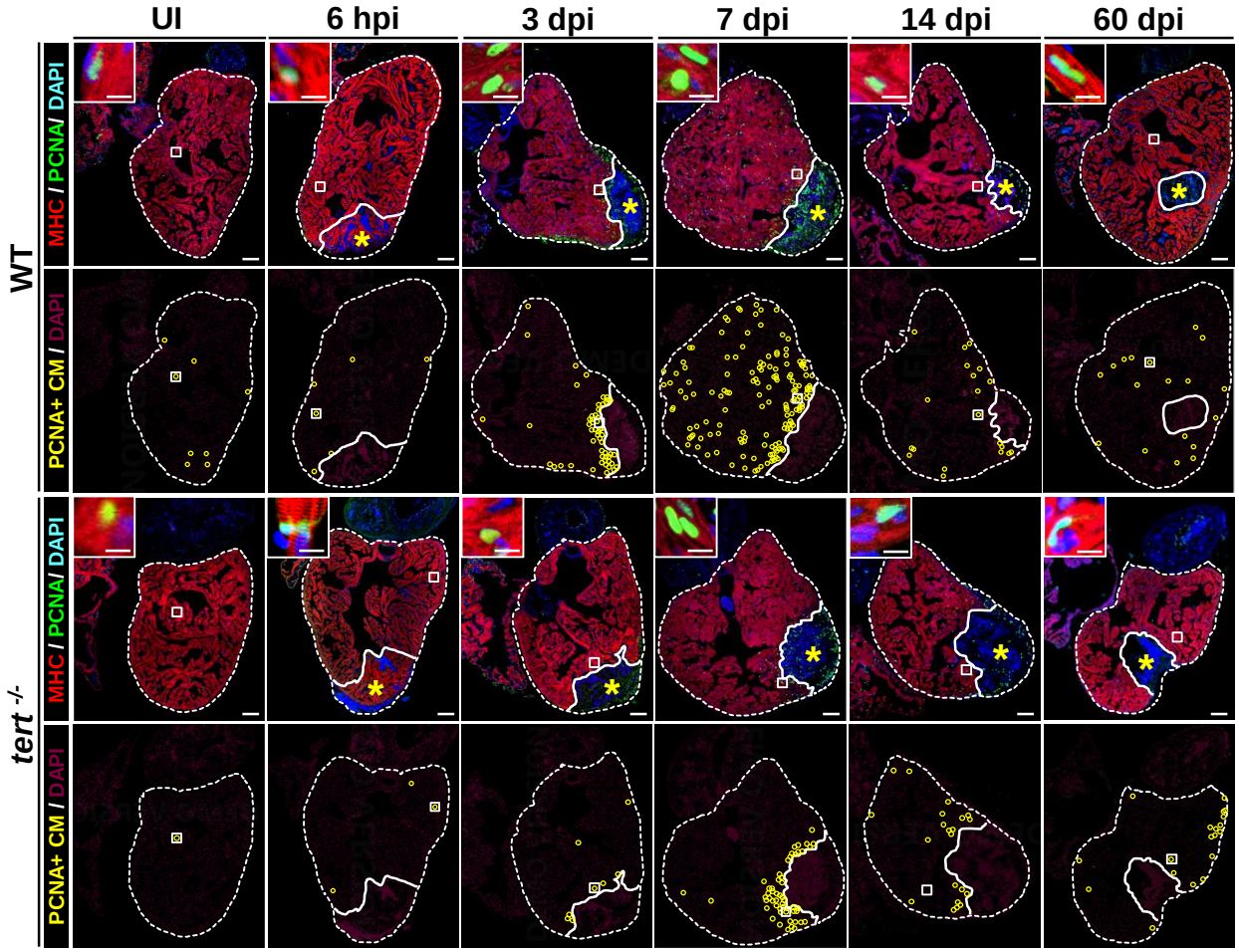

Figure R 16. Location of proliferating cardiomyocytes within the heart ventricle during regeneration. WT and *tert*$^{-/-}$ heart sections immunostained with anti-myosin heavy chain (MHC) to mark cardiomyocytes (red) and anti-PCNA to mark cells in S-phase (green); nuclei are counterstained with DAPI (blue). The lower rows show the location of PCNA+ cardiomyocytes during regeneration (yellow circles). Nuclear area is shown in magenta. Dotted lines outline the ventricle; white lines indicate injured area; asterisks mark the initial injury site. Inset panels show high-magnification views of representative PCNA+ cardiomyocytes in the boxed areas. dpi, days postinjury; hpi; hours postinjury;. Scale bars: 100 μm (whole mount views), 10 μm (magnifications).

To further characterize the impaired proliferative capacity of *tert*$^{-/-}$ regenerating hearts, we injected WT and *tert*$^{-/-}$ hearts with bromodeoxyuridine (BrdU) 3 and 7 dpi and collected hearts at 7 and 14 dpi respectively. To assess DNA synthesis we stained sections with antibodies against BrdU and the mitosis marker phosphorylated histone H3 (pH3) (**Figure R 17**). For both stainings

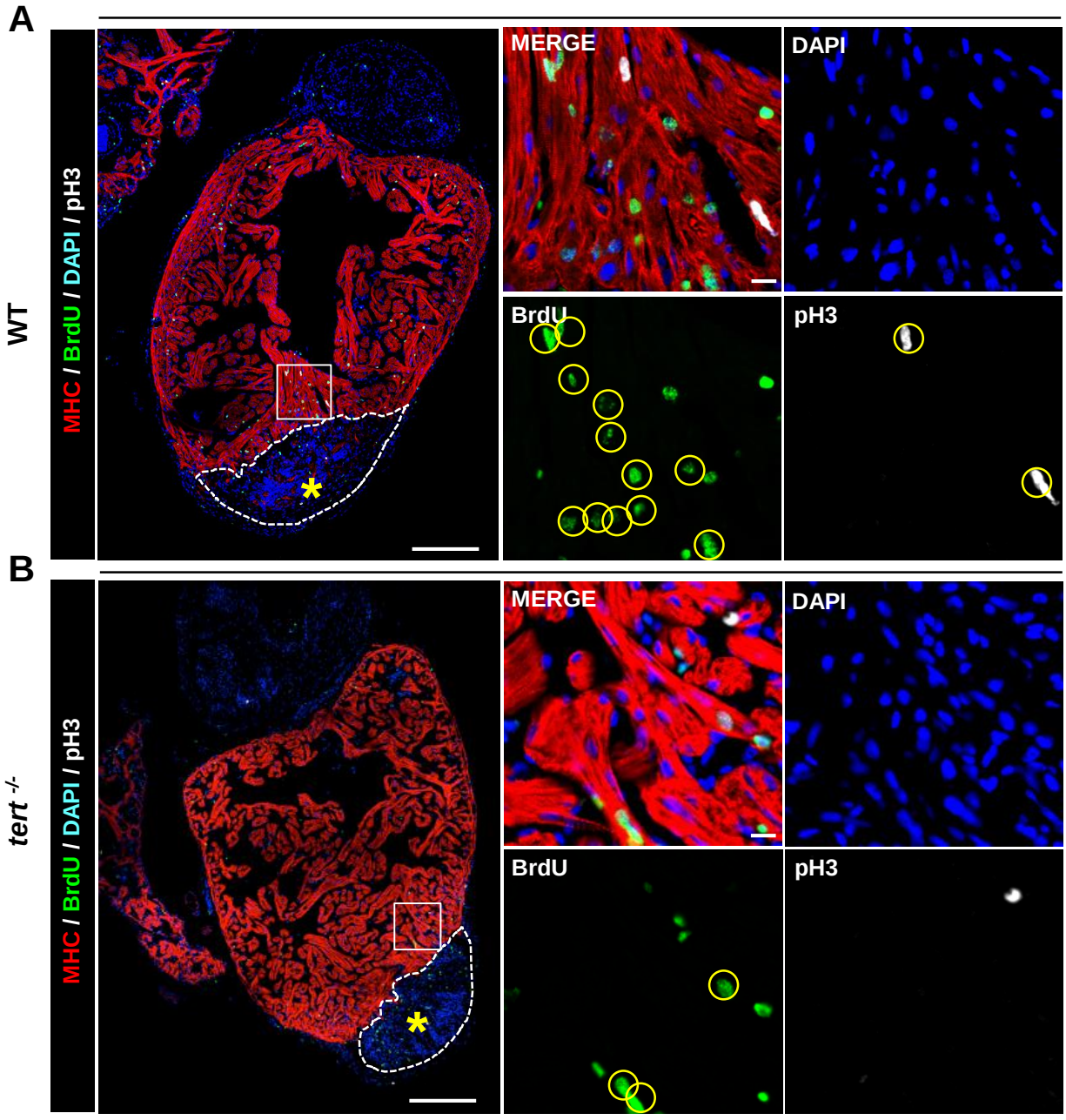

Figure R 17. Cardiomyocyte expansion during zebrafish heart regeneration. (A, B) Immunofluorescence staining on WT (A) and *tert*$^{-/-}$ (B) hearts with anti-myosin heavy chain (MHC, red), anti-BrDU (green) and anti-phospho histone 3 (pH3, white). Nuclei are counterstained with

DAPI. Boxed areas are shown at higher magnification; yellow circles highlight BrdU/MHC and pH3/MHC double positive cardiomyocytes. Note that fewer pH3 and BrdU-positive cardiomyocytes are found in the *tert*$^{-/-}$ heart. Scale bars: 100 µm (whole section views), 10 µm (magnifications).

in *tert*$^{-/-}$ hearts we observed large reductions in the number of cycling cardiac cells in general but in cardiomyocytes in particular (**Figure R 18A**). Further quantification of BrdU positive cells both in the entire cardiac cell population and in cardiomyocytes, indicated at least 3-fold fewer number of cycling cells, found in the *tert*$^{-/-}$ hearts (**Figure R 18B**). The pH3 marker revealed an even greater mean reduction in the number of proliferating cells (**Figure R 18C**).

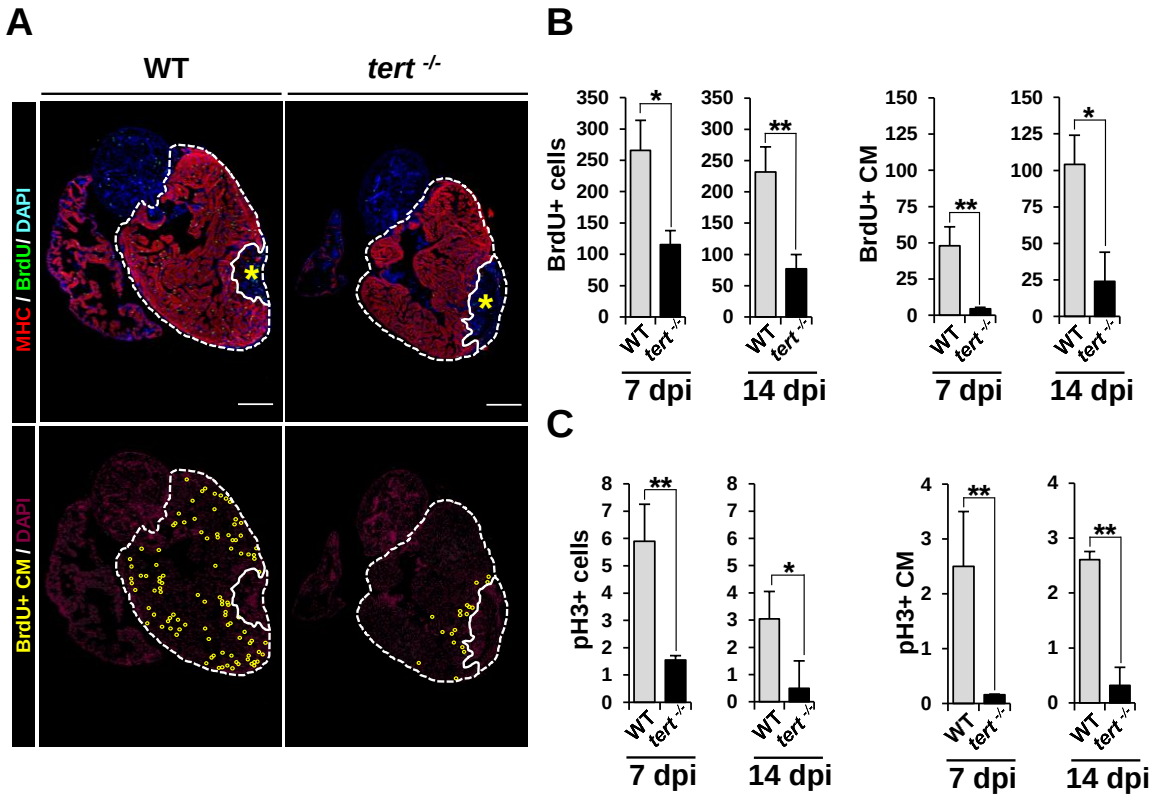

Figure R 18. *tert* loss of function leads to reduced proliferation. (A) WT and *tert*$^{-/-}$ heart sections immunostained with anti-myosin heavy chain (MHC) to mark cardiomyocytes (red) and anti-BrdU to mark cells in S-phase (green); nuclei are counterstained with DAPI (blue). The lower row shows the location of BrdU+ cardiomyocytes during regeneration (yellow circles). Nuclear area is shown in magenta. Dotted lines outline the ventricle; white lines indicate injured area; asterisks mark the initial injury site. (C, D) Quantification of pH3+ and BrdU-labeled cardiac cells and cardiomyocytes at 7 and 14 dpi. Data are means ± SEM. *, $p<0.05$; **, $p<0.01$. (unpaired Student's t-test).

Whole heart RNA-seq analysis detected that the expression of genes associated with proliferation - cyclins, cdks, replication licensing factors and processivity factors implicated in a proliferation response – at 3 dpi was lower in *tert*$^{-/-}$ hearts compared to WT (**Figure R 19**).

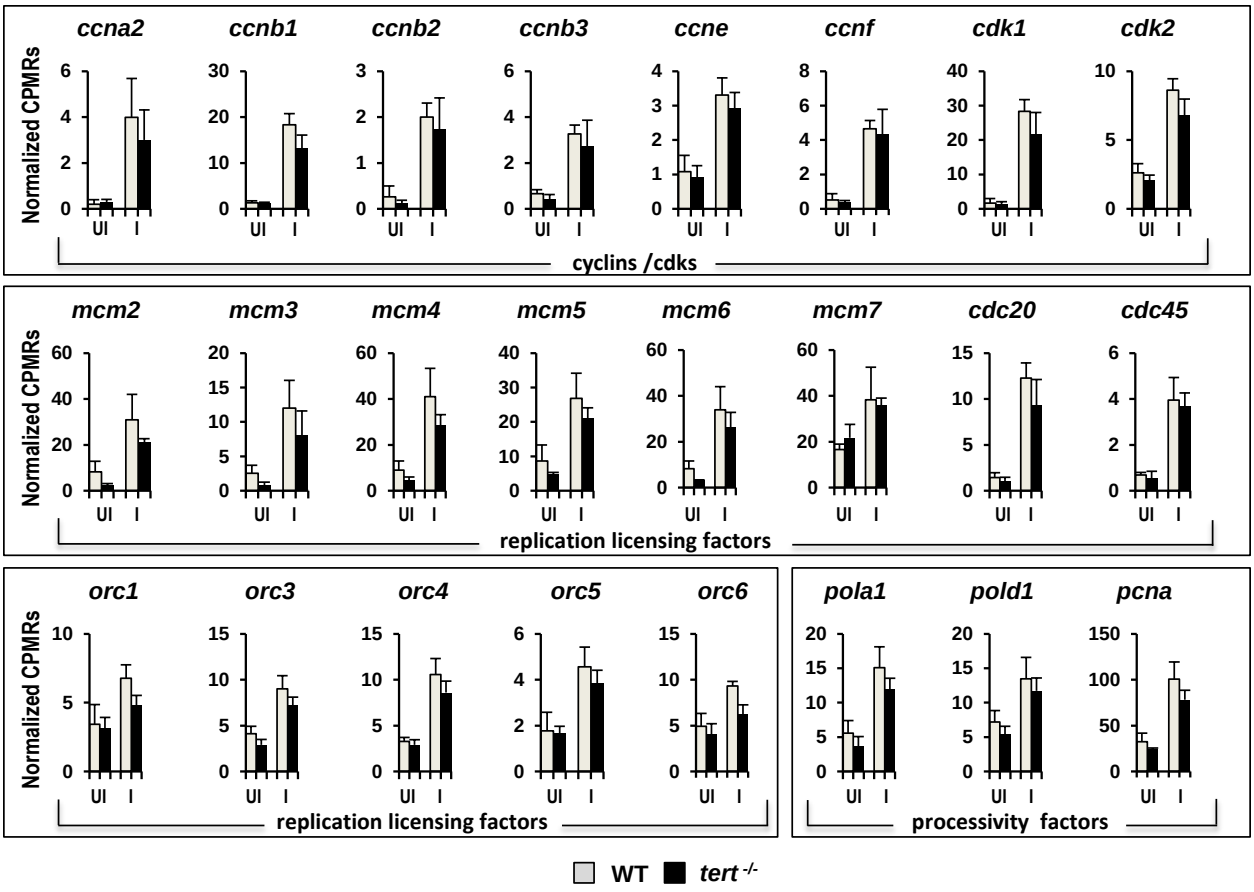

Figure R 19. Proliferation-related factors are upregulated during zebrafish heart regeneration. RNA expression of cyclins, cdks, replication licensing factors and processivity factors implicated in a proliferation response at 3 dpi in WT and *tert*$^{-/-}$ hearts. Data are means ± SEM of values obtained from an RNA-seq experiment of 4 biological replicates, each replicate consisting of 3 pooled hearts. CPM, counts per million; dpi, days postinjury. *p<0.05, ** p<0.01, *** p<0.001 (Benjamini-Hochberg adjusted p-values).

Moreover we performed Gene Set Enrichment Analysis (GSEA) and confirmed that cell-proliferation-associated pathways were significantly downregulated in *tert*$^{-/-}$ hearts compared to WT (**Table R 2**).

customized pathway collection	WT I vs. UI	tert$^{(-/-)}$ I vs. UI	UI tert$^{(-/-)}$vs. WT	I tert$^{(-/-)}$ vs. WT
BioCarta_cellcycle_pathway	I	I	n.s.	WT
KEGG_cell_cycle	I	I	WT	WT
Reactome_cell_cycle_checkpoints	I	I	WT	n.s.
Reactome_cell_cycle_mitotic	I	I	WT	WT
Reactome_ cell_cycle	I	I	WT	WT
Reactome_regulation_of_mitotic_ cell_cycle	I	I	n.s.	n.s.

Table R 2. Heart injury leads to upregulation of cell-proliferation-associated pathways in zebrafish. Bioinformatic analysis of the *tert* loss-of-function on cell proliferation. Upregulation of cell-proliferation-associated pathways upon heart injury. WT injured hearts show significant difference in upregulation levels comparing with *tert*$^{-/-}$ hearts in most of the pathways. UI, uninjured; I, 3 dpi; n.s. not significant.

Our results suggest that in absence of telomerase activity proliferation is impaired and consequently the regeneration process cannot proceed normally.

9. *tert* silencing in the injured hearts inhibits the proliferative response of cardiac cells

We used antisense Morpholino (MO)-mediated knockdown technology as a temporal and spatially-restricted approach to dissect the effect of *tert* on cardiac cell proliferation during zebrafish heart regeneration. Next to the use of mutant lines this constitutes the most common approach to analyze gene function in zebrafish (Stainier et al., 2015). Two different MOs were used: *tert* vivo-MO (Imamura et al., 2008) and *gfp* vivo-MO (Huang et al., 2003). First the efficiency of the MOs was measured by TRAP assay. As expected, we found that *tert* silencing led to a significant downregulation of telomerase activity in *tert* vivoMO treated hearts at 3 days postinjury (**Figure R 20A**). We established an *ex vivo* culture system to determine the effects of the morpholinos. After culture *ex vivo* for 3 days, untreated injured hearts contained PCNA-positive cardiac cells, including cardiomyocytes, at the periphery of the heart ventricles. However, we found that *tert* vivo MO administration during *ex vivo* culture inhibits cardiac cells proliferation (**Figure R 20B, Figure R 20C**). These results further suggest that *tert* has a critical role in promoting cardiac cell proliferation in regenerating heart.

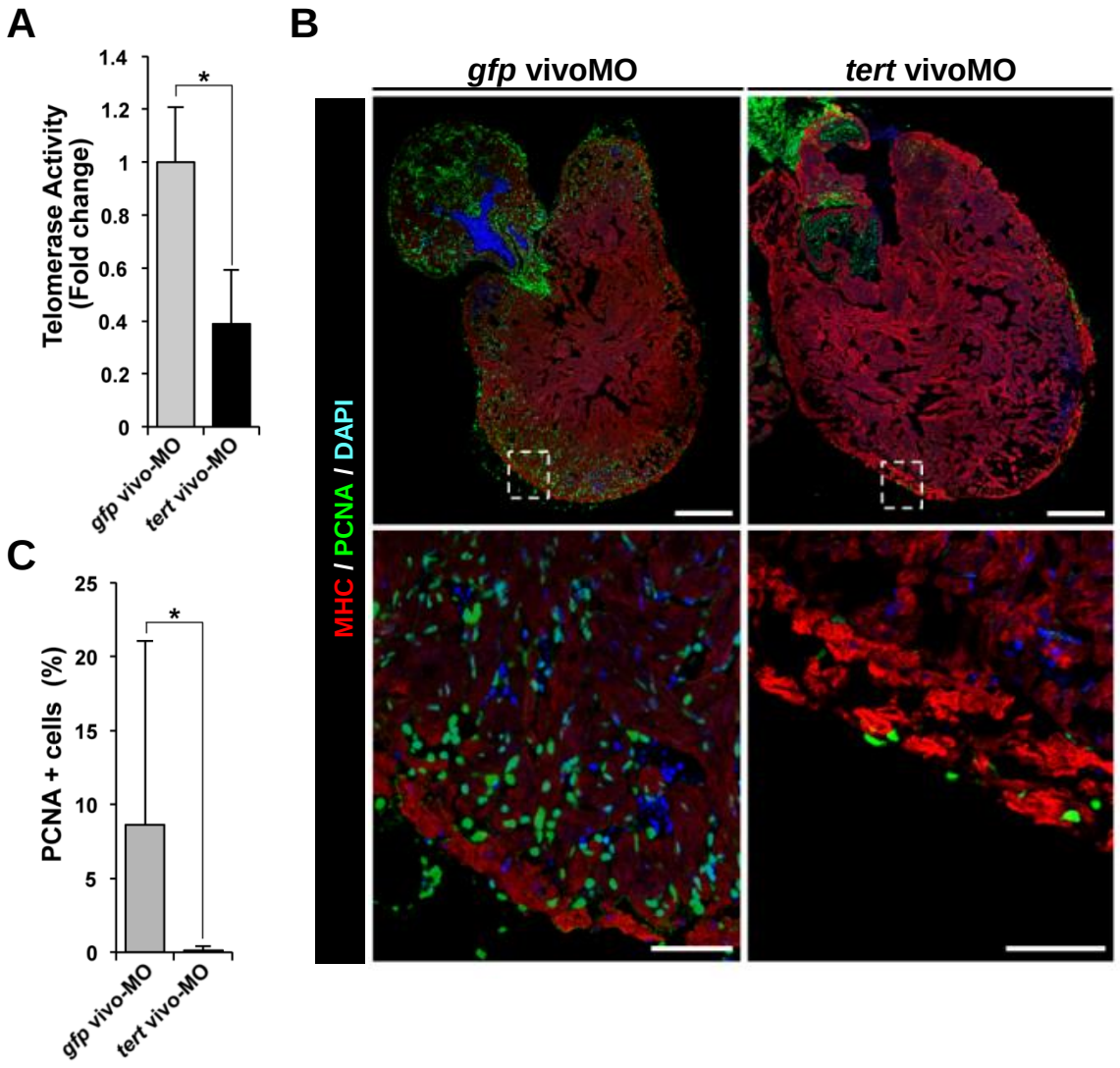

Figure R 20. *tert* silencing in the injured hearts inhibits the proliferative response of cardiac cells. (A) *tert* activity assay in stab-injured hearts cultured for 3 days in the presence of 10 μM *gfp vivo* Morpholino or *tert vivo* Morpholino. Data are means ± SD from 2 pools of 3 hearts per condition ($p<0.05$, unpaired Student's t-test). A second experiment using 2 additional control and *tert* vivoMO replicates at 15 μM (3 pooled hearts per replicate) yielded the same result (data not shown). (B) Immunfluorescence analysis of *gfp* and *tert* vivoMO-treated hearts. Stab-injured hearts were immunostained for PCNA (green) and myosin heavy chain (MHC, red), and nuclei were counterstained with DAPI (blue). Boxed areas are shown at higher magnification in the lower panels. Bars, 200 μm (whole section images) 50 μm (zoomed views). (C) Quantification of the percentage of PCNA-positive cells per total cell nuclei in hearts treated with *gfp* or *tert* vivoMO. Data are means ± SD from 4-5 hearts per condition ($p<0.05$, unpaired Student's t-test).

10. Injury-induced telomerase hyperactivation triggers the global transient telomere elongation in WT hearts

We next investigated how telomerase influences proliferation. Since the canonical function of telomerase is to lengthen telomeres, and long telomeres provide proliferation potential, we conducted a telomapping assay to determine whether telomerase hyperactivation leads to changes in telomere length during heart regeneration (Flores et al., 2008). The average telomere length of cells in injured WT hearts increased globally, affecting cells from the entire section (**Figure R 21**).

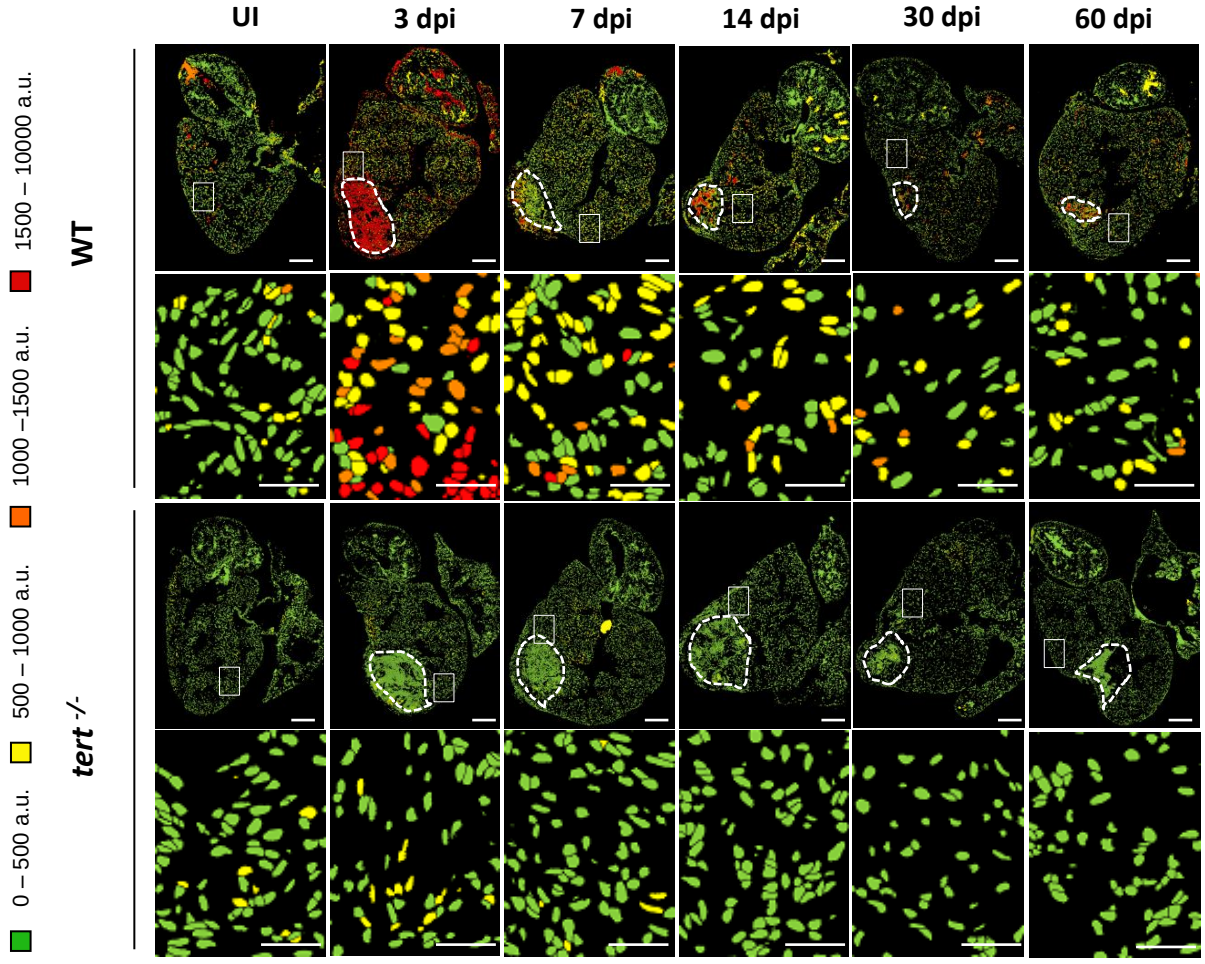

Figure R 21. Heart cryoinjury induces a telomerase-dependent increase in telomere reserves. Representative telomap images of sections of uninjured WT and *tert*$^{-/-}$ hearts and at the indicated days after cryoinjury. In the telomap images, each nuclei is assigned to a proper color from the four-color

code, according to its average telomere fluorescence in a.u. The cells with the longest telomeres are visualized in red, and the cells with the shortest telomeres are presented in green. Note in WT hearts the injury-induced global transient increase in the number of cells with long telomeres, peaking 3 dpi and followed by subsequent gradual decrease. This response is not present in *tert*$^{-/-}$ hearts. Dotted lines mark the injured area. The second and fourth rows show higher magnifications of the box area highlighted in the entire heart section images. Scale bars 100 μm for entire sections and 50 μm for magnifications. UI, uninjured; dpi, days postinjury; a.u., arbitrary units.

Quantification of the average telomere length in each cell on sections of whole WT heart showed that cardiac telomeres transiently elongate during heart regeneration, with a lengthening peak at 3 dpi (**Figure R 22**). We focused on the injury-induced telomere dynamics exclusively for the cardiac cell population by excluding cells found in the injury site. To this end we measured telomere fluorescence frequency of cardiac WT and *tert*$^{-/-}$ cells in uninjured hearts and hearts at 3, 7, 14, 30, and 60 days after injury. At 3 dpi we observed that the increase in the number of nuclei with long telomeres in WT hearts was followed by subsequent gradual decrease of telomere length at the later time points. In contrast, telomere length in *tert*$^{-/-}$ hearts decreased at 3 dpi. At 60 dpi the average length of the telomeres reached half of the value observed in uninjured fish (**Figure R 22**).

Substantial telomere lengthening was detected not only in the cardiac cells population but in non-cardiac cell types as well. Telomere elongation was especially evident in cells that had accumulated within the wound region in WT hearts at 3 dpi (**Figure 21)**. Because cardiac muscle damage triggered a rapid infiltration of the injury site by inflammatory and other circulating cells (Frangogiannis, 2014), we performed telomere analysis on blood samples collected from the dorsal aorta from uninjured and at 3 days post heart injury WT and *tert*$^{-/-}$ zebrafish. There was a significant increase of telomere length in blood samples obtained from the WT zebrafish animals at 3 dpi in contrast to those obtained from *tert*$^{-/-}$ siblings (**Figure R 23**). This suggests that *tert* ablation affects both cardiac and non-cardiac cells in response to the heart injury.

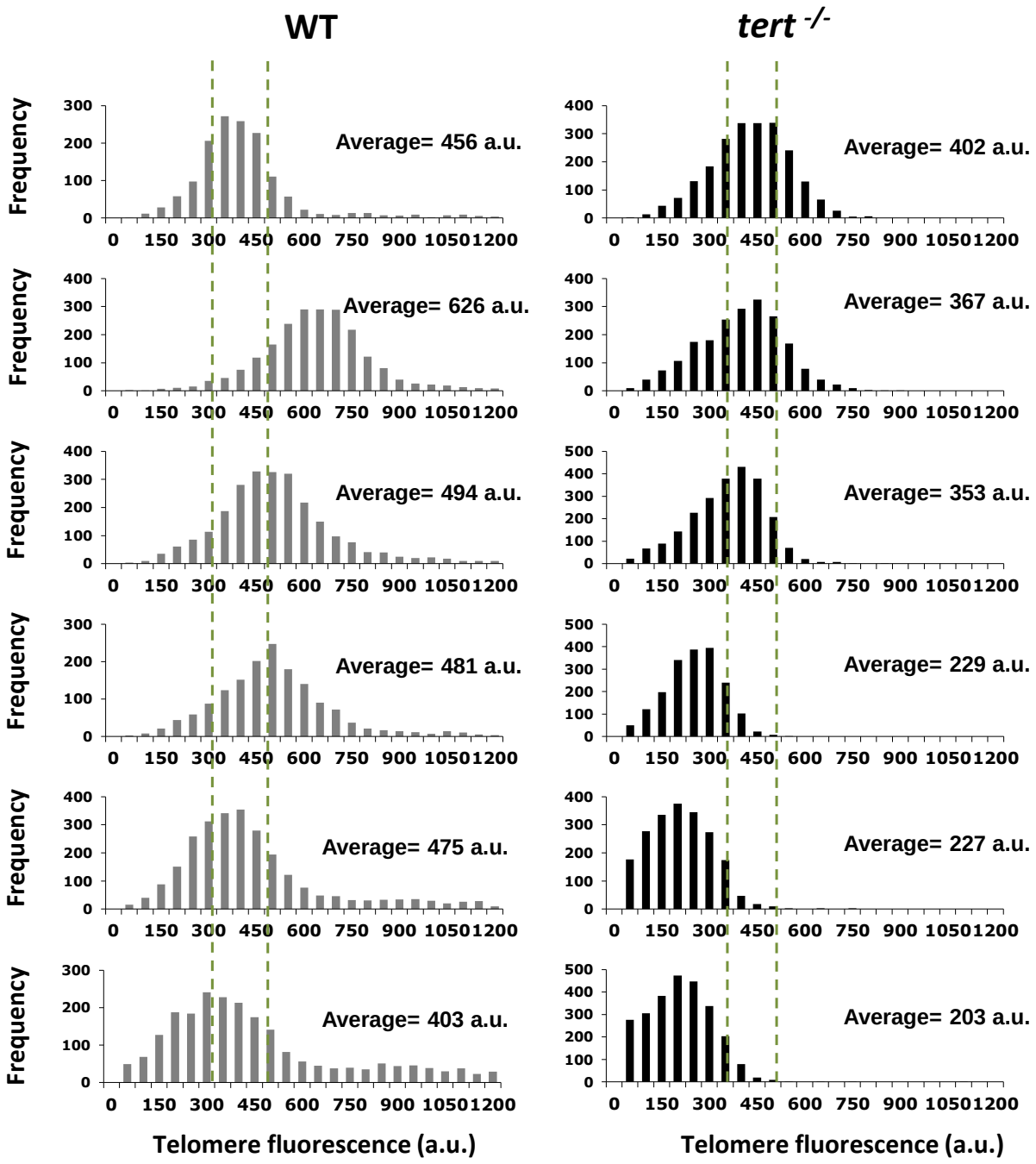

Figure R 22. Transient injury-induced telomere elongation in WT zebrafish hearts. Telomere fluorescence frequency histograms of cardiac WT and *tert*$^{-/-}$ cells in uninjured hearts and hearts at 3, 7, 14, 30 and 60 days after cryoinjury. Mean telomere fluorescence is indicated in arbitrary units (a.u.). The injury site was excluded from the analysis. Note the increase in the number of cells with long telomeres at 3 dpi in WT hearts, followed by reestablishment of the initial profile. This response is lacking in *tert*$^{-/-}$ cells, and at later stages cells have shorter telomeres than initially.

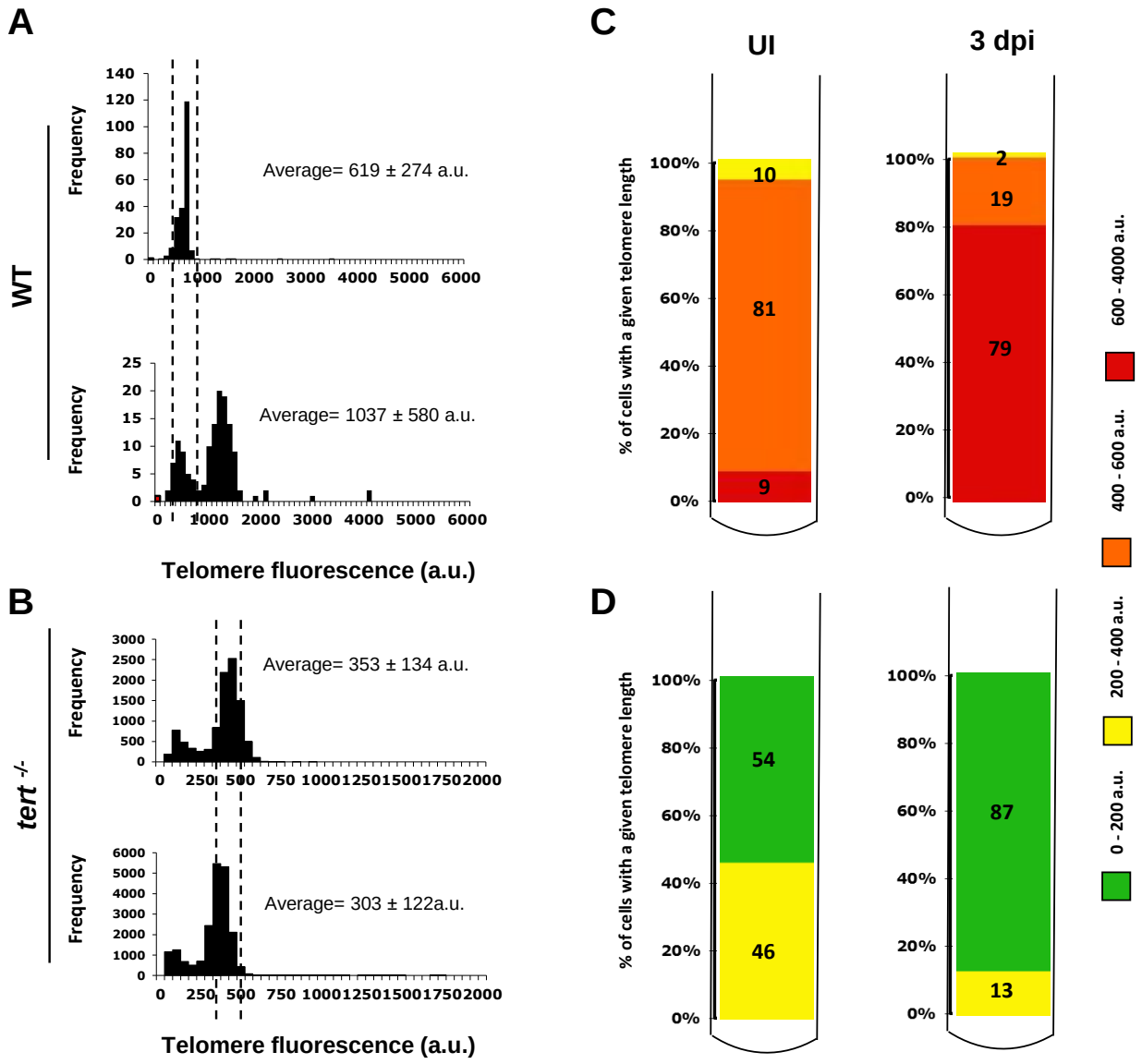

Figure R 23. Injury-induced telomere lengthening in circulating cells from the WT zebrafish. (A,B) Telomere length fluorescence frequency histograms of circulating cells from the WT (A) and *tert*$^{-/-}$ (B) uninjured fish and fish at 3 days after heart cryoinjury. Mean telomere fluorescence is indicated in arbitrary units (a.u.). Note the specific enrichment of cells with long telomeres at 3 dpi in WT hearts. (C,D) The percentage of the circulating cells showing a given telomere fluorescence from the WT fish (C) and *tert*$^{-/-}$ fish(D).Note that the frequency of the cells with the longest telomeres increased in WT zebrafish after the heart injury. The cells with the longest telomeres were not present in the *tert*$^{-/-}$ fish, neither before nor after heart injury. A total of 4 animals per condition per genotype were used for quantification. UI, uninjured; dpi, days postinjury; a.u., arbitrary units.

Given that telomere length has been linked to the cell cycle in several types of cells and organs (Lansdorp, 1995; Lee et al., 1998), we compared the telomere length of proliferative and non-proliferative cardiac cells. Single-cell profiling of telomere length and analysis of PCNA expression revealed the presence of cells with very long telomeres within the proliferating WT cardiac cells population. This suggests the existence of a subclass of cardiac cells with higher proliferative potential due to the longer telomeres (**Figure R 24**). We noticed that during regeneration telomeres lengthened not only in actively proliferating cells but also in non-proliferating cells, demonstrating that telomere elongation is a general process affecting all cells within the regenerating heart (**Figure R 24**).

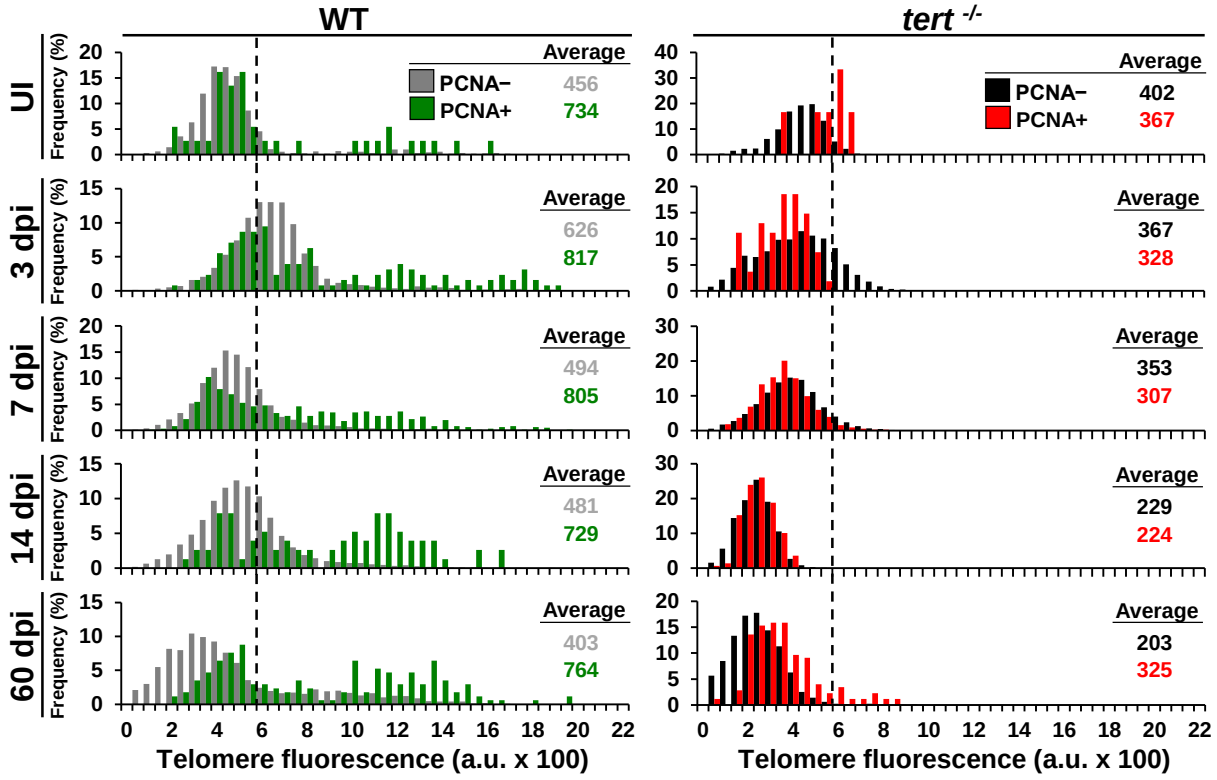

Figure R 24. Long telomeres mark a subset of proliferating cardiac cells. Telomere fluorescence frequency histograms of PCNA- and PCNA+ WT and *tert*$^{-/-}$ cells in uninjured hearts and hearts at 3, 7, 14, 30 and 60 days after cryoinjury. Histograms show frequencies for total cardiac cells. Telomere fluorescence averages are indicated in arbitrary units (a.u.). Note that the subpopulation of proliferating cells with long telomeres is lacking in *tert*$^{-/-}$ hearts. UI, uninjured; a.u. arbitrary units; dpi, days postinjury; PCNA, proliferating nuclear cell antigen; WT, wildtype.

To determine telomere length in proliferating cardiomyocytes, we co-immunostained sections for myosin heavy chain (MHC), PCNA and telomeres (**Figure R 25A**). We noticed that in uninjured WT hearts, cardiomyocyte telomere length was heterogeneous, with telomeres longer in proliferating cells. In addition, after injury, the number of proliferating cardiomyocytes with long telomeres (>600 arbitrary units, a.u.) increased to peak at 7 dpi but then gradually declined (**Figure R 25B**).

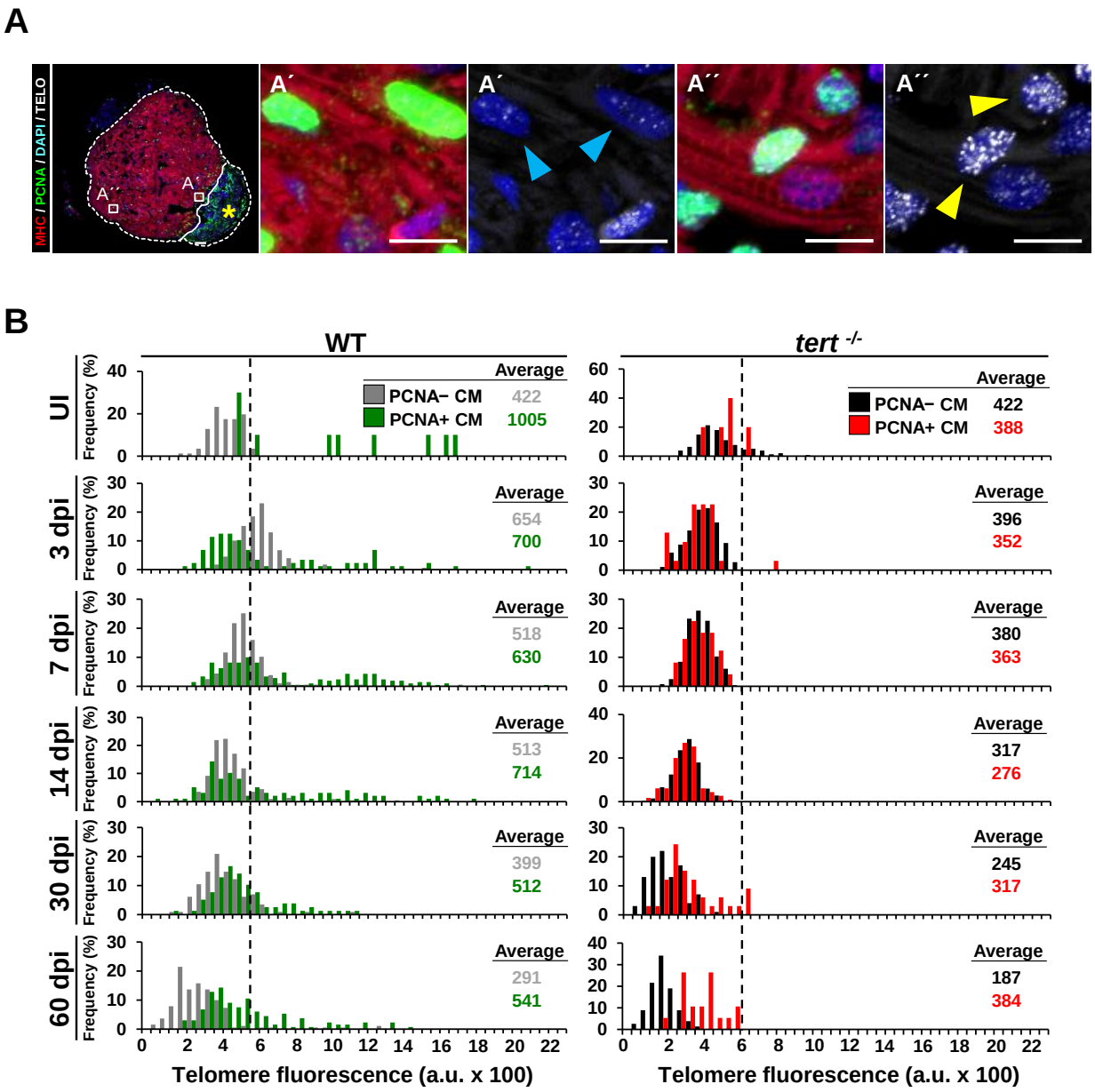

Figure R 25. Long telomeres mark a subset of proliferating cardiomyocytes. (A) Representative section of WT zebrafish heart immunostained for the cardiomyocyte marker MHC (red), the proliferation marker PCNA (green), and telomeres (white), with nuclear counterstaining with DAPI (blue). Asterisks mark the injured area. White line marks the injured area. The box area highlighted in the entire heart section images show higher magnifications on the right side. Scale bars 100 μm for entire sections and 10 μm for magnifications. Representative proliferating cardiomyocytes located close to the injury site (A´) and in the remote region (A´´). Arrowheads indicate PCNA-positive cardiomyocytes with short (blue arrowhead) or long (yellow arrowhead) telomeres. **(B)** Telomere fluorescence frequency histograms of PCNA- and PCNA+ WT and *tert*$^{-/-}$ cells in uninjured hearts and hearts at 3, 7, 14, 30 and 60 days after cryoinjury. Histograms show frequencies for cardiomyocytes. Telomere fluorescence averages are indicated in arbitrary units (a.u.). Note that the subpopulation of proliferating cardiomyocytes with long telomeres is lacking in *tert*$^{-/-}$ hearts. UI, uninjured; a.u. arbitrary units; CM, cardiomyoctes; dpi, days postinjury; PCNA, proliferating nuclear cell antigen.

These results suggest that despite undergoing telomerase hyperactivation after cryoinjury, telomerase activity levels become insufficient to maintain telomere reserves in cardiomyocytes and other cardiac cells. The successive rounds of cell division taking place during regeneration are likely to contribute to telomere erosion (Satyanarayana et al., 2003; Jiang & Rudolph, 2007). Consistent with this idea, telomeres shortened abruptly in cells close to the injury, the region with the highest proliferation rate (**Figure R 26**).

We confirmed that the initial increase in telomere length observed in cardiomyocytes of WT hearts at 3dpi and subsequent global telomere shortening at later stages of the regeneration process occurred both as average increase per nucleus and per single telomere spot (**Figure R 27**). The telomere dynamics profile of *tert*$^{-/-}$ cardiomyocytes was similar to the profile of the entire *tert*$^{-/-}$ cardiac cells population. It showed gradual injury-induced decrease and no evidence for longer telomeres in the cardiomyocytes population (**Figure R 27**).

Moreover telomere length dynamics triggered upon zebrafish heart injury were similar for all cardiac cells population. There was an injury-induced initial increase in telomere length not only in cardiomyocytes, but in epicardial (**Figure R 28A**) and endocardial (**Figure R 28B, C**) cells of WT hearts. These results suggest that injury-induced telomerase hyperactivation triggers global response of zebrafish heart.

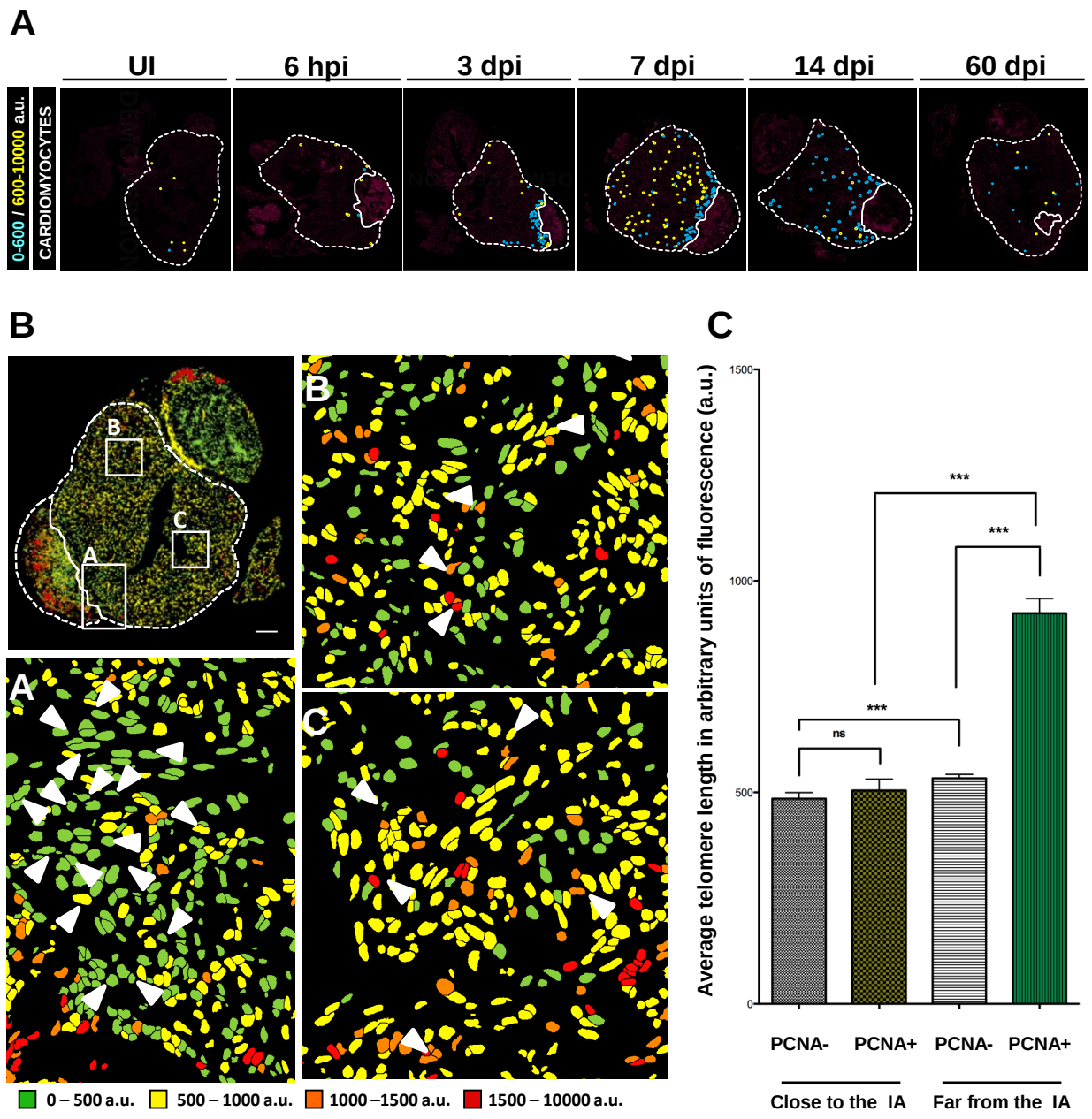

Figure R 26. Telomeres shortened abruptly in cells close to the injury, the region with the highest proliferation rate. (A) The locations of proliferating cardiomyocytes in WT zebrafish heart at the indicated time points. The panels depict proliferating cardiomyocytes with relatively short telomeres (<600 a.u.) in light blue and those with relatively long telomeres (> 600 a.u.) in yellow. **(B)** Representative telomere length pseudocolor images of section from WT zebrafish heart at 7 dpi. Nuclei are colored according to their average telomere fluorescence in arbitrary units. The cells with the longest telomeres are visualized in red, and the cells with the shortest telomeres are presented in green. Note in WT heart followed injury-induced global transient increase in the number of cells with

long telomeres, telomeres of proliferating cells shortened abruptly close to the injury site. White arrows indicate proliferating cardiomyocytes. Dotted lines mark the ventricle. Scale bars 100 μm for entire sections and 50 μm for magnifications. (C) Quantification of the average telomere length of proliferating (PCNA+) and non-proliferating (PCNA-) cells close to the injured area and from the regions far from the injury. Data are means ± SD from 4-5 hearts per condition (**p<0.01, *** p<0.001, Mann-Whitney test).PCNA, proliferating cell nuclear antigen; IA, injured area; dpi, days postinjury; a.u., arbitrary units.

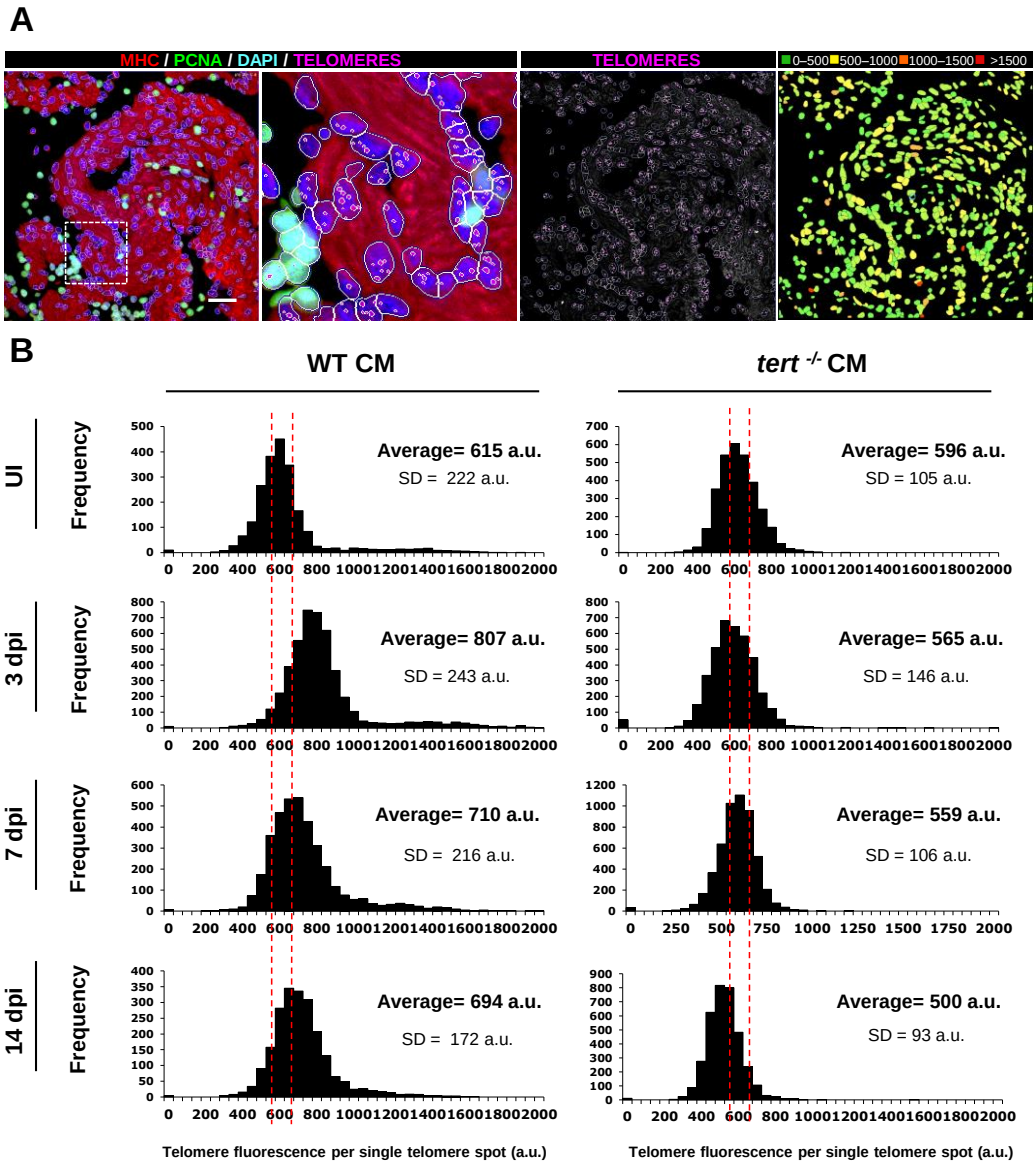

Figure R 27. Heart cryoinjury induces a telomerase-dependent increase in telomere reserves of cardiomyocytes per single telomere spot. (A) Immunofluorescence of WT zebrafish hearts for

cardiomyocyte marker MHC (red), the proliferation marker PCNA (green), telomeres (magenta) with nuclear counterstaining with DAPI (blue) – left panel. Telomap image, nuclei are colored according to their average fluorescence in arbitrary units- right panel (B). Telomere fluorescence frequency histograms per single telomere spot of cardiomyocytes from the WT and *tert*$^{-/-}$ uninjured hearts and hearts at 3, 7 and 14 days after cryoinjury. Mean telomere fluorescence is indicated in arbitrary units (a.u.). Note the increase in the number of CMs with long telomeres at 3 dpi in WT hearts, followed by reestablishment of the initial profile. This response is lacking in *tert*$^{-/-}$ CMs, and telomeres shorten at the later stages. Quantification based on minimum 4hearts per condition per genotype, minimum 3 sections per heart. CM, cardiomyocyte; dpi, days postinjury; a.u., arbitrary units.

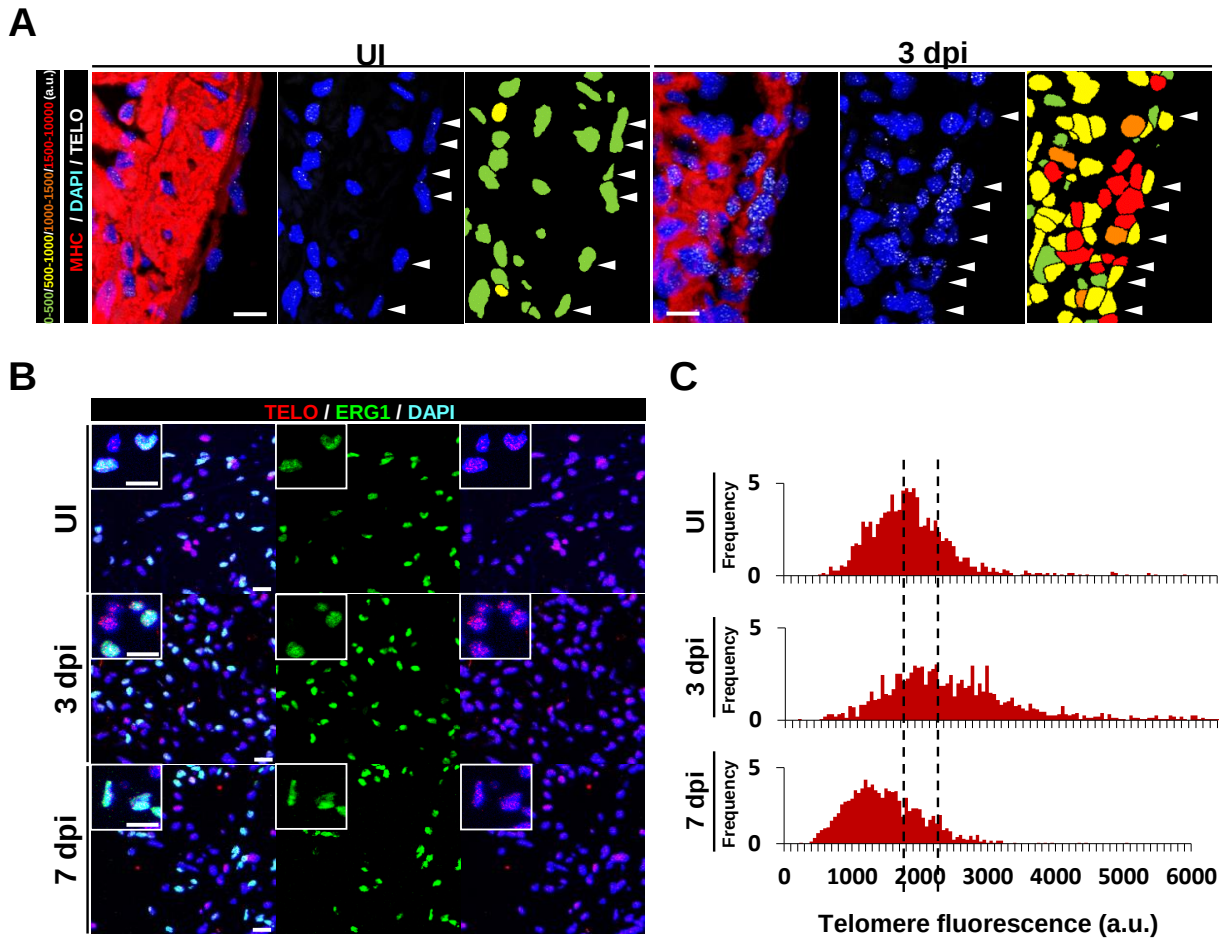

Figure R 28. . Heart cryoinjury induces a telomerase-dependent increase in telomere reserves of epicardial and endocardial cells. (A) Representative magnifications of epicardial region of the zebrafish hearts immunostained for the cardiomyocyte marker MHC (red) and telomeres (white), with

nuclear counterstaining with DAPI (blue). Telomere length in the epicardium region of uninjured and at 3 dpi WT zebrafish hearts. Telomap image, nuclei are colored according to their average fluorescence in arbitrary units- right panel (right side). White arrowheads indicate epicardial cells. (B) Immunostaining of the endocardium (endothelial cell marker erg1; green) combined with Q-FISH detection of telomere length (red) in uninjured, 3 dpi and 7 dpi WT zebrafish hearts. Nuclei are counterstained with DAPI (blue). (C) Representative histograms showing the frequency of telomere fluorescence in arbitrary units (a.u.) in endocardial cells upon cryoinjury. a.u. arbitrary units; dpi, days postinjury; WT, wildtype. Scale bars: 10 μm.

11. The injury-induced telomere elongation in WT hearts does not signify reversal of telomere aging (telomere rejuvenation)

Telomere length has been proposed as a biomarker of aging in the zebrafish model (Anchelin et al., 2011). During the aging process, telomeres undergo progressive shortening mostly due to rounds of cell divisions that consequently decrease the further cell proliferation. Injury-induced global telomere elongation observed in cardiac cells of WT animals at 3 dpi might constitute, together with the cardiomyocyte dedifferentiation and reexpression of embryonic cardiac markers, another feature of transient heart rejuvenation, thus supporting cell proliferation. We measured the average telomere length of cells from uninjured WT zebrafish hearts at three different stages: 1,5 month, 5 months and 18 months old, corresponding respectively to juvenile, young adult and older adult (**Figure R 29**).

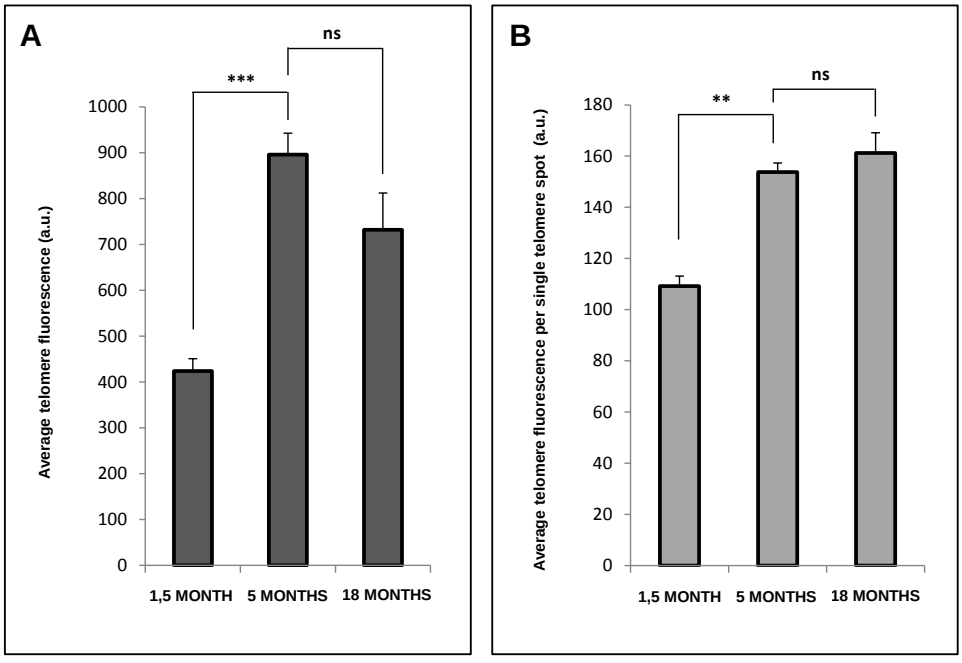

Figure R 29. Injury-induced WT cells telomere elongation is not telomere rejuvenation. Average telomere fluorescence of cardiac WT cells in uninjured juvenile (1,5 month), young adult (5 months) and older adult (18 months) hearts. Quantification of fluorescence per nucleus (A) and per single telomere spot (B). Mean telomere fluorescence is indicated in arbitrary units (a.u.). Data are means of at least 4 sections per heart from 3-6 hearts per condition. **, $p<0.01$; ***, $p<0.001$, ns, not significant (Mann-Whitney test).

We found that telomere length in WT zebrafish heart increased between juvenile and the young adult stage and was maintained in the old adult. We quantified the average telomere fluorescence intensity in arbitrary units (a.u.) and we observed that young adult fish hearts presented almost double average telomere length than the hearts from the juvenile stage (**Figure R 29A**). As expected this increase was significant. Furthermore we confirmed that the increase in the average telomere length was present not only per nuclei, but also for the single telomere spot measurement (**Figure R 29B**). The differences in average telomere fluorescence (a.u.) between the cells from the young adult and older adult zebrafish hearts were not significant.

These data suggest that the transient telomere elongation that we observe upon ventricular injury cannot be considered as a reversal of aging process that affects the proliferative cell capacity.

12. The absence of telomerase is an important contributor to DNA damage

We found that after the injury the number of cells with short telomeres increases. Short and dysfunctional telomeres limit the cellular proliferative capacity by eliciting a DNA damage response. To assess the levels of DNA damage before and after injury in WT and *tert*$^{-/-}$ hearts, we measured the protein levels of the DNA damage marker γ-H2AX (Rogakou et al., 1998). First, we performed Western blot on the protein extracts obtained from pools of uninjured and 3 dpi WT and *tert*$^{-/-}$ whole hearts (**Figure R 30A**). There was a significant increase in phosphorylation of histone H2AX between WT and *tert*$^{-/-}$ hearts without injury, measured by γ-H2AX average signal intensity. We found that ventricular injury triggered an additional increase in the gH2AX signal intensity, although significant only in *tert*$^{-/-}$ hearts, suggesting that the absence of telomerase contributes to the injury-induced DNA damage levels (**Figure R 30B**).

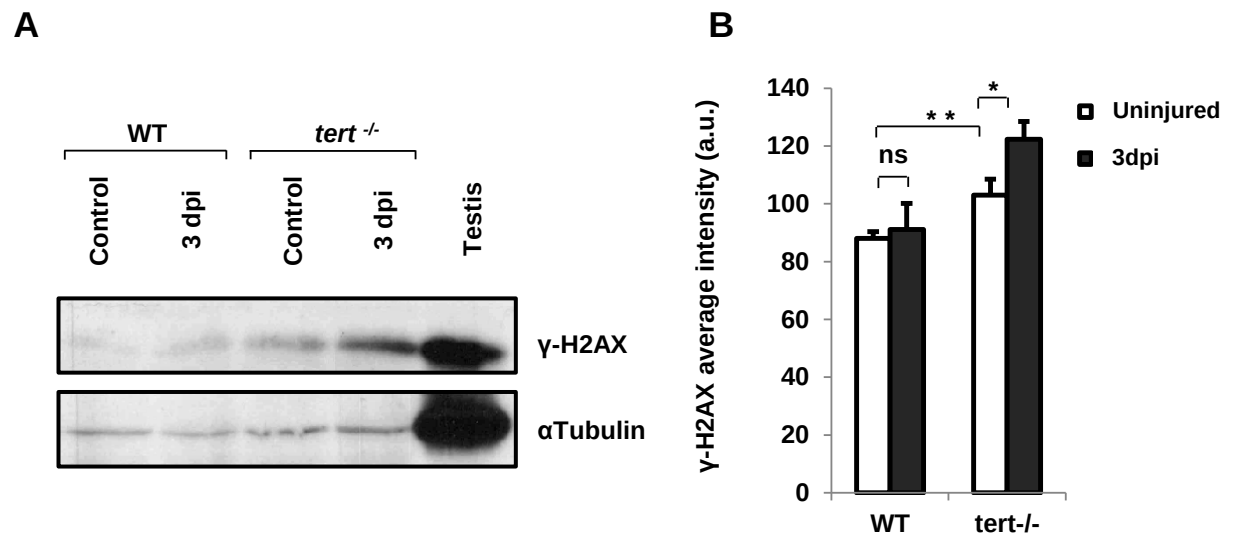

Figure R 30. DNA damage increases after ventricular cryoinjury in the absence of telomerase. (A) Representative Western blot of γ -H2AX expression in WT and *tert*$^{-/-}$ hearts without injury and in hearts at 3 dpi.(B) Quantification of Western blot signal intensities (n = 9 hearts/condition). Data are means ± SEM.*p < 0.05 (Mann-Whitney test).

To determine the location of cardiac cells, presenting γ-H2AX foci, we performed immunostaining of γ-H2AX, myosin heavy chain (MHC) and DAPI to counterstain nucleus, on uninjured and 3 dpi WT and *tert*$^{-/-}$ heart sections (**Figure R 31**).

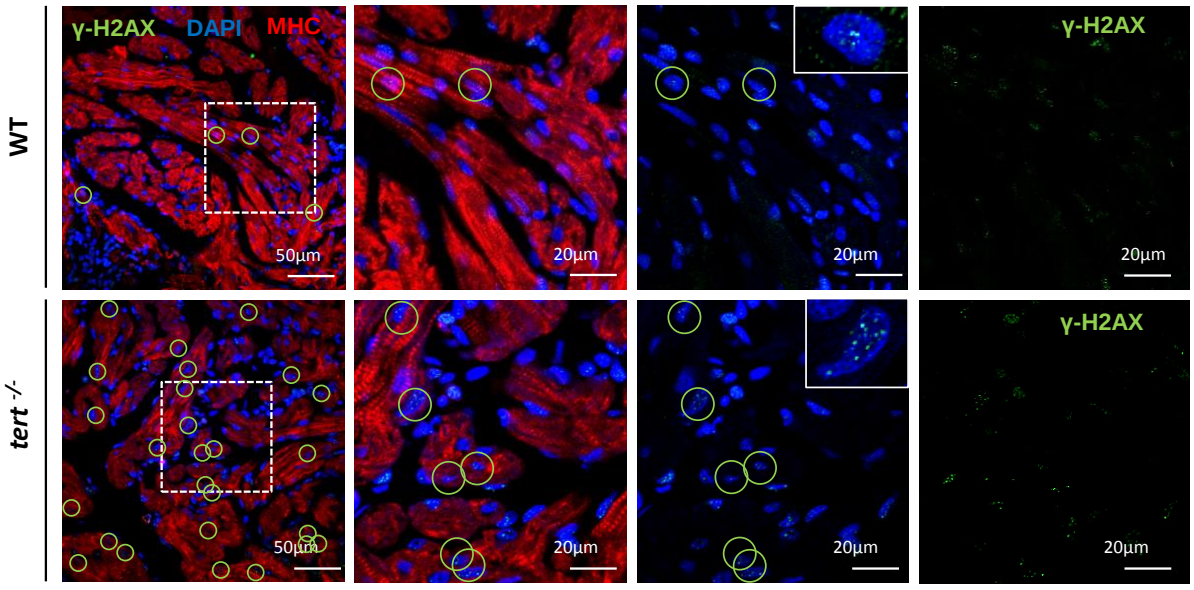

Figure R 31. Damage Increases Strongly after Ventricular Cryoinjury in the Absence of Telomerase. Representative staining of γ-H2AX foci (green) in cardiac cells in uninjured and 3 dpi WT and *tert*$^{-/-}$ hearts. Cardiomyocytes are immunostained with anti-MHC (red), and nuclei are counterstained with DAPI (blue). Examples of γ-H2AX^{+} cardiomyocytes are outlined with green circles. Boxed areas are shown at a higher magnification. Scale bars, 20 μm.

We wondered whether the cardiomyocyte population in particular was susceptible to DNA damage. To determine this we co-immunostained sections with myosin heavy chain (MHC), γ-H2AX and DAPI. Cardiomyocytes presenting DNA damage foci were spread globally in the ventricles of uninjured hearts and hearts at 3 dpi (**Figure R 32A**). The high percentage of cardiomyocytes with γ-H2AX foci confirmed that *tert*$^{-/-}$ hearts have a higher basal level of DNA damage (**Figure R 32B**). A weak but significant increase in the number of cardiomyocytes presenting γ-H2AX foci upon injury was present in WT hearts, but both the basal numbers of γ-H2AX positive cardiac myocytes and the injury-induced increase of DNA damage were significantly higher in *tert*$^{-/-}$ hearts (**Figure R 32A, C**).

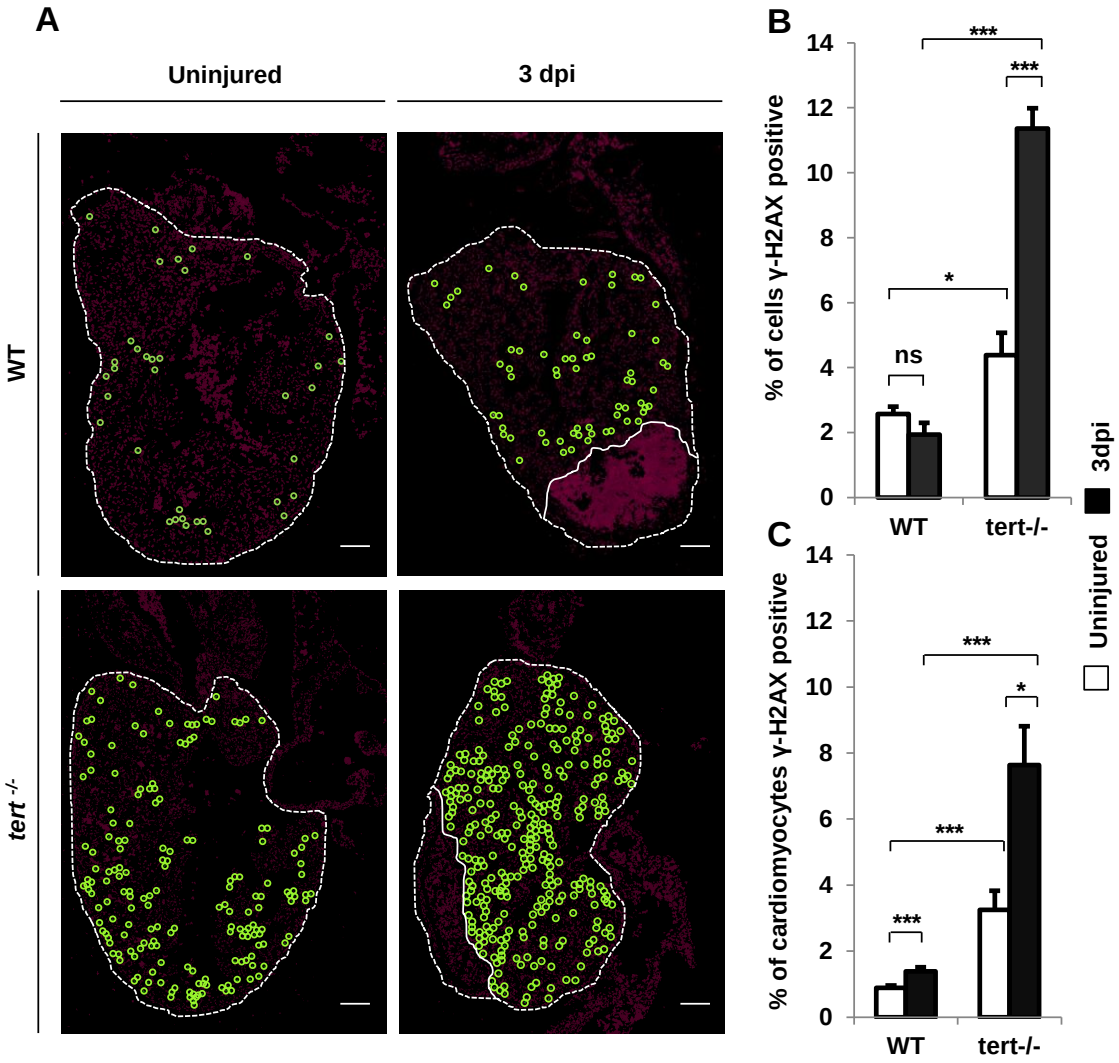

Figure R 32. Damage Increases Strongly after Ventricular Cryoinjury in the Absence of Telomerase. (A) Distribution of γ-H2AX-positive cardiomyocytes (green circles) in uninjured and 3 dpi WT and *tert*$^{-/-}$ hearts. The nuclear area is shown in magenta. The ventricle and injured area are outlined by dotted lines. Scale bars, 100 µm. (B , C) Percentages of (B) γ-H2AX-positive cardiac cells and (C) γ-H2AX-positive cardiomyocytes in uninjured and 3 dpi WT and *tert*$^{-/-}$ hearts. Data are means ± SEM of cells counted on a minimum of 3 sections/heart in four hearts. *p < 0.05, **p < 0.01, ***p < 0.001 (Student's t test).

The DNA damage response limits the cellular proliferative capacity of many cell types (Behrens et al., 2014). To assess whether DNA damage directly affects proliferation of cardiac cells we co-immunostained WT and *tert*$^{-/-}$ 3dpi heart sections with γ-H2AX and BrdU antibodies after injecting BrdU intraperitoneally 8 hours beforehand. This analysis revealed that the vast majority of BrdU-positive cells were γ-H2AX negative in both, WT and *tert*$^{-/-}$ hearts, providing indirect confirmation that the presence of DNA damage foci is limiting cell proliferation (**Figure R 33**).

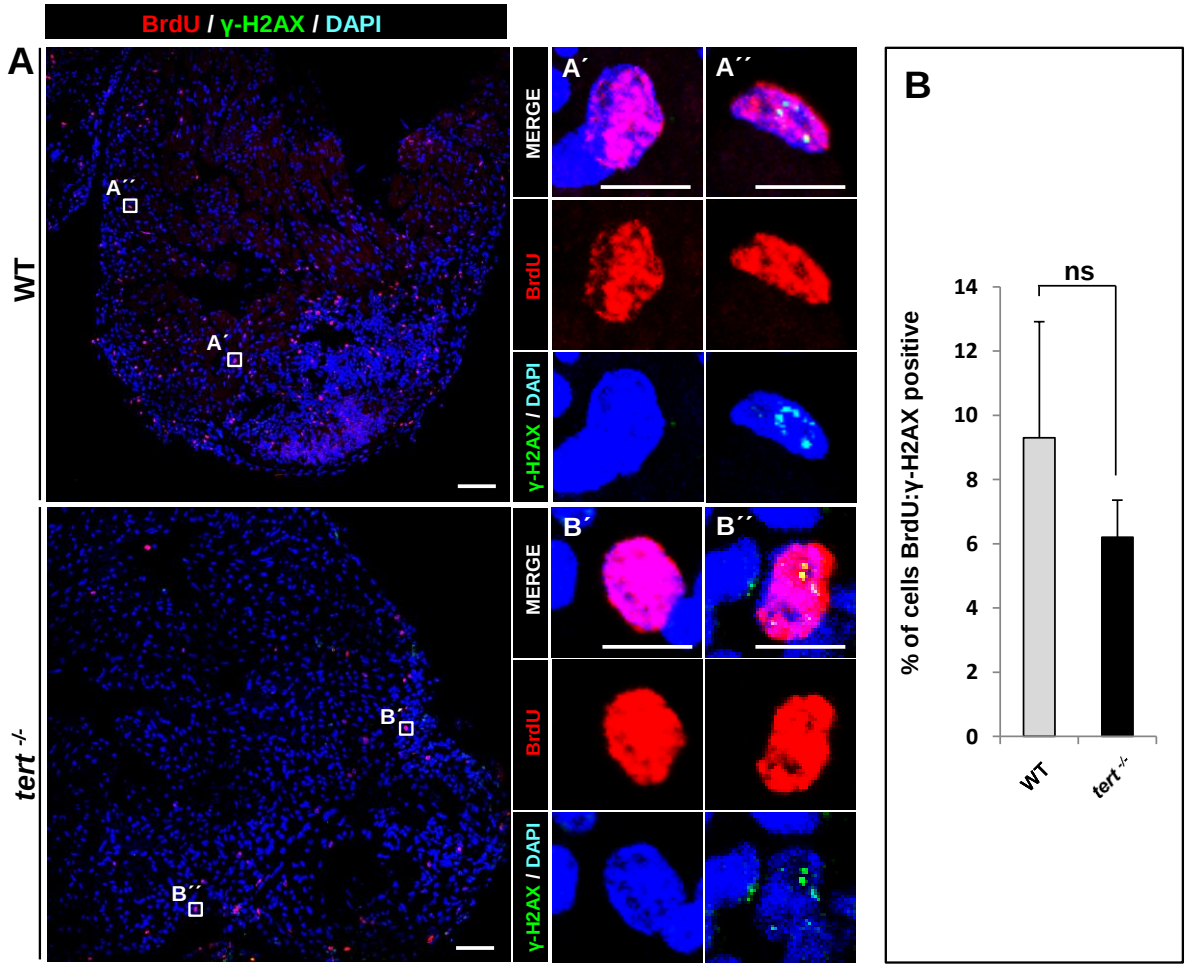

Figure R 33. Cardiac cells with accumulated DNA damage are less prone to proliferate. (A) Immunofluorescence staining on a WT and a *tert*$^{-/-}$ heart section with anti-BrdU (red) and anti-γH2AX (green). Nuclei are counterstained with DAPI (blue). (A1-A4) Boxed areas in the whole-mount heart views of WT (A1,A2) and *tert*$^{-/-}$ (A3,A4) are shown at high magnification in the right panels to exemplify individual BrDU-positive cells. Scale bars: 100 μm (whole mount views), 10 μm (magnifications). (B) Quantification of cells double positive for BrDU and γH2AX. Data are means ± SEM of 4 sections/heart from a total of 3 hearts per condition (p=0.106, unpaired Student's t-test). ns, not significant.

We wondered whether the presence of critically short or dysfunctional telomeres was an important contributor to the observed levels of DNA damage. We performed Q-FISH on γ-H2AX-stained WT and *tert*$^{-/-}$ heart sections at 3 dpi. In order to establish a correlation between both signals, we manually counted the number of cells with telomere dysfunction-induced foci (TIFs) (**Figure R 34**). Interestingly we could not find any DNA damage foci at critically short or dysfunctional telomeres in uninjured hearts irrespective of the genotype, although a very low number of TIFs was identified in 3 dpi WT and *tert*$^{-/-}$ hearts (0.2% of total damage) (**Figure R 34**). This might suggest that the DNA damage response induced upon heart injury is related with different forms of stresses (mechanical, oxidative etc.) rather than with the critically short and dysfunctional telomeres.

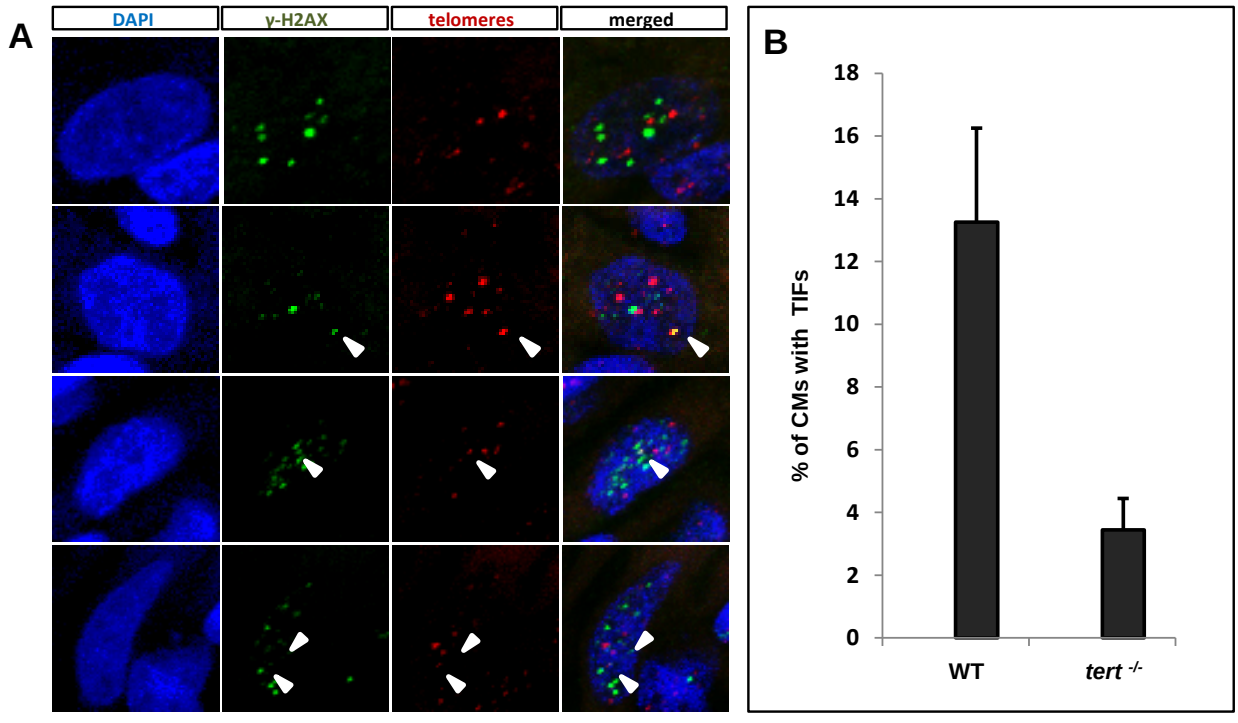

Figure R 34. Critically short or dysfunctional telomeres are not the main contributor to DNA damage. Representative staining and quantification of γ-H2AX foci (green) and telomeres (red) in

cardiomyocytes in 3 dpi WT and *tert*$^{-/-}$ hearts. Cardiomyocytes are immunostained with anti-MHC (red) and nuclei are counterstained with DAPI (blue). White arrows show TIFs. TIF, telomere dysfunction-induced foci; ns, non significant, Scale bar: 20 μm.

13. The apoptotic response is not correlated with DNA damage levels during the initial phase of zebrafish heart regeneration

DNA damage can elicit three types of cellular response: apoptotis, a transient cell cycle arrest or a permanent cell cycle arrest called senescence (d'Adda di Fagagna et al., 2003; review d'Adda di Fagagna 2008). To study apoptosis we performed a TUNEL assay in WT and *tert*$^{-/-}$ uninjured hearts and at 3, 7, 14, 30 and 60 dpi (**Figure R 35A**). We found a significant increase in the percentage of apoptotic cardiac cells, including cardiomyocytes, in *tert*$^{-/-}$ hearts at 14 dpi and later timepoints (**Figure R 35B**). This suggests that injury-induced apoptosis is the later event in telomerase deficient zebrafish hearts and appears as a consequence rather than a cause of DNA damage.

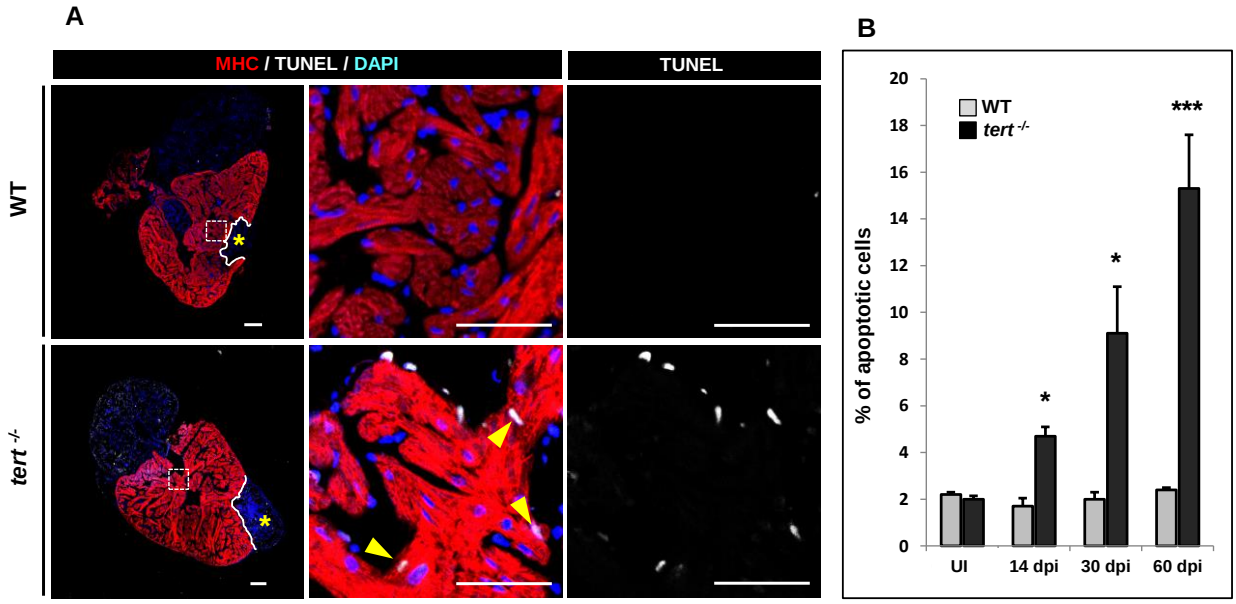

Figure R 35. Injury-induced increase in the apoptotic response. (A) Representative staining and of TUNEL positive cardiac cells in uninjured and at 14, 30, and 60 dpi WT and *tert*$^{-/-}$ hearts. Cardiomyocytes are immunostained with anti-MHC (red), nuclei are counterstained with DAPI (blue) and TUNEL-positive cells are white. Yellow arrows show cardiomyocytes. White lines outline injured area; asterisks mark the initial injury site. dpi, days postinjury; Scale bars: 100 μm (whole

section views), 50 μm (magnifications). (B) Quantification of the average percentage of apoptotic cells. Data are means of at least 4 sections per heart from 4 hearts per time point, *, $p<0.05$, ***, $p<0.001$ (Mann-Whitney test), UI, uninjured.

14. The absence of telomerase significantly contributes to injury-induced senescence

DNA damage and cell cycle blockade can lead to cellular senescence (d'Adda di Fagagna et al., 2003). Because heart injury promoted further phosphorylation of H2AX and led to significant increase of injury induced DNA damage in *tert*$^{-/-}$ hearts, we wondered whether *tert* deficiency can result in permanent cell cycle arrest (senescence), which may explain the severe reduction of cellular proliferation. We therefore used a β-galactosidase assay to detect senescence in WT and *tert*$^{-/-}$ hearts. First we confirmed the specificity of this assay with whole-mount staining in young and old animals. Both in the liver and intestines, which are prone to aging (Jurk et al., 2014; Wang et al., 2009), we observed a very strong senescence-associated β-gal signal (**Figure R 36A**). Next we compared the senescence-associated β-galactosidase signal in hearts from WT and *tert*$^{-/-}$ siblings in uninjured and injured conditions. Uninjured hearts of either WT or *tert*$^{-/-}$ animals did not show senescence by either whole-mount staining and paraffin sections from uninjured hearts (**Figure R 36B**), whole-mount staining and paraffin sections from the heart at 3 and 7 dpi (**Figure R 36C**), or freshly prepared cryosections (**Figure R 37)**. In contrast injury-induced senescence signal was found in WT and *tert*$^{-/-}$ hearts at 3 and 7 dpi (**Figure R 36C, Figure R 37**). Senescent cells were almost exclusively limited to the injured region WT hearts at 3 dpi, whereas the signal was distributed more broadly in injured *tert*$^{-/-}$ hearts, extending beyond the injured area and border zone to remote regions of the ventricle (**Figure R 36C, Figure R 37**). This staining was maintained at later stages of regeneration (7 dpi) (**Figure R 36C, Figure R 37**).

These data suggest that the injury-induced senescence is increased in the absence of telomerase activity. This might at least partially explain the severe inhibition of cardiac cell proliferation observed in *tert*$^{-/-}$ hearts upon heart injury.

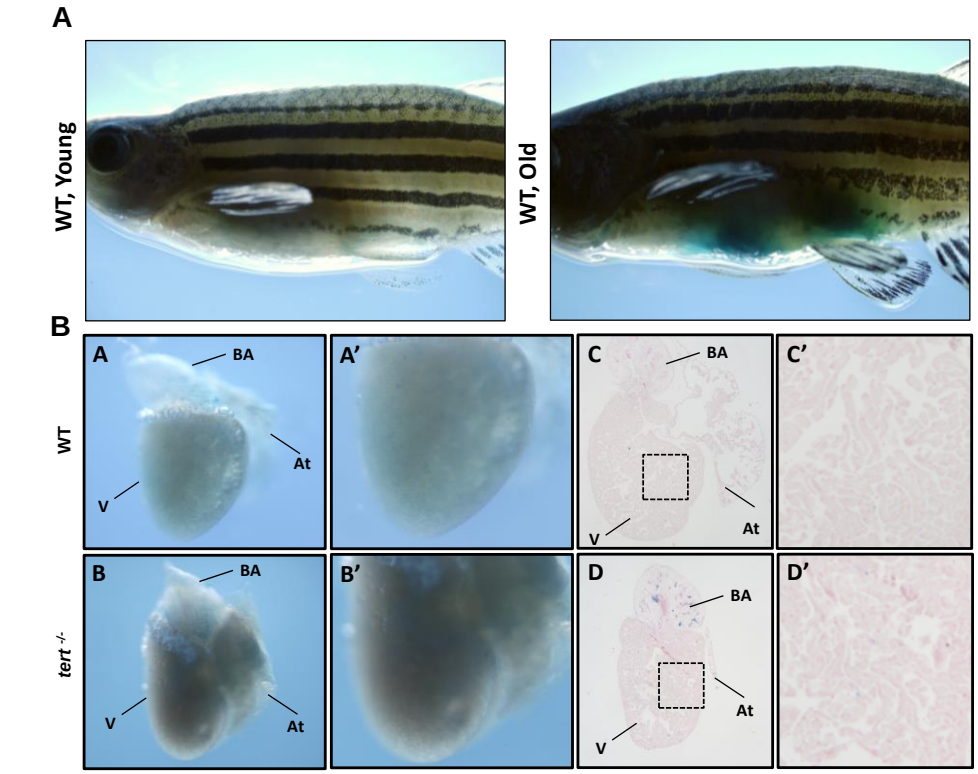
A
WT, Young
WT, Old
B
WT
tert -/-
A
A'
B
B'
C
C'
D
D'
BA
At
V

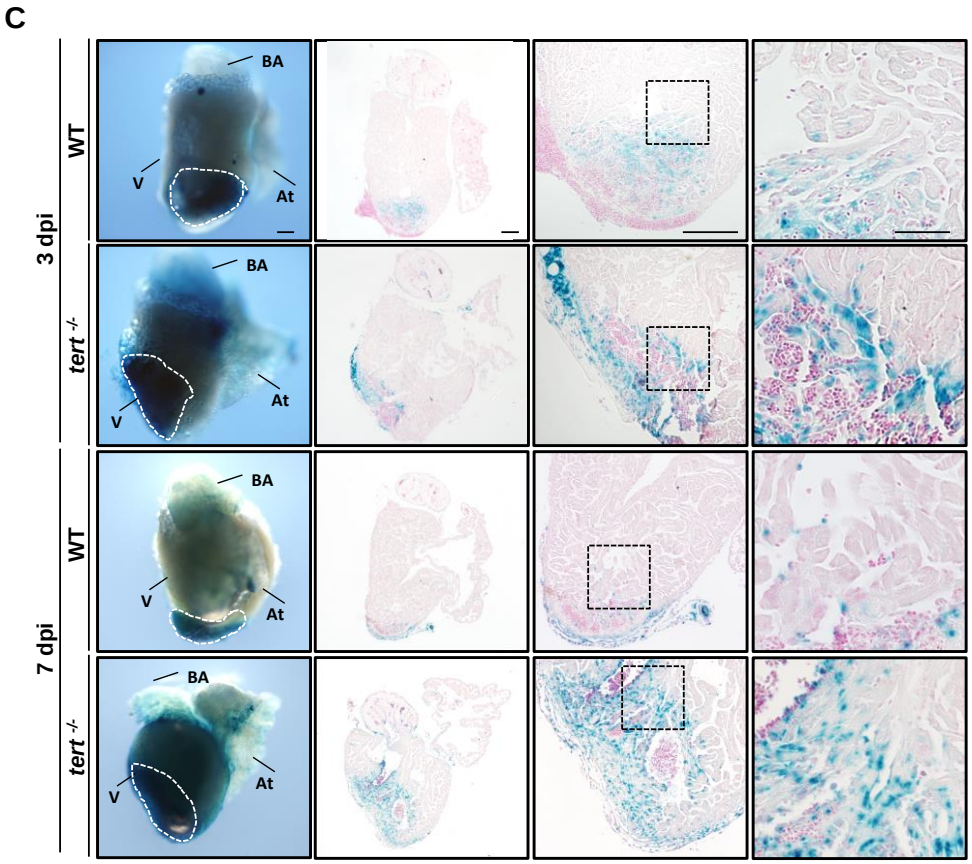
C
3 dpi
7 dpi
WT
tert -/-
BA
At
V

Figure R 36. Senescent response during homeostasis and heart regeneration in WT and *tert*$^{-/-}$ zebrafish. (A) Whole mount staining of uninjured WT young and old zebrafish for SA-*β*-galactosidase. Note detectable senescence signal in the liver and intestine of old animals. (B) Whole mounts and paraffine sectionsof uninjured WT and *tert*$^{-/-}$ hearts stained for SA-*β*- galactosidase. There is no detectable senescent signal. Scale bars: 100 μm and 10um for magnifications. (C) Whole mount views and paraffine sections of 3 dpi and 7 dpi WT and *tert*$^{-/-}$ hearts stained for SA-β-galactosidase. Note elevated senescence signal in *tert*$^{-/-}$ hearts. Magnified views are shown of the injured area (IA). White dotted line indicate injury area.V, ventricle; At, atrium; BA, bulbus arteriosus.

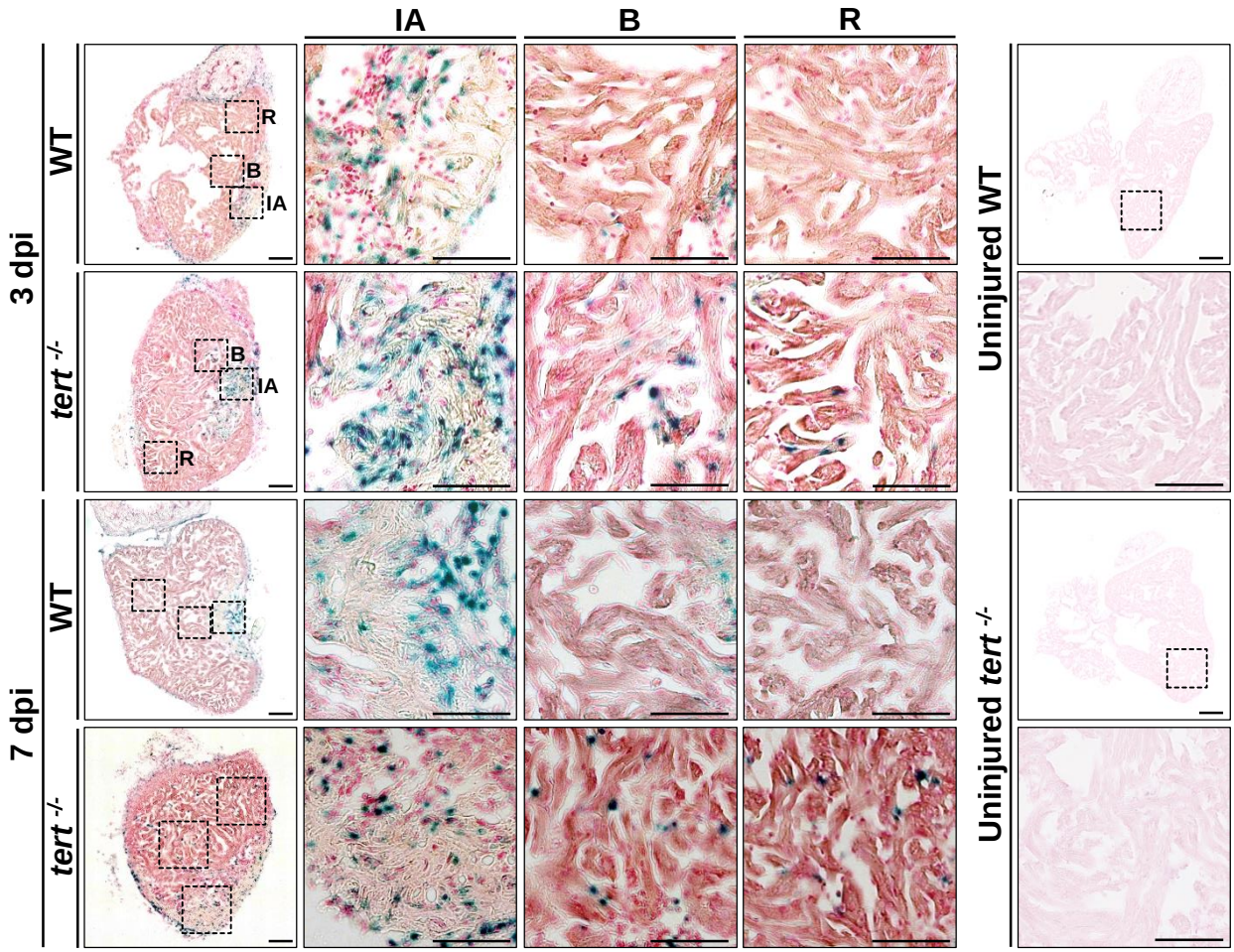

Figure R 37. *tert*$^{-/-}$ hearts acquire a senescence phenotype after ventricular cryoinjury. Cryosections of uninjured and at 3 dpi and 7 dpi WT and *tert*$^{-/-}$ hearts stained for SA-β- galactosidase. Magnified views are shown of the injured area (IA), injury border (B) and remote zone of the ventricle (R). Scale bars: 100 μm and 10um for magnifications. Dpi, days postinjury.

DISCUSSION

To advance human health and find new targets for therapy, the initial requirement is to understand how our genes work in nature. In this endeavor animal models are invaluable tools. There is an increased number of studies highlighting the importance of the zebrafish (Danio rerio), a lower vertebrate that has emerged as a model organism for human diseases research (reviewed in Lieschke & Currie, 2007; Howe et al., 2013). For effective modeling of human disease it is essential to comprehend the extent to which zebrafish genes structure and function are related to human genes. Interestingly, the vast majority of genes detected in zebrafish have a human counterpart. Comparative studies between zebrafish and human reference genomes have revealed that approximately 70% of all human genes and strikingly of 84% of those linked to human diseases have at least one zebrafish orthologue (Howe et al., 2013).

Here we set out to explore the association of constitutive telomerase activity and telomere length in the zebrafish heart with the tissue-renewing capacity of cardiac cells in this model. To this end, our study focused on two aspects of the heart regeneration process in zebrafish heart: first, the role of *tert* by analyzing WT and *tert* mutant fish and second, the injury-induced telomere dynamics in the regenerating cardiac tissue of adult zebrafish after cryoinjury.

Cryoinjury is a potent incentive to induce heart regeneration process in zebrafish. We find that an insult to the myocardium triggers telomerase hyperactivation in the zebrafish WT heart. This is concomitant with a global striking telomere elongation of all cardiac cells. Long telomeres provide cells proliferative potential. We find that *tert* expression and telomerase activation are prerequisites to robust cellular proliferation by maintaining telomere length and genome integrity. Moreover our data reveal a telomere-independent role for telomerase as a cell protector against DNA damage response in the zebrafish heart. Thus in the presence of telomerase damaged cardiac muscle is replaced with newly formed myocardium. Consequently, failure to activate telomerase in *tert* deficient zebrafish is a reason for restricted zebrafish heart regenerative capacity. We find that heart injury in the absence of telomerase aggravates telomere shortening and dysfunction, decreases proliferation thus regenerative potential of *tert*$^{-/-}$ zebrafish hearts. We demonstrate that limited proliferative capacity in cardiomyocytes is caused by accumulation of DNA damage that leads to permanent cell cycle arrest (senescence).

Based on our findings we propose a following working model (**Figure D 1**):

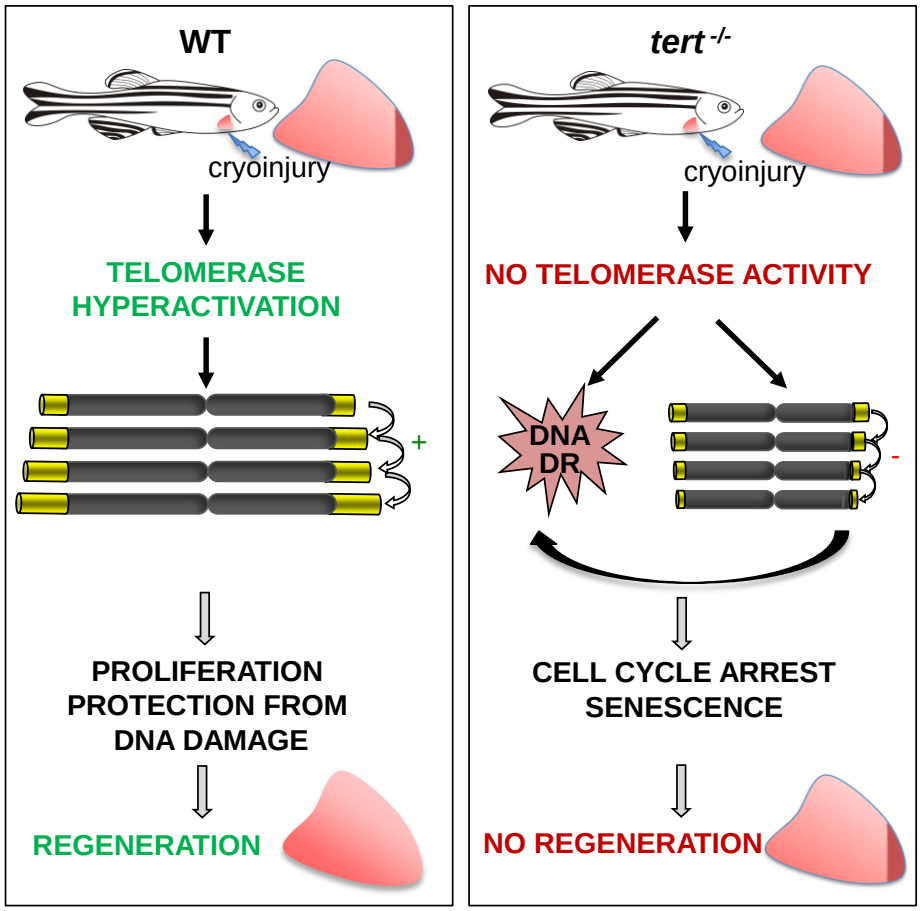

Figure D 1: Graphical model of zebrafish heart regeneration in presence and absence of telomerase activity.

1. The *tert* gene is upregulated upon heart injury in zebrafish.

In contrast to the situation in mammals, zebrafish maintain high telomerase activity in adult tissues throughout their entire lifespan (Anchelin et al., 2011, 2013). This feature is of great interest as it may contribute to the zebrafish's remarkable capacity for indefinite growth in the context of organ regeneration including the heart (reviewed in Poss, 2007).

First, we confirmed that the zebrafish *tert* mutant lacks telomerase activity in the heart and can be considered a *tert* knockout (*tert*$^{-/-}$), as has been proposed previously in other zebrafish tissues (Anchelin et al., 2011; Kishi et al., 2003). Interestingly, we observed that the expression

of *tert* mRNA was significantly higher in *tert*$^{-/-}$ uninjured hearts compared to WT, suggesting the existence of a regulatory mechanism that induces a compensatory activation of the *tert* promoter in the absence of telomerase activity. In contrast, telomerase activity in WT hearts was transiently upregulated in response to the injury which correlated with a significant increase in *tert* gene expression at 3 days post injury (dpi), pointing toward transcriptional activation as a likely regulatory mechanism. As we expected, no further increase in the *tert* mRNA nonsense transcripts was observed after injury in *tert*$^{-/-}$ hearts. Moreover, we showed that under homeostatic conditions the WT zebrafish heart possess constitutive telomerase activity at different stages of adult life, which is consistent with detectable activity of this enzyme in other zebrafish somatic tissues (Anchelin et al., 2011; Kishi et al., 2003). Furthermore, we did not observe significant differences in size, morphology and function of *tert*$^{-/-}$ hearts compared with those of WT siblings, suggesting that heart development is not affected per se in the absence of *tert*. The lack of an obvious phenotype in *tert*$^{-/-}$ hearts from 6 to 9 months of age is consistent with the lack of phenotypic alterations in low-turnover *tert*$^{-/-}$ tissues at young ages, which may be owed to a sufficiently large telomere reserve under homeostatic conditions (Anchelin et al., 2013; Henriques et al., 2013).

2. **Telomerase deficiency impairs regeneration of the zebrafish heart**

The most important finding of our study was, however, that *tert* deficient zebrafish exhibit a very poor regenerative response following cardiac injury. We observed that in contrast to WT fish injured *tert*$^{-/-}$ cardiac muscle was replaced with scar-like tissue rather than regenerated myocardium and also failed to recover the contractile function. Strikingly, this closely recapitulates the pathophysiological processes after myocardial infarction (MI) in the human heart where telomerase is normally not active.

The finding that in WT zebrafish heart injury-induced fibrotic tissue deposition is reversible and removed over time until a full re-establishment of myocardial structure and function (Chablais et al., 2011; González-Rosa et al., 2011), strongly suggests telomerase as a key factor in cardiac regeneration. In support of this, Oh et al. (2001) could demonstrate that transgenic telomerase expression in mice can delay the cell cycle exit and promotes survival of CMs. Moreover, telomerase reactivation in the adult mouse heart has been shown to have a cardioprotective effect after MI (Bär et al. 2014).

After establishing that telomerase is essential for zebrafish heart regeneration we investigated which part of the regeneration process was affected by *tert* deficiency and in which cell type telomerase activity is required to promote regeneration. Myocardial injury triggers a rapid inflammatory response, leading to the infiltration of the injury site first by leukocytes, including neutrophils and later by monocytes/ macrophages and other circulating cells (review Frangogiannis, 2014). The injury-triggered inflammatory responses induce the expression of chemokines and cytokines, which recruit inflammatory cells in order to clear the infarct zone of dead cells and matrix debris. This is a programmed process that serves to stimulate repair and heal damage tissues. The inflammatory response, particularly the infiltration of macrophages, plays a key role in promoting cardiac regeneration in the neonatal mouse heart (Aurora et al., 2014). However, an inadequate or excessive inflammatory response may lead to improper cellular repair, tissue damage, and dysfunction. Accordingly, chronic inflammation in adult mammalian hearts leads to continued fibrosis and cardiomyocyte loss, which contributes to adverse cardiac remodeling, the development of heart failure and ultimately inhibits cardiac regeneration (reviewed in Frangogiannis, 2014). Because *tert* knock-down was reported to impair differentiation of multiple blood cell types, including inflammatory cells (Imamura et al, 2008), an important question to answer was whether *tert* deficiency could result in an impaired inflammatory response triggered by cryoinjury, thus explaining the observed regeneration blockade. However, our results revealed that *tert*$^{-/-}$ zebrafish hearts do not have a defective inflammatory response and therefore, a contribution to the impaired regeneration of the cardiac muscle in *tert*$^{-/-}$ is unlikely.

We also show that the rapid organ-wide activation of the endocardium and epicardium, critical in order to support cardiomyocytes proliferation, (Kikuchi et al., 2011; Lepilina et al., 2006) was not affected in the absence of telomerase. The dedifferentiation of cardiomyocytes that we observed upon zebrafish heart injury is reminiscent of that seen in embryonic mammalian cardiomyocytes. Disassembly of sarcomere structures has been shown to be a feature of proliferating cardiomyocytes in the embryonic mouse heart (Ahuja et al., 2004). *Gata4* gene expression is also induced in myocardium during the embryonic development of the mouse heart, and its function is required for cardiomyocyte proliferation (Zeisberg et al., 2005). Therefore these results suggest that some mechanisms used for regenerating zebrafish heart are also conserved in the mammalian hearts. Injury-induced expression of myocardial differentiation

factors, such as *gata4*, *nkx2.5*, *hand2*, *tbx20* and *tbx5* was unaffected by the absence of *tert* although we could not detect significant upregulation in injured hearts as has been previously described (Kikuchi et al., 2011; Lepilina et al., 2006). Discrepancy with other studies (Jopling et al., 2010; Lien et al., 2006), may be explained by the fact that the mRNA from whole hearts was used for the analysis (RNAseq and qRT-PCRs) potentially diluting ventricular and cardiomyocyte specific gene expression. We find that *tert*$^{-/-}$ cardiomyocytes have the potential to dedifferentiate and the capacity to re-express embryonic markers in the same way as cardiomyocytes from WT hearts. Thus the ability to dedifferentiate can be ruled out as the discriminating trait to explain the differences in the regeneration potential between both genotypes.

Knowing that pre-existing mature cardiomyocytes from both genotypes (WT and *tert*$^{-/-}$) dedifferentiate to a more primitive state, allowing efficient CMs proliferation and myocardial renewal we asked if the proliferative capacity of *tert*$^{-/-}$ cardiac muscle cells appears to be limited. Although the mechanism of CM division in mammals (Senyo et al., 2012; reviewed in Senyo et al., 2014) seems to be similar to zebrafish, they lack the ability of massive CM cell cycle re-entry which correlates with lack of telomerase. We provided experimental evidence that cardiomyocytes proliferation, the primary source for regenerating myocardium, was delayed and severely reduced in *tert*$^{-/-}$ zebrafish hearts. In line with this, Gene Set Enrichment Analysis (GSEA) additionally showed that cell proliferation-associated pathways were significantly underrepresented in *tert*$^{-/-}$ hearts compared to WT.

To address the role of *tert* in a temporal and spatial manner we completed the analysis on *tert* mutant animals by the use of anti-sense technology, namely morpholino (MO) antisense oligonucleotide administration, that together with the use of mutant lines, are presently the most common approaches to analyze gene function in zebrafish (Rossi et al., 2015). Using this approach, we found that *tert* vivo MO administration leads to reduced *tert* activity and concomitant inhibition of cardiac cell proliferation. These preliminary results further supported through a temporally and spatially restricted approach, the function of *tert* in promoting cardiac cell proliferation in the injured heart.

3. Telomeres shorten faster in the *tert* mutant hearts

To gain further insight into injury-induced and telomerase-dependent cardiomyocyte proliferation we studied cardiac telomere length dynamics upon stress caused by heart injury. Mammalian tissues require strict regulation of cell proliferation and differentiation to facilitate both tissue maintenance with normal homeostasis and efficient repair in settings of organ damage. As known from studies in mice and humans these processes are limited by progressive telomere shortening in the absence of telomerase and subsequent onset of replicative senescence (Calado & Dumitriu, 2013). It is well established that hTERT expression and telomerase activation are prerequisites to robust cellular proliferation by maintaining telomere length and genome integrity (Shay & Wright 2011). Accumulating evidence indicates that TERT in mammals may have other important functions independent of its enzymatic activity in telomere maintenance. Numerous of experiments have suggested the existence of telomere length-independent activities for telomerase in cellular transformation (Artandi et al., 2002; Gonzalez-Suarez et al., 2001; Stewart et al., 2002), proliferation (Smith et al., 2003; reviewed in Blasco, 2002; Chang & DePinho, 2002; Stampfer et al., 2001), stem-cell biology (Armstrong et al., 2005; Imamura et al., 2008; Yang et al., 2008), cell survival (Lee et al., 2008), and chromatin regulation (Masutomi et al., 2005 Galati et al., 2013; Robin et al., 2014). However, the mechanism governing this activation is not fully understood.

We found that telomerase hyperactivation after injury occurs concomitant with changes in telomere length during heart regeneration. We observed that telomeres elongate transiently in regenerating WT hearts, which affected all cardiac cell types (cardiomyocytes, epicardial and endocardial cells). In contrast telomere shortening is gradual and persists in injured *tert*$^{-/-}$ hearts. Given that longer telomeres provide an increased proliferation potential this finding is consistent with the observed sustained telomerase activity and regenerative ability of WT hearts. Furthermore, we distinguished a subpopulation of cardiomyocytes which possess very long telomeres, and thus, presumably have an extended proliferative lifespan and a higher regenerative capacity. However, the telomerase hyperactivation that takes place subsequent to injury is insufficient for the long-term maintenance of telomere reserves in regenerating myocardium. This is likely owed to successive rounds of cell division and replication-associated telomere erosion taking place during regeneration. Interestingly, in spite of the initial global telomere lengthening in cardiac cells, the subsequent telomere shortening takes place in both proliferating and non-proliferating cardiac cells in WT hearts. Moreover, we observed significant

telomere erosion in low-proliferative *tert*$^{-/-}$ hearts, suggesting the existence of an additional, replication-independent factor, likely contributing to overall telomere attrition. In support of this notion, telomere shortening after ischemic events such as MI has been reported even for post-mitotic tissues, such as the heart (Oh et al., 2003). Indeed, oxidative or mechanical stress-induced telomere shortening that is independent on cell division, has been identified as a trigger for telomere erosion (von Zglinicki, 2002; Correia-Melo et al., 2014; Kawanishi & Oikawa, 2004; Oh et al., 2003).

4. The DNA damage and senescence are likely contributors to the regenerative blockade of *tert*$^{-/-}$ zebrafish hearts.

The canonical function of telomerase is the synthesis of telomeric DNA repeats and the maintenance of the length and homeostasis of telomeres. Increasing evidence is emerging that implicates telomerase in regeneration, not only by maintaining the telomeres, but also via mechanisms independent of telomere maintenance (Cong & Shay, 2008; Martinez & Blasco, 2011). Cardiomyocytes proliferation after heart injury in *tert*$^{-/-}$ zebrafish hearts was drastically reduced. However, this was not associated with CMs enhanced apoptosis in *tert*$^{-/-}$ hearts, suggesting a decreased regenerative capacity of *tert*$^{-/-}$ CMs. The reduced proliferative potential in the *tert*$^{-/-}$ cardiomyocytes seems to be caused at least partially by activation of DNA damage checkpoints, as has been proposed previously in other cell types in mice (Sperka et al., 2012; Rossi et al., 2007; Wang et al., 2013). Eukaryotic cells respond to DNA damage by activating signaling pathways that promote cell cycle arrest and DNA repair (**Figure D 2**). Telomeres shortening or deprotection triggers a DNA damage response pathway (Collado et al. 2007) involving checkpoints in the cell cycle where transient cell cycle arrest allow sufficient time for DNA repair. Moreover if the damage is too severe this transient cell cycle arrest may become permanent (cellular senescence) (Hartwell & Weinert, 1989; Harper & Elledge, 2007). The DNA damage checkpoint results in the appearance or the maintenance of histone modifications, among them phosphorylation of histone H2AX, giving rise to a modified protein denoted here as γH2AX (Clémenson & Marsolier-Kergoat, 2009). Injury-induced fast proliferating cardiac cells might be more sensitive to the consequences of DNA damage checkpoint activation. We demonstrated that although WT and *tert*$^{-/-}$ uninjured hearts presented some initial levels of DNA damage spread out globally within the ventricles, the levels were already elevated in *tert*$^{-/-}$ hearts.

This latter observation was strengthened by the finding that a heart injury promotes further phosphorylation of histone H2AX only in the *tert*$^{-/-}$ hearts. Telomerase deficiency led to an increase in number of cardiac cells presenting DNA damage upon injury. Despite the fact that WT animals did not significantly increase the total number of cardiac cells with DNA damage, the number of γH2AX positive cardiomyocytes significantly increased, suggesting that this population of cardiac cells were particularly susceptible to the injury-induced H2AX phoshorylation.

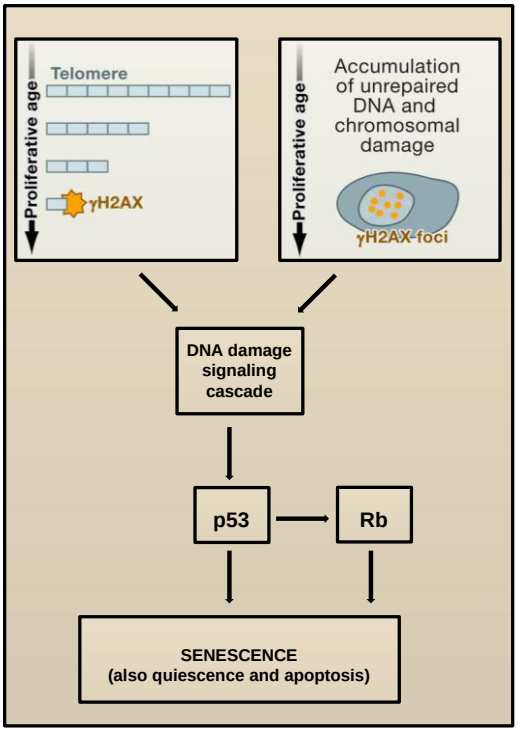

Figure D 2: **"Hayflick Factors" Record the Proliferative History of Cells and Tissues.**Telomere shortening and accumulation of DNA damage summarized together with their main effectors, the tumor suppressors p53 and retinoblastoma (Rb). Modified from Collado et al., 2007.

Based on the analysis of correlation between proliferation marker (BrdU) and a marker of DNA damage (γH2AX), our study shows that the DNA damage response limits the proliferative capacity of the cell. We demonstrate that only a minority of BrdU+ cells were also γH2AX+, both in wildtype and *tert* mutant hearts. This result is an indirect indication that the DNA damage response pathway is important for limiting cell proliferation, supporting the working model that

the increase in DNA damage found in *tert* mutant hearts leads to an arrest in cell cycle progression. In support of our data, we found that there was a significant decrease in expression of genes from the Cell Cycle KEGG (Kyoto Encyclopedia of Genes and Genomes) pathway in *tert*$^{-/-}$ vs wildtype hearts.

During the initial phase of the regeneration process (3 dpi) elevated levels of DNA damage did not correlate with telomere shortening and only around 0.2% of total damage on all cardiac cells (4-12% on CMs) correlated with telomere induced foci (TIFs) in *tert*$^{-/-}$ hearts. Downstream components of the DNA damage response (DDR) in mammals, such as p53 and H2AX, have not been found to have a major impact on telomere length regulation (Chin et al., 1999; Fernandez-Capetillo et al., 2003). This suggests that the DNA damage response in telomerase deficient zebrafish hearts is initially not related to short or dysfunctional telomeres, pointing to other uncharacterized *tert*-dependent activities as a source for DNA protection from damage. Moreover telomere shortening might be a consequence rather than a cause of DNA damage. We cannot exclude the scenario that accelerated telomeres shortening in the absence of telomerase is an important contributor to DNA damage at a later stage of the regeneration process.

Telomere dysfunction inducing a persistent DDR is a major cause of cellular senescence (d'Adda di Fagagna et al., 2003). Severe telomere dysfunction is induced by telomere shortening in late-generation telomerase *Terc*$^{-/-}$ knockout mice, where it compromises the function of tissue-specific stem and progenitor cells thus limits regenerative capacity (Choudhury et al., 2007). However, telomere shortening is just one mechanism that causes telomere dysfunction. Senescent cells harbouring dysfunctional telomeres, which are recognized by persistent telomere-associated DNA damage foci, accumulate even in tissues of ageing mice with long telomeres, suggesting that telomere dysfunction may contribute to age-related decline in tissue function and regeneration during normal ageing of mice (Hewitt et al., 2012).

We demonstrated an injury-triggered senescence response (permanent cell cycle arrest) occurred regardless of the absence of telomerase. Using a senescence-associated β-galactosidase assay we detected senescent cells in WT hearts at 3 and 7 dpi, albeit at lower levels than their *tert*$^{-/-}$ siblings. In WT hearts senescence signals were almost exclusively limited to the injured zone, whereas in injured *tert*$^{-/-}$ hearts the signal was distributed more broadly, extending beyond the injury area and border zone to remote regions of the ventricle, consistent with the organ-wide

deficit of proliferating *tert*$^{-/-}$ cardiac cells. However, senescence is not only a cell-autonomous process. By secreting bioactive molecules including interleukins, numerous cytokines, chemokines, growth factors and proteases (Acosta et al., 2008; Rodier et al., 2009) senescent cells induce powerful bystander effects that spread senescence to the neighboring normal cells (Nelson et al., 2012; Acosta et al., 2013). Given that senescence associated secretory phenotype (SASP) signals are higher in *tert*$^{-/-}$ hearts (data not shown), we hypothesized that these cells, when senescent, might exert a stronger bystander effect. We tested senescence by beta-Gal staining. Based on our findings we speculated that loss of *tert* activity reinforces cellular senescence by both autocrine and paracrine signaling and thus impairs proliferation. We therefore expected faster accumulation of senescent cells in hearts from *tert*$^{-/-}$ fish. In this context, it is interesting to discuss the beneficial/detrimental effects of the senescence associated secreting phenotype (SASP) (Campisi et al., 2013; Munoz-Espin & Serrano, 2014). However this findings need further investigation. A possible function of the SASP may be to ensure that damaged cells communicate their compromised state to surrounding cells to prepare the tissue for repair and stimulating immune system for their clearance. The cytokine response might also function in a paracrine manner to suppress or promote the proliferation of neighboring cells in damaged tissues upon injury. While this may provide a plausible explanation for an activation of the regenerative processes in the wild-type setting, cell with a limited telomere reserve in *tert*$^{-/-}$ may just not be able to respond to these signals.

5. Implications of our findings

Our findings may have implications for human health in the context of cardiac diseases. Our finding that *tert* activity is required to promote regeneration and cardiomyocyte proliferation is proof of concept that maybe in the future this knowledge can be exploited for the development of therapeutic strategies in human heart failure. Further investigation is warranted, addressing for example the cardiac cell type including myocytes in which *tert* activity is necessary during heart regeneration. To this end, inducible lines using the Cre/lox technology to specifically overexpress or downregulate *tert* in different cell types may be used. Alternatively, crossing inducible *tert* gain of function lines in cardiomyocytes, endocardial or epicardial cells is a valid strategy to further study the *tert's* effect on regeneration.

CONCLUSIONS

The results obtain in this work lead to the following conclusions:

1. Absence of telomerase activity impairs zebrafish heart regeneration.

2. Telomerase hyperactivation is an early event during zebrafish heart regeneration.

3. Injury-induced hyperactivation of telomerase triggers global telomere elongation in the zebrafish heart.

4. Telomeres reserves cannot be maintained without telomerase under the high demands triggered upon heart insult.

5. Long telomeres support robust cardiomyocyte proliferation.

6. *tert* protects cardiac cells from DNA damage and senescence not only upon cardiac injury but also during homeostasis.

CONCLUSIONES

Los resultados obtenidos en esta tesis nos llevan a las siguientes conclusiones:

1. La ausencia de telomerasa afecta a la regeneración cardiaca en el pez cebra.

2. La criolesión cardiaca en el pez cebra provoca un aumento de la actividad telomerasa.

3. El incremento en la actividad telomerasa causado por la lesión provoca un alargamiento de los telómeros en el corazón del pez cebra.

4. Las reservas teloméricas no pueden mantenerse sin telomerasa tras la lesión cardiaca.

5. Los telómeros largos son necesarios para la correcta proliferación de los cardiomiocitos

6. Tert protege a las células del corazón del pez cebra del daño al ADN y de la senescencia no sólo tras una lesión cardiaca, sino también durante la homeostasis.

BIBLIOGRAPHY

Acosta JC, O'Loghlen A, Banito A, Guijarro MV, Augert A, Raguz S, Fumagalli M, Da Costa M, Brown C, Popov N, Takatsu Y, Melamed J, d'Adda di Fagagna F, Bernard D, Hernando E, Gil J. (2008). Chemokine signaling via the CXCR2 receptor reinforces senescence. Cell.;133(6):1006-18.

Acosta JC, Banito A, Wuestefeld T, Georgilis A, Janich P, Morton JP, Athineos D, Kang TW, Lasitschka F, Andrulis M, Pascual G, Morris KJ, Khan S, Jin H, Dharmalingam G, Snijders AP, Carroll T, Capper D, Pritchard C, Inman GJ, Longerich T, Sansom OJ, Benitah SA, Zender L, Gil J. (2013). A complex secretory program orchestrated by the inflammasome controls paracrine senescence. Nat Cell Biol.;15(8):978-90.

Ahuja P., Sdek P., MacLellan W.R. (2007). Cardiac myocyte cell cycle control in development, disease, and regeneration. Physiol Rev.;87(2):521-44.

Ambrus A, Chen D, Dai J, Bialis T, Jones RA, Yang D. (2006). Human telomeric sequence forms a hybrid-type intramolecular G-quadruplex structure with mixed parallel/antiparallel strands in potassium solution. Nucleic Acids Res. 34(9):2723-35.

Anchelin, M., Alcaraz-Pérez, F., Martínez, C.M., Bernabé-García, M., Mulero, V., and Cayuela, M.L. (2013). Premature aging in telomerase-deficient zebrafish. In Dis Model Mech, pp. 1101-1112.

Anchelin, M., Murcia, L., Alcaraz-Pérez, F., García-Navarro, E.M., and Cayuela, M.L. (2011). Behaviour of telomere and telomerase during aging and regeneration in zebrafish. In PloS one, pp. e16955.

Anversa, P., Kajstura, J., Olivetti, G. (1996) Myocyte death in heart failure. Curr. Opin. Cardiol. 11, 245-251.

Arends, M. J. Wyllie, A. H. (1991) Apoptosis: mechanisms and roles in pathology. Int. Rev. Exp. Pathol. 32, 223-254.

Armanios MY, (2007) Telomerase mutations in families with idiopathic pulmonary fibrosis. N. Engl. J. Med. 356:1317–1326.

Armanios M, Blackburn EH. (2012). The telomere syndromes. Nat Rev Genet. 13(10):693-704.

Armstrong L, Saretzki G, Peters H, Wappler I, Evans J, Hole N, von Zglinicki T, Lako M. (2005). Overexpression of telomerase confers growth advantage, stress resistance, and enhanced differentiation of ESCs toward the hematopoietic lineage. Stem Cells. 2005; 23:516–529.

Artandi SE, Steven E. Artandi, Scott Alson, Maja K. Tietze, Norman E. Sharpless, Siqin Ye, Roger A. Greenberg, Diego H. Castrillon, James W. Horner, Sarah R. Weiler, Ruben D. Carrasco, Ronald A. DePinho (2002). Constitutive telomerase expression promotes mammary carcinomas in aging mice. Proc Natl Acad Sci USA; 99:8191–8196

Aurora, A.B., Porrello, E.R., Tan, W., Mahmoud, A.I., Hill, J.A., Bassel-Duby, R., Sadek, H.A., and Olson, E.N. (2014). Macrophages are required for neonatal heart regeneration. The Journal of clinical investigation 124, 1382-1392.

Bakkers, J. (2011). Zebrafish as a model to study cardiac development and human cardiac disease. Cardiovasc Res 91, 279–288.

Bär C, Bernardes de Jesus B, Serrano R, Tejera A, Ayuso E, Jimenez V, Formentini I, Bobadilla M, Mizrahi J, de Martino A, Gomez G, Pisano D, Mulero F, Wollert KC, Bosch F, Blasco MA. (2014). Telomerase expression confers cardioprotection in the adult mouse heart after acute myocardial infarction. Nat. Commun 18; 5:5863.

Bekaert S., Derradji H., Baatout S. (2004). Telomere biology in mammalian germ cells and during development. Dev Biol. 274(1):15-30.

Behrens, A., van Deursen, J.M., Rudolph, K.L., and Schumacher, B. (2014). Impact of genomic damage and ageing on stem cell function. Nature cell biology *16*, 201-207.

Beltrami, A. P., Urbanek, K., Kajstura, J., Yan, S. M., Finato, N., Bussani, R., Nadal-Ginard, B., Silvestri, F., Leri, A., Beltrami, C. A., et al. (2001). Evidence that human cardiac myocytes divide after myocardial infarction. N Engl J Med 344, 1750–1757.

Benjamini, Y., and Hochberg, Y. (1995). Controlling the false discovery rate: a practical and powerful approach to multiple testing. In Journal of the Royal Statistical Society Series B pp. 289-300.

Bergmann, O., Bhardwaj, R.D., Bernard, S., Zdunek, S., Barnabé-Heider, F., Walsh, S., Zupicich, J., Alkass, K., Buchholz, B.A., Druid, H., *et al.* (2009). Evidence for cardiomyocyte renewal in humans. In Science, pp. 98-102.

Bernhardt, R R ., Tongiorgi, E ., Anzini, P ., Schachner, M (1996) Increased expression of specific recognition molecules by retinal ganglion cells and by optic pathway glia accompanies the successful regeneration of retinal axons in adult zebrafish. J Comp Neurol. 1996 Dec 9;376(2):253-64.

Bilousova G, Marusyk A, Porter CC, Cardiff RD, DeGregori J. (2005). Impaired DNA Replication within Progenitor Cell Pools Promotes Leukemogenesis. PLoS Biol. 3(12):e401.

Blasco M. (2002). Telomerase beyond telomeres. Review, Nature Reviews Cancer 2, 627-633.

Calado R.T., Dumitriu B. (2013). Telomere dynamics in mice and humans. Semin Hematol. 50(2): 165-174.

Caldecott KW. (2008). Single-strand break repair and genetic disease. Nat Rev Genet. 9(8):619-31. doi: 10.1038/nrg2380.

Campisi J. (2013). Aging, cellular senescence, and cancer. Annu Rev Physiol.;75:685-705.

Carmona, R., Macías, D., Guadix, J. A., Portillo, V., Pérez-Pomares, J. M. and Munoz-Chapuli,

R. (2007). A simple technique of image analysis for specific nuclear immunolocalization of proteins. J Microsc 225, 96–99.

Caulfield, J. B., Leinbach, R. and Gold, H. (1976). The relationship of myocardial infarct size and prognosis. Circulation 53, I141–4.

Chablais, F., Veit, J., Rainer, G., and Jaźwińska, A. (2011). The zebrafish heart regenerates after cryoinjury-induced myocardial infarction. In BMC Dev Biol, pp. 21. Couzin-Frankel, J. (2014). The elusive heart fix. In Science, pp. 252-257.

Chang, S. & DePinho, R.A. (2002). Telomerase extracurricular activities. Proc. Natl Acad. Sci. USA 99, 12520–12522.

Chen, J.L. & Greider, C.W. (2004). Telomerase RNA structure and function: implications for dyskeratosis congenita. Trends Biochem. Sci. 29, 183−192.

Chin L, Artandi SE, Shen Q, Tam A, Lee SL, Gottlieb GJ, Greider CW, DePinho RA. (1999). p53 deficiency rescues the adverse effects of telomere loss and cooperates with telomere dysfunction to accelerate carcinogenesis. Cell.;97(4):527-38.

Choi, W.-Y. and Poss, K. D. (2012). Cardiac regeneration. Curr. Top. Dev. Biol. 100, 319–344.

Choudhury AR, Ju Z, Djojosubroto MW, Schienke A, Lechel A, Schaetzlein S, Jiang H, Stepczynska A, Wang C, Buer J, Lee HW, von Zglinicki T, Ganser A, Schirmacher P, Nakauchi H, Rudolph KL. (2007). Cdkn1a deletion improves stem cell function and lifespan of mice with dysfunctional telomeres without accelerating cancer formation. Nat Genet.;39(1):99-105.

Ciccia A, Elledge SJ. (2010). The DNA Damage Response: Making it safe to play with knives. Mol Cell. 40(2):179-204.

Clémenson C, Marsolier-Kergoat MC. (2009). DNA damage checkpoint inactivation: adaptation and recovery. DNA Repair (Amst). 8(9):1101-9.

Collado M, Blasco MA, Serrano M. (2007). Cellular senescence in cancer and aging. Cell.;130(2):223-33.

Cong Y, Shay JW. (2008). Actions of human telomerase beyond telomeres. Cell Res. 18(7):725-32.

Cong YS, Wright WE, Shay JW. (2002). Human Telomerase and Its Regulation Microbiol Mol Biol Rev. 66(3):407-25.

Correia-Melo C., Hewitt G., Passos J.F. (2014). Telomeres, oxidative stress and inflammatory factors: partners in cellular senescence? Longev Healthspan; 3: 12046-2395.

d'Adda di Fagagna, F., Reaper, P.M., Clay-Farrace, L., Fiegler, H., Carr, P., Von Zglinicki, T., Saretzki, G., Carter, N.P., and Jackson, S.P. (2003). A DNA damage checkpoint response in telomere-initiated senescence. In Nature, pp. 194-198.

Diep, C. Q., Ma, D., Deo, R. C., Holm, T. M., Naylor, R. W., Arora, N., Wingert, R. A., Bollig, F., Djordjevic, G., Lichman, B., et al. (2011). Identification of adult nephron progenitors capable of kidney regeneration in zebrafish. Nature 470, 95–100.

Díez, J., Querejeta, R., López, B., González, A., Larman, M. and Martínez Ubago, J. L. (2002). Losartan-dependent regression of myocardial fibrosis is associated with reduction of left ventricular chamber stiffness in hypertensive patients. Circulation 105, 2512–2517.

Donate LE, Blasco MA (2011).Telomeres in cancer and ageing. Philos T Roy Soc B 366, 76-84.

Evans, M.A., Smart, N., Dube, K.N., Bollini, S., Clark, J.E., Evans, H.G., Taams, L.S., Richardson, R., Levesque, M., Martin, P., *et al.* (2013). Thymosin beta4-sulfoxide attenuates inflammatory cell infiltration and promotes cardiac wound healing. Nature communications *4*, 2081.

Fan, D., Takawale, A., Lee, J. and Kassiri, Z. (2012). Cardiac fibroblasts, fibrosis and extracellular matrix remodeling in heart disease. Fibrogenesis Tissue Repair 5, 15.

Fang, Y., Gupta, V., Karra, R., Holdway, J.E., Kikuchi, K., and Poss, K.D. (2013). Translational profiling of cardiomyocytes identifies an early Jak1/Stat3 injury response required for zebrafish heart regeneration.

Fernandez-Capetillo O, Liebe B, Scherthan H, Nussenzweig A. (2003). H2AX regulates meiotic telomere clustering. J Cell Biol.;163(1):15-20.

Flores, I., and Blasco, M.A. (2010). The role of telomeres and telomerase in stem cell aging. In FEBS Lett, pp. 3826-3830.

Flores, I., Canela, A., Vera, E., Tejera, A., Cotsarelis, G., and Blasco, M.A. (2008). The longest telomeres: a general signature of adult stem cell compartments. In Genes Dev, pp. 654-667.

Flores, I., Cayuela, M.L., and Blasco, M.A. (2005). Effects of telomerase and telomere length on epidermal stem cell behavior. In Science, pp. 1253-1256.

Forsyth, N.R., Wright, W.E., and Shay, J.W. (2002). Telomerase and differentiation in multicellular organisms: turn it off, turn it on, and turn it off again. In Differentiation, pp. 188-197.

Frangogiannis, N. G. (2006). The mechanistic basis of infarct healing. Antioxid. Redox Signal. 8, 1907–1939.

Frangogiannis, N. G. (2012). Regulation of the Inflammatory Response in Cardiac Repair. Circulation Research 110, 159–173.

Frangogiannis, N.G. (2014). The inflammatory response in myocardial injury, repair, and remodelling. Nature reviews Cardiology *11*, 255-265.

Galati A, Micheli E, Cacchione S. (2013). Chromatin Structure in Telomere Dynamics. Front Oncol. 7;3:46.

Gamba L, Harrison M, Lien CL. (2014). Cardiac regeneration in model organisms. Curr Treat Options Cardiovasc Med. 2014 Mar;16(3):288.

Gemberling, M., Bailey, T.J., Hyde, D.R., and Poss, K.D. (2013). The zebrafish as a model for complex tissue regeneration. In Trends Genet, pp. 611-620.

Gobbini E., Trovesi C., Cassani C., Longhese M.P. (2014). Telomere uncapping at the crossroad between cell cycle arrest and carcinogenesis. Molecular and Cellular Oncology 1, e29901;

González-Rosa, J.M., Guzman-Martinez, G., Marques, I.J., Sanchez-Iranzo, H., Jimenez-Borreguero, L.J., and Mercader, N. (2014). Use of echocardiography reveals reestablishment of ventricular pumping efficiency and partial ventricular wall motion recovery upon ventricular cryoinjury in the zebrafish. PloS one *9*, e115604.

González-Rosa, J.M., Martín, V., Peralta, M., Torres, M., and Mercader, N. (2011). Extensive scar formation and regression during heart regeneration after cryoinjury in zebrafish. In Development, pp. 1663-1674.

González-Rosa, J.M., and Mercader, N. (2012). Cryoinjury as a myocardial infarction model for the study of cardiac regeneration in the zebrafish. In Nature Protocols, pp. 782-788.

Gonzalez-Suarez E, Samper E, Ramírez A, Flores JM, Martín-Caballero J, Jorcano JL, Blasco MA. (2001). Increased epidermal tumors and increased skin wound healing in transgenic mice overexpressing the catalytic subunit of telomerase, mTERT, in basal keratinocytes. EMBO J.; 20:2619–2630.

Greider, C.W., Blackburn, E.H. (1985). Identification of a specific telomere terminal transferase activity in Tetrahymena extracts. Cell, pp. 405-413.

Grimes A., Chandra S.B.C. (2009). Significance of cellular senescence in aging and cancer. Cancer Res Treat. 41(4):187-195.

Greenberg RA, Allsopp RC, Chin L, Morin GB, DePinho RA. (1998). Expression of mouse telomerase reverse transcriptase during development, differentiation and proliferation. Oncogene. 16(13):1723-30.

Gut, P., Baeza-Raja, B., Andersson, O., Hasenkamp, L., Hsiao, J., Hesselson, D., Akassoglou, K., Verdin, E., Hirschey, M. D. and Stainier, D. Y. R. (2013). Whole-organism screening for gluconeogenesis identifies activators of fasting metabolism. Nat Chem Biol 9, 97–104.

Hahn WC, (1999) Inhibition of telomerase limits the growth of human cancer cells. Nat. Med. 5:1164–1170.

Harper JW, Elledge SJ. (2007). The DNA damage response: ten years after. Mol Cell.;28(5):739-45.

Harris JA, Cheng AG, Cunningham LL, MacDonald G, Raible DW, Rubel EW. (2003). Neomycin-induced hair cell death and rapid regeneration in the lateral line of zebrafish (Danio rerio). J Assoc Res Otolaryngol. 4(2):219-34.

Hartwell LH, Weinert TA. (1989). Checkpoints: controls that ensure the order of cell cycle events. Science.;246(4930):629-34.

Henriques, C.M., Carneiro, M.C., Tenente, I.M., Jacinto, A., and Ferreira, M.G. (2013). Telomerase is required for zebrafish lifespan. In PLoS Genet, pp. e1003214.

Herbert, B.-S., Hochreiter, A.E., Wright, W.E., and Shay, J.W. (2006). Nonradioactive detection of telomerase activity using the telomeric repeat amplification protocol. In Nature Protocols, pp. 1583-1590.

Heusch, G. (2004). Myocardial hibernation: a delicate balance. In AJP: Heart and Circulatory Physiology, pp. H984-H999.

Hewitt G, Jurk D, Marques FD, Correia-Melo C, Hardy T, Gackowska A, Anderson R, Taschuk M, Mann J, Passos JF. (2012). Telomeres are favoured targets of a persistent DNA damage response in ageing and stress-induced senescence. Nat Commun.;3:708.

Howe K, Clark MD, Torroja CF, Torrance J, Berthelot C, Muffato M, Collins JE, Humphray S, McLaren K, Matthews L, McLaren S, Sealy I, Caccamo M, Churcher C, Scott C, Barrett JC, Koch R, Rauch GJ, White S, Chow W, Kilian B, Quintais LT, Widaa S, Langford C, Yang F, Schuster SC, Carter NP, Harrow J, Ning Z, Herrero J, Searle SM, Enright A, Geisler R, Plasterk RH, Lee C, Westerfield M, de Jong PJ, Zon LI, Postlethwait JH, Nüsslein-Volhard C, Hubbard TJ, Roest Crollius H, Rogers J, Stemple DL. (2013). The zebrafish reference genome sequence and its relationship to the human genome. Nature; 496(7446):498-503.

Hu, N., Yost, H. J. and Clark, E. B. (2001). Cardiac morphology and blood pressure in the adult zebrafish. Anat Rec 264, 1–12.

Huang, C.J., Tu, C.T., Hsiao, C.D., Hsieh, F.J., and Tsai, H.J. (2003). Germ-line transmission of a myocardium-specific GFP transgene reveals critical regulatory elements in the cardiac myosin light chain 2 promoter of zebrafish. Developmental dynamics : an official publication of the American Association of Anatomists 228, 30-40.

Hsieh, P. C. H., Segers, V. F. M., Davis, M. E., MacGillivray, C., Gannon, J., Molkentin, J. D., Robbins, J. and Lee, R. T. (2007). Evidence from a genetic fate-mapping study that stem cells refresh adult mammalian cardiomyocytes after injury. Nat. Med. 13, 970–974.

Hwang, W. Y., Fu, Y., Reyon, D., Maeder, M. L., Tsai, S. Q., Sander, J. D., Peterson, R. T., Yeh, J.-R. J. and Joung, J. K. (2013). Efficient genome editing in zebrafish using a CRISPR-Cas system. Nature Biotechnology 1–3.

Imamura, S., Uchiyama, J., Koshimizu, E., Hanai, J., Raftopoulou, C., Murphey, R.D., Bayliss, P.E., Imai, Y., Burns, C.E., Masutomi, K. (2008). A noncanonical function of zebrafish telomerase reverse transcriptase is required for developmental hematopoiesis. PloS one *3*, e3364.

Itou, J., Akiyama, R., Pehoski, S., Yu, X., Kawakami, H., and Kawakami, Y. (2014). Regenerative responses after mild heart injuries for cardiomyocyte proliferation in zebrafish. Developmental dynamics: an official publication of the American Association of Anatomists 243, 1477-1486.

Itou, J., Kawakami, H., Burgoyne, T., and Kawakami, Y. (2012). Life-long preservation of the regenerative capacity in the fin and heart in zebrafish. In Biology open (Company of Biologists), pp. 739-746.

Jennings, R. B., Murry, C. E., Steenbergen, C. and Reimer, K. A. (1990). Development of cell injury in sustained acute ischemia. Circulation 82, II2–12.

Jesty, S. A., Steffey, M. A., Lee, F. K., Breitbach, M., Hesse, M., Reining, S., Lee, J. C., Doran, R. M., Nikitin, A. Y., Fleischmann, B. K., et al. (2012). c-kit+ precursors support postinfarction myogenesis in the neonatal, but not adult, heart. Proc Natl Acad Sci USA 109, 13380–13385.

Jiang H., Ju Z., Rudolph K.L. (2007). Telomere shortening and ageing. Gerontol Geriat 40:314-324.

Johnson SL, Weston JA. (1995). Temperature-sensitive mutations that cause syage-specific defects in Zebrafish fin regeneration. Genetics, 141(4):1583-95.

Jopling, C., Sleep, E., Raya, M., Martí, M., Raya, A., and Izpisua Belmonte, J.C. (2010). Zebrafish heart regeneration occurs by cardiomyocyte dedifferentiation and proliferation. In Nature, pp. 606-609.

Joung, J. K. and Sander, J. D. (2013). TALENs: a widely applicable technology for targeted genome editing. Nature Reviews Molecular Cell Biology 14, 49–55.

Kajstura, J., Urbanek, K., Perl, S., Hosoda, T., Zheng, H., Ogórek, B., Ferreira-Martins, J., Goichberg, P., Rondon-Clavo, C., Sanada, F., et al. (2010). Cardiomyogenesis in the adult human heart. Circulation Research 107, 305–315.

Kawanishi S, Oikawa S. (2004). Mechanism of telomere shortening by oxidative stress. Ann N Y Acad Sci.;1019:278-84.

Kikuchi, K., Holdway, J.E., Major, R.J., Blum, N., Dahn, R.D., Begemann, G., and Poss, K.D. (2011). Retinoic acid production by endocardium and epicardium is an injury response essential for zebrafish heart regeneration. In Developmental cell, pp. 397-404.

Kikuchi, K., Holdway, J.E., Werdich, A.A., Anderson, R.M., Fang, Y., Egnaczyk, G.F., Evans, T., MacRae, C.A., Stainier, D.Y.R., and Poss, K.D. (2010). Primary contribution to zebrafish heart regeneration by gata4+ cardiomyocytes. In Nature, pp. 601-605.

Kikuchi, K., and Poss, K.D. (2012). Cardiac regenerative capacity and mechanisms. In Annu Rev Cell Dev Biol, pp. 719-741.

Kim NW, (1994) Specific association of human telomerase activity with immortal cells and cancer. Science 266:2011–2015.

Kipling, D., Cook, H.J. (1990). Hypervariable ultra-long telomeres in mice. Nature, 347, 400-402.

Kishi S., Uchiyama J., Baughman A.M., Goto T., Lin M. C., Tsai S.B. (2003). The zebrafish as a vertebrate model of functional aging and very gradual senescence. Exp.Gerontol. 38(7):777-86.

Kroehne, V., Freudenreich, D., Hans, S., Kaslin, J. and Brand, M. (2011). Regeneration of the adult zebrafish brain from neurogenic radial glia-type progenitors. Development 138, 4831–4841.

Laflamme, M. A. and Murry, C. E. (2011). Heart regeneration. Nature 473, 326–335.

Lawson, N.D., and Weinstein, B.M. (2002). In vivo imaging of embryonic vascular development using transgenic zebrafish. Developmental biology *248*, 307-318.

Lee HW, et al. Essential role of mouse telomerase in highly proliferative organs. Nature. 1998;392:569–574.

Lee J, Sung YH, Cheong C, Choi YS, Jeon HK, Sun W, Hahn WC, Ishikawa F, Lee HW. TERT promotes cellular and organismal survival independently of telomerase activity. Oncogene. 2008;27:3754–3760.

Leeder S, et al. A Race Against Time: The Challenge of Cardiovascular Disease in Developing Countries. New York: Trustees of Columbia University; 2004.

Lepilina, A., Coon, A.N., Kikuchi, K., Holdway, J.E., Roberts, R.W., Burns, C.G., and Poss, K.D. (2006). A dynamic epicardial injury response supports progenitor cell activity during zebrafish heart regeneration. In Cell, pp. 607-619.

Li, B., and Dewey, C.N. (2011). RSEM: accurate transcript quantification from RNASeq data with or without a reference genome. In BMC Bioinformatics, pp. 323.

Lien, C.-L., Schebesta, M., Makino, S., Weber, G. J. and Keating, M. T. (2006). Gene expression analysis of zebrafish heart regeneration. PLoS Biol 4, e260.

Lie-Venema, H., van den Akker, N. M. S., Bax, N. A. M., Winter, E. M., Maas, S., Kekarainen, T., Hoeben, R. C., deRuiter, M. C., Poelmann, R. E. and Gittenberger-de Groot, A. C. (2007). Origin, fate, and function of epicardium-derived cells (EPDCs) in normal and abnormal cardiac development. ScientificWorldJournal 7, 1777–1798.

Lieschke G.J., Currie P.D. (2007). Animal models of human disease: zebrafish swim into view. Nature Reviews Genetics 8, 353-367.

Lin J., Epel E., Blackburn E. (2012). Telomeres and lifestyle factors: roles in cellular senescence. Mutat Res 730(1-2):85-9.

Loeb L.A. (2011). Human cancers express mutator phenotypes: origin, consequences and targeting. Nat Rev Cancer.11(6): 450-457.

Loffredo, F. S., Steinhauser, M. L., Gannon, J. and Lee, R. T. (2011). Bone marrow-derived cell therapy stimulates endogenous cardiomyocyte progenitors and promotes cardiac repair. Cell Stem Cell 8, 389–398.

Londoño-Vallejo JA, DerSarkissian H, Cazes L, Thomas G. (2001). Differences in telomere length between homologous chromosomes in humans. Nucleic Acids Res. 29(15):3164-71.

Lopez AD, Mathers CD, Ezzati M, Jamison DT, editors. Global Burden of Disease and Risk Factors. ed. D.C.P. Project. New York, NY: The World Bank and Oxford University Press; 2006. p. 552.

Lund, T.C., Glass, T.J., Tolar, J., and Blazar, B.R. (2009). Expression of telomerase and telomere length are unaffected by either age or limb regeneration in Danio rerio. In PloS one, pp. e7688.

Maicher A, Kastner L, Luke B. (2012). Telomeres and disease: enter TERRA. RNA Biol. 9(6):843-9.

Mallo, M., Schrewe, H., Martin, J.F., Olson, E.N., and Ohnemus, S. (2000). Assembling a functional tympanic membrane: signals from the external acoustic meatus coordinate development of the malleal manubrium. In Development, pp. 4127-4136.

Martin, M. (2011). Cutadapt removes adapter sequences from high-throughput sequencing reads. In EMBnet j, pp. pp. 10-12.

Martínez P, Blasco MA. (2011). Telomeric and extra-telomeric roles for telomerase and the telomere-binding proteins. Nat Rev Cancer. 11(3):161-76.

Masutomi K, Possemato R, Wong J.M.Y., Currier J.L., Tothova Z., Manola J.B., Ganesan S., Lansdorp P.M., Collins K., Hahn W.C. (2005). The telomerase reverse transcriptase regulates chromatin state and DNA damage responses. Proc Natl Acad Sci USA ;102:8222–8227.

McClintock, B. (1941). "The stability of broken ends of chromosomes in Zea mays." Genetics 26:234-282.

Mollova, M., Bersell, K., Walsh, S., Savla, J., Das, L.T., Park, S.-Y., Silberstein, L.E., dos Remedios, C.G., Graham, D., Colan, S., *et al.* (2013). Cardiomyocyte proliferation contributes to heart growth in young humans. In Proc Natl Acad Sci USA, pp. 1446-1451.

Morrison S.J., Prowse K.R., Ho P., Weissman I.L. (1996). Telomerase activity in hematopoietic cells is associated with self-renewal potential. Immunity. 5(3):207-16.

Moss JB, Koustubhan P, Greenman M, Parsons MJ, Walter I, Moss LG.(2009). Regeneration of the pancreas in adult zebrafish. Diabetes. 2009 Aug;58(8):1844-51.

Mozaffarian D, Benjamin EJ, Go AS, Arnett DK, Blaha MJ, Cushman M, de Ferranti S, Després JP, Fullerton HJ, Howard VJ, Huffman MD, Judd SE, Kissela BM, Lackland DT, Lichtman JH, Lisabeth LD, Liu S, Mackey RH, Matchar DB, McGuire DK, Mohler ER 3rd, Moy CS, Muntner P, Mussolino ME, Nasir K, Neumar RW, Nichol G, Palaniappan L, Pandey DK, Reeves MJ, Rodriguez CJ, Sorlie PD, Stein J, Towfighi A, Turan TN, Virani SS, Willey JZ, Woo D, Yeh RW, Turner MB; American Heart Association Statistics Committee and Stroke Statistics Subcommittee. (2015). Heart disease and stroke statistics—2015 update: a report from American Heart Association. Circulation. 27;131(4):e29-322.

Muller, H. J. (1938). The remaking of chromosomes. The Collecting Net 13, 181-195,198.

Mummery, C.L., and Lee, R.T. (2013). Is heart regeneration on the right track? In Nature Medicine, pp. 412-413.

Muñoz-Espín D, Serrano M. (2014). Cellular senescence: from physiology to pathology. Nat Rev Mol Cell Biol.;15(7):482-96.

Murry, C. E., Reinecke, H. & Pabon, L. M. (2006). Regeneration gaps: observations on stem cells and cardiac repair. J. Am. Coll. Cardiol. 47, 1777–1785.

Nelson ND, Bertuch AA. (2012). Dyskeratosis congenita as a disorder of telomere maintenance. Mutat Res. 730(1-2):43-51.

North, T. E., Goessling, W., Walkley, C. R., Lengerke, C., Kopani, K. R., Lord, A. M., Weber, G.J., Bowman, T. V., Jang, I.-H., Grosser, T., et al. (2007). Prostaglandin E2 regulates vertebrate haematopoietic stem cell homeostasis. *Nature* 447, 1007–1011.

Ogami M, Ikura Y, Ohsawa M, Matsuo T, Kayo S, Yoshimi N, Hai E, Shirai N, Ehara S, Komatsu R, Naruko T, Ueda M. (2004). Telomere shortening in human coronary artery diseases. Arterioscler Thromb Vasc Biol. 24(3):546-50.

Oh H., Taffet G. E., Youker K.A., Entman M.L., Overbeek P.A., Michael L.H., Schneider M.D., (2001). Telomerase Reverse Transcriptase Promotes Cardiac Muscle Cell Proliferation, Hypertrophy, and Survival. Proc Natl Acad Sci USA. 98(18):10308-13.

Oh, H., Wang, S.C., Prahash, A., Sano, M., Moravec, C.S., Taffet, G.E., Michael, L.H., Youker, K.A., Entman, M.L., and Schneider, M.D. (2003). Telomere attrition and Chk2 activation in human heart failure. In Proc Natl Acad Sci USA, pp. 5378-5383.

Olivetti, G., Capasso, J. M., Sonnenblick, E. H. and Anversa, P. (1990). Side-to-side slippage of myocytes participates in ventricular wall remodeling acutely after myocardial infarction in rats. Circulation Research 67, 23–34.

Olovnikov, A. M. (1973). A theory of marginotomy. J. Theor. Biol. 41, 181-190.

Parente, V., Balasso, S., Pompilio, G., Verduci, L., Colombo, G.I., Milano, G., Guerrini, U., Squadroni, L., Cotelli, F., Pozzoli, O., et al. (2013). Hypoxia/reoxygenation cardiac injury and regeneration in zebrafish adult heart. In PloS one, pp. e53748.

Parrinello S, Coppe JP, Krtolica A, Campisi J. (2005). Stromal-epithelial interactions in aging and cancer: senescent fibroblasts alter epithelial cell differentiation. J Cell Sci. 118(Pt 3):485-96.

Passos JF, Saretzki G, von Zglinicki T. (2007). DNA damage in telomeres and mitochondria during cellular senescence: is there a connection? Nucleic Acids Res. 35(22):7505-13.

Pasumarthi KB, Field LJ. (2002). Cardiomyocyte cell cycle regulation. Circ Res. 90(10):1044-54. Review.

Pieperhoff, S., Wilson, K.S., Baily, J., de Mora, K., Maqsood, S., Vass, S., Taylor, J., Del-Pozo, J., MacRae, C.A., Mullins, J.J., *et al.* (2014). Heart on a plate: histological and functional assessment of isolated adult zebrafish hearts maintained in culture. PloS one *9*, e96771.

Porrello, E.R., Mahmoud, A.I., Simpson, E., Hill, J.A., Richardson, J.A., Olson, E.N., and Sadek, H.A. (2011). Transient regenerative potential of the neonatal mouse heart. In Science, pp. 1078-1080.

Porrello, E.R., Mahmoud, A.I., Simpson, E., Johnson, B.A., Grinsfelder, D., Canseco, D., Mammen, P.P., Rothermel, B.A., Olson, E.N., and Sadek, H.A. (2013). Regulation of neonatal and adult mammalian heart regeneration by the miR-15 family. In Proc Natl Acad Sci USA, pp. 187-192.

Poss, K. D. (2007). Getting to the heart of regeneration in zebrafish. Semin Cell Dev Biol 18, 36–45.
Poss, K. D. (2010). Advances in understanding tissue regenerative capacity and mechanisms in animals. Nat Rev Genet 11, 710–722.

Poss, K. D., Nechiporuk, A., Hillam, A. M., Johnson, S. L. and Keating, M. T. (2002b). Mps1 defines a proximal blastemal proliferative compartment essential for zebrafish fin regeneration. Development 129, 5141–5149.

Poss, K.D., Wilson, L.G., and Keating, M.T. (2002a). Heart regeneration in zebrafish. In Science, pp. 2188-2190.

Poss, K. D., Keating, M. T. and Nechiporuk, A. (2003). Tales of regeneration in zebrafish. Dev Dyn 226, 202–210.

Prescott J., Wentzensen I.M., Savage S.A., De Vivo I. (2012). Epidemiologic evidence for a role of telomere dysfunction in cancer etiology. Mutat Res 730(1-2):75-84.

Raya, A., Koth, C.M., Büscher, D., Kawakami, Y., Itoh, T., Raya, R.M., Sternik, G., Tsai, H.-J., Rodríguez-Esteban, C., and Izpisua Belmonte, J.C. (2003). Activation of Notch signaling pathway precedes heart regeneration in zebrafish. In Proc Natl Acad Sci USA, pp. 11889-11895.

Robin J.D., Ludlow A.T., Batten K., Magdinier F., Stadler G., Wagner K.R.,Shay J.W., Wright W.E.(2014). Telomere position effect: regulation of gene expression with progressive telomere shortening over long distances**.** Genes Dev. 28(22): 2464–2476.

Robinson, M.D., McCarthy, D.J., and Smyth, G.K. (2010). edgeR: a Bioconductor package for differential expression analysis of digital gene expression data. In Bioinformatics, pp. 139-140.

Rodier F, Coppé JP, Patil CK, Hoeijmakers WA, Muñoz DP, Raza SR, Freund A, Campeau E, Davalos AR, Campisi J. (2009). Persistent DNA damage signalling triggers senescence-associated inflammatory cytokine secretion. Nat Cell Biol.;11(8):973-9.

Rogakou, E.P., Pilch, D.R., Orr, A.H., Ivanova, V.S., and Bonner, W.M. (1998). DNA double-stranded breaks induce histone H2AX phosphorylation on serine 139. In J Biol Chem, pp. 5858-5868.

Rossi A, Kontarakis Z, Gerri C, Nolte H, Hölper S, Krüger M, Stainier DY. (2015). Genetic compensation induced by deleterious mutations but not gene knockdowns. Nature. 524(7564):230-3.

Rudolph KL, (2000) Inhibition of experimental liver cirrhosis in mice by telomerase gene delivery. Science 287:1253–1258.

Sabbah, H. N., Sharov, V. G., Goldstein, S. (1998) Programmed cell death in the progression of heart failure. Ann. Med. 30 (Suppl. 1) 33-38.

Sadler KC, Krahn KN, Gaur NA, Ukomadu C. (2007). Liver growth in the embryo and during liver regeneration in zebrafish requires the cell cycle regulator, uhrf1. Proc Natl Acad Sci U S A. 104(5):1570-5.

Samper E, (2001) Restoration of telomerase activity rescues chromosomal instability and premature aging in Terc$^{-/-}$ mice with short telomeres. EMBO Rep. 2:800–807.

Saretzki, G., and von Zglinicki, T. (2002). Replicative aging, telomeres, and oxidative stress. In Annals of the New York Academy of Sciences, pp. 24-29.

Schnabel, K., Wu, C.-C., Kurth, T., and Weidinger, G. (2011). Regeneration of Cryoinjury Induced Necrotic Heart Lesions in Zebrafish Is Associated with Epicardial Activation and Cardiomyocyte Proliferation. In PloS one (Public Library of Science), pp. e18503.

Senyo, S. E., Steinhauser, M. L., Pizzimenti, C. L., Yang, V. K., Cai, L., Wang, M., Wu, T.-D., Guerquin-Kern, J.-L., Lechene, C. P. and Lee, R. T. (2013). Mammalian heart renewal by pre-existing cardiomyocytes. Nature 493, 433–436.

Senyo S.E., Lee R.T., Kühn B. (2014). Cardiac regeneration based on mechanisms of cardiomyocyte proliferation and differentiation. Stem Cell Res; volume13, Issue 3, pp. 532-541.

Sfeir A., de Lange T. (2012). Removal of shelterin reveals the telomere end-protection problem. Science. 336(6081):593-7.

Shay J.W., Wright W.E. (2011). Role of telomeres and telomerase in cancer. Semin. Cancer Biol. 21, 349-353.

Sherr CJ, McCormick F. (2002). The RB and p53 pathways in cancer. Cancer Cell 2002 Aug;2(2):103-12.

Smith LL, Coller HA, Roberts JM. (2003). Telomerase modulates expression of growth-controlling genes and enhances cell proliferation. Nature Cell Biol;5:474–479.

Soonpaa, M. H. and Field, L. J. (1997). Assessment of cardiomyocyte DNA synthesis in normal and injured adult mouse hearts. Am. J. Physiol. 272, H220–6.

Sperka T, Wang J, Rudolph KL. (2012). DNA damage checkpoints in stem cells, ageing and cancer. Nat Rev Mol Cell Biol. 13(9):579-90.

Stainier, D. Y., Fouquet, B., Chen, J. N., Warren, K. S., Weinstein, B. M., Meiler, S. E., Mohideen, M. A., Neuhauss, S. C., Solnica-Krezel, L., Schier, A. F., et al. (1996). Mutations affecting the formation and function of the cardiovascular system in the zebrafish embryo. Development 123, 285–292.

Stampfer MR, Garbe J, Levine G, Lichtsteiner S, Vasserot AP, Yaswen P. (2001). Expression of the telomerase catalytic subunit, hTERT, induces resistance to transforming growth factor βgrowth inhibition in *p16INK4A(-)* human mammary epithelial cells. Proc. Natl Acad. Sci. USA 98, 4498–4503.

Starling JA, Maule J, Hastie ND, Allshire RC. (1990). Extensive telomere repeat arrays in mouse are hypervariable. Nucleic Acids Res. 18(23):6881-8.

Starr J.M., McGurn B., Harris S.E., Whalley L.J., Deary I.J., Shiels P.G. (2006). Association between telomere length and heart disease in a narrow age cohort of older people. Exp Gerontology 42(6):571-3.

Staudt, D. and Stainier, D. (2012). Uncovering the Molecular and Cellular Mechanisms of Heart Development Using the Zebrafish. Annu. Rev. Genet. 46, 397–418.

Steinhauser, M. L. and Lee, R. T. (2011). Regeneration of the heart. EMBO Mol Med 3, 701–712.

Stewart SA, , Hahn WC, O'Connor BF, Banner EN, Lundberg AS, Modha P, Mizuno H, Brooks MW, Fleming M, Zimonjic DB, Popescu NC, Weinberg RA. (2002). Telomerase contributes to tumorigenesis by a telomere length-independent mechanism. Proc Natl Acad Sci USA.; 99:12606–12611.

Subramanian, A., Tamayo, P., Mootha, V.K., Mukherjee, S., Ebert, B.L., Gillette, M.A., Paulovich, A., Pomeroy, S.L., Golub, T.R., Lander, E.S., *et al.* (2005). Gene set enrichment analysis: a knowledge-based approach for interpreting genome-wide expression profiles. Proceedings of the National Academy of Sciences of the United States of America *102*, 15545-15550.

Szibor M, Pöling J, Warnecke H, Kubin T, Braun T. (2014). Remodeling and dedifferentiation of adult cardiomyocytes during disease and regeneration. Cell Mol Life Sci. 71(10):1907-16.

Takeuchi, T. (2014). Regulation of cardiomyocyte proliferation during development and regeneration. In Dev Growth Differ, pp. 402-409.

Tümpel, S., and Rudolph, K.L. (2012). The role of telomere shortening in somatic stem cells and tissue aging: lessons from telomerase model systems. In Annals of the New York Academy of Sciences, pp. 28-39.

Urnov, F. D., Rebar, E. J., Holmes, M. C., Zhang, H. S. and Gregory, P. D. (2010). Genome editing with engineered zinc finger nucleases. Nat Rev Genet 11, 636–646.

Vihtelic, T. S. and Hyde, D. R. (2000). Light-induced rod and cone cell death and regeneration in the adult albino zebrafish (Danio rerio) retina. J. Neurobiol. 44, 289–307.

von Zglinicki T.(2002). Oxidative stress shortens telomeres. Trends Biochem Sci. 27(7):339-44.

Vulliamy T, Marrone A, Goldman F, Dearlove A, Bessler M, Mason PJ, Dokal I. (2001). The RNA component of telomerase is mutated in autosomal dominant dyskeratosis congenita. Nature. 413(6854):432-5.

Wang, J., Karra, R., Dickson, A.L., and Poss, K.D. (2013). Fibronectin is deposited by injury-activated epicardial cells and is necessary for zebrafish heart regeneration. In Dev Biol, pp. 427-435.

Wang, J., Panáková, D., Kikuchi, K., Holdway, J.E., Gemberling, M., Burris, J.S., Singh, S.P., Dickson, A.L., Lin, Y.-F., Sabeh, M.K., *et al.* (2011). The regenerative capacity of zebrafish reverses cardiac failure caused by genetic cardiomyocyte depletion. In Development, pp. 3421-3430.

Watson, J. D. (1972). Origin of concatemeric T7 DNA. Nat New Biol 239(94):197-201.

Wencker, D., Chandra, M., Nguyen, K., Miao, W., Garantziotis, S., Factor, S. M., Shirani, J., Armstrong, R. C., Kitsis, R. N. (2003) A mechanistic role for cardiac myocyte apoptosis in heart failure. J. Clin. Invest. 111, 1497-1504.

WHO (2011). Global Atlas on Cardiovascular disease, prevention and control.

Willett, C.E., Cortes, A., Zuasti, A., and Zapata, A.G. (1999). Early hematopoiesis and developing lymphoid organs in the zebrafish. In Dev Dyn, pp. 323-336.

Wills, A. A., Holdway, J. E., Major, R. J. and Poss, K. D. (2008). Regulated addition of new myocardial and epicardial cells fosters homeostatic cardiac growth and maintenance in adult zebrafish. Development 135, 183–192.

Wong KK, et al. Telomere dysfunction impairs DNA repair and enhances sensitivity to ionizing radiation. Nature Genet. 2000;26:85–88.

Wright, W.E., Piatyszek, M.A., Rainey, W.E., Byrd, W., and Shay, J.W. (1996). Telomerase activity in human germline and embryonic tissues and cells. Developmental genetics *18*, 173-179.

Yang C, Przyborski S, Cooke MJ, Zhang X, Stewart R, Anyfantis G, Atkinson SP, Saretzki G, Armstrong L, Lako M. (2008) A key role for telomerase reverse transcriptase unit in modulating human embryonic stem cell proliferation, cell cycle dynamics, and *in vitro* differentiation. Stem Cells;26:850–863.

Zaragoza C, Gomez-Guerrero C, Martin-Ventura JL, Blanco-Colio L, Lavin B, Mallavia B, Tarin C, Mas S, Ortiz A, Egido J. (2011). Animal models of cardiovascular diseases. J Biomed Biotechnol. 2011:497841.

Zeisberg EM[1], Ma Q, Juraszek AL, Moses K, Schwartz RJ, Izumo S, Pu WT. (2005). Morphogenesis of the right ventricle requires myocardial expression of Gata4. J Clin Invest. 115(6):1522-31.

Zhang X, (1999) Telomere shortening and apoptosis in telomerase-inhibited human tumor cells. Genes Dev. 13:2388–2399.

Movie S 1. Doppler Echocardiography Recording of an Uninjured Wild-Type Zebrafish Heart

Movie S 2. Doppler Echocardiography Recording of an Uninjured tert $^{-/-}$ Zebrafish Heart

Movie S 3. Doppler Echocardiography Recording of a Wild-Type Zebrafish Heart at 3 dpi

Movie S 4. Doppler Echocardiography Recording of a tert $^{-/-}$ Zebrafish Heart at 3 dpi

Movie S 5. Doppler Echocardiography Recording of a Wild-Type Zebrafish Heart at 60 dpi

Movie S 6. Doppler Echocardiography Recording of a tert $^{-/-}$ Zebrafish Heart at 60 dpi

APPENDIX

Article

Cell Reports

Telomerase Is Essential for Zebrafish Heart Regeneration

Graphical Abstract

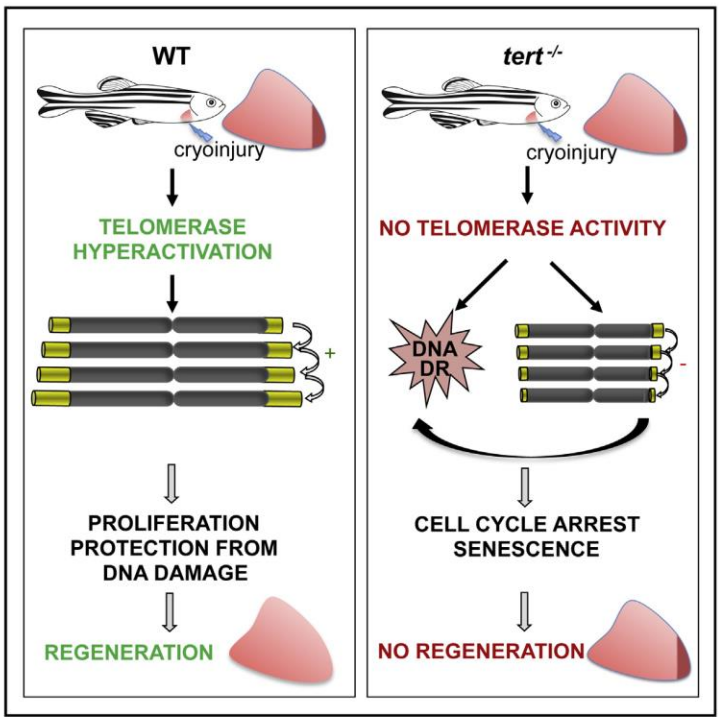

Authors

Dorota Bednarek, Juan Manuel González-Rosa, Gabriela Guzmán-Martínez, ..., Luis Jesús Jiménez-Borreguero, Nadia Mercader, Ignacio Flores

Correspondence

nmercader@cnic.es (N.M.), iflores@cnic.es (I.F.)

In Brief

Bednarek et al. find that telomerase, well known for its role in elongating telomere ends, is essential during zebrafish heart regeneration. Cardiac injury hyperactivates telomerase and increases telomere length in cardiac cells. In telomerase-null mutants, cardiac cells accumulate DNA damage and do not efficiently proliferate in response to injury.

Highlights

- Telomerase hyperactivation is an early event during zebrafish heart regeneration
- Telomerase loss of function impairs cardiac regeneration
- The proliferative response of cardiomyocytes is inhibited in *tert*$^{-/-}$ zebrafish
- Telomerase protects cardiac cells from DNA damage and limits cellular senescence

Accession Numbers

GSE71755

Bednarek et al., 2015, Cell Reports *12*, 1691–1703
September 8, 2015
http://dx.doi.org/10.1016/j.celrep.2015.07.064

Cell Reports
Article

Telomerase Is Essential for Zebrafish Heart Regeneration

Dorota Bednarek,[1] Juan Manuel González-Rosa,[2,6,7] Gabriela Guzmán-Martínez,[3] Óscar Gutiérrez-Gutiérrez,[1] Tania Aguado,[1] Carlota Sánchez-Ferrer,[1] Inês João Marques,[2] María Galardi-Castilla,[2] Irene de Diego,[1] Manuel José Gómez,[4] Alfonso Cortés,[5] Agustín Zapata,[5] Luis Jesús Jiménez-Borreguero,[3] Nadia Mercader,[2,8,*] and Ignacio Flores[1,*]

[1]Regeneration and Aging Group
[2]Development of the Epicardium and Its Role during Regeneration Group
[3]Cardiovascular Imaging in Humans
[4]Bioinformatic Unit
Centro Nacional de Investigaciones Cardiovasculares (CNIC-ISCIII), Melchor Fernández Almagro 3, 28029 Madrid, Spain
[5]Electron Microscopy Center, Complutense University, Madrid 28040, Spain
[6]Present address: Cardiovascular Research Center, Massachusetts General Hospital, Charlestown, MA 02129, USA
[7]Present address: Harvard Medical School, Boston, MA 02115, USA
[8]Present Address: Institute of Anatomy, University of Bern, Bern, Switzerland
*Correspondence: nmercader@cnic.es (N.M.), iflores@cnic.es (I.F.)
http://dx.doi.org/10.1016/j.celrep.2015.07.064

SUMMARY

After myocardial infarction in humans, lost cardiomyocytes are replaced by an irreversible fibrotic scar. In contrast, zebrafish hearts efficiently regenerate after injury. Complete regeneration of the zebrafish heart is driven by the strong proliferation response of its cardiomyocytes to injury. Here we show that, after cardiac injury in zebrafish, telomerase becomes hyperactivated, and telomeres elongate transiently, preceding a peak of cardiomyocyte proliferation and full organ recovery. Using a telomerase-mutant zebrafish model, we found that telomerase loss drastically decreases cardiomyocyte proliferation and fibrotic tissue regression after cryoinjury and that cardiac function does not recover. The impaired cardiomyocyte proliferation response is accompanied by the absence of cardiomyocytes with long telomeres and an increased proportion of cardiomyocytes showing DNA damage and senescence characteristics. These findings demonstrate the importance of telomerase function in heart regeneration and highlight the potential of telomerase therapy as a means of stimulating cell proliferation upon myocardial infarction.

INTRODUCTION

Heart disease is the leading cause of human death in the world. Currently, the only effective treatment for the loss of cardiomyocytes after infarction or heart failure is transplantation. Great hope has been placed on stem cell therapies, but, although data from clinical trials are promising, they fall far short of fulfilling expectations. This has led many researchers to consider taking a step back from the "bedside to the bench" before continuing with more clinical trials (Couzin-Frankel, 2014; Mummery and Lee, 2013). Understanding the repair mechanisms operating in vertebrates with a strong cardiac repair capacity may help to identify new molecules and pathways that could be used to promote heart regeneration in humans.

The zebrafish has become a powerful model for investigating regenerative processes because of its capacity to completely repair several organs, including the heart, after injury (Gemberling et al., 2013). The zebrafish heart can regenerate after ventricular resection (Poss et al., 2002; Raya et al., 2003), genetic ablation of cardiomyocytes (Wang et al., 2011), hypoxia-reoxygenation injury (Parente et al., 2013), and ventricular cryoinjury (Chablais et al., 2011; González-Rosa et al., 2011; Schnabel et al., 2011). Cryoinjury causes local damage to all cardiac cell types and leads to a transient fibrotic tissue deposition reminiscent of the fibrotic scar formed in mammals after myocardial infarction (Chablais et al., 2011; González-Rosa et al., 2011). In the zebrafish, dead cardiomyocytes are replaced not by stem cells but by preexisting cardiomyocytes, which first dedifferentiate and then proliferate to replace the injured tissue with newly formed myocardium (Jopling et al., 2010; Kikuchi et al., 2010). This cardiomyocyte proliferation and remodeling requires paracrine-like contributions from the endocardial lining of the heart lumen and from the epicardium, the outer mesothelial layer covering the myocardium. Early after cardiac injury, the endocardium and epicardium start to re-express developmental genes (Kikuchi et al., 2011; Lepilina et al., 2006). One of these genes encodes retinaldehyde dehydrogenase aldh1a2, an enzyme involved in retinoic acid production that is proposed to be necessary for cardiomyocyte proliferation (Kikuchi et al., 2011). The endocardium also activates the expression of *il11a*, which triggers a jak1/stat3 signaling pathway in cardiomyocytes (Fang et al., 2013). In parallel, the epicardium starts to release extracellular matrix components such as fibronectin, which has been suggested to promote cardiomyocyte regeneration through interaction with integrin β 3 (itgβ3) (Wang et al., 2013).

A similar ability to proliferate in response to injury is shown by cardiomyocytes of neonatal mice (Porrello et al., 2011, 2013), and a limited degree of cardiomyocyte turnover has been reported in humans (Bergmann et al., 2009; Mollova et al., 2013). These observations suggest a new avenue for the treatment of heart failure based on enhancing the endogenous proliferation capacity of cardiomyocytes (Kikuchi and Poss, 2012; Takeuchi, 2014).

Successful DNA replication and extensive cell proliferation require the presence of functional telomeres, the capping structure at the end of chromosomes. Telomeres become shortened because of the end replication problem and other degradative activities (Saretzki and von Zglinicki, 2002). The ability of a cell to proliferate is therefore tightly linked to its ability to maintain healthy telomeres and avoid DNA damage. Telomerase is a ribonucleoprotein enzyme that maintains telomere length by adding DNA repeats to chromosome ends (Greider and Blackburn, 1985). Because of its ability to counteract telomere erosion, telomerase is associated with the proliferation potential of cells and tissues (Flores and Blasco, 2010; Flores et al., 2005) and has been implicated in mouse liver regeneration (Tümpel and Rudolph, 2012). Telomerase can be detected in zebrafish of all ages (Anchelin et al., 2011; Lund et al., 2009), and its expression level correlates with the life-long regenerative capacity of heart and fin tissues (Itou et al., 2012). In contrast, telomerase expression is suppressed rapidly postnatally in human and mouse tissues, with the exception of those with high turnover, reinforcing the association between telomerase activity and repair potential (Forsyth et al., 2002). Remarkably, human and zebrafish telomeres are of a similar size, making the zebrafish a good model for studying the contribution of telomere biology to regeneration (Henriques et al., 2013). Recent reports have described a zebrafish null mutant for the gene encoding telomerase reverse transcriptase (*tert*), the catalytic subunit of the telomerase enzyme (Anchelin et al., 2013; Henriques et al., 2013). Loss of *tert* leads to premature aging in several organs, including the liver, intestine, and pancreas. However, the impact of loss of *tert* on zebrafish organ regeneration remains unexplored.

Here we analyzed the role of tert during zebrafish cardiac regeneration. We report that ventricular cryoinjury upregulates *tert* gene expression and telomerase activity in cardiac cells. In *tert*-null fish, cardiac regeneration is inhibited, and a fibrotic scar remains. This inability to regenerate is mainly due to a strong inhibition of the proliferation response associated with accumulation of cardiac cells with damaged DNA and senescence characteristics. These results highlight the potential of telomere restitution as an approach to reawakening hibernating myocardium after cardiac injury.

RESULTS

Zebrafish cardiomyocytes are able to proliferate throughout life (Itou et al., 2012) but markedly increase their proliferation index upon injury (Chablais et al., 2011; González-Rosa et al., 2011; Poss et al., 2002; Raya et al., 2003; Schnabel et al., 2011; Wang et al., 2011). Telomerase activity is linked to the ability of cells and tissues to proliferate (Flores and Blasco, 2010; Flores et al., 2005). We therefore first compared telomerase activity in zebrafish hearts under homeostatic conditions and during regeneration. A PCR-based telomerase activity assay revealed amplification bands in uninjured heart tissues from 6- to 9-month-old zebrafish, confirming telomerase activity in adults under homeostatic conditions (Figure 1A). There were no significant differences in telomerase activity between the hearts of 6- and 10-month-old fish (Figures 1B and 1C). Cryoinjury of the ventricular apex (one quarter of the ventricle) provoked a transient increase in the processivity and intensity of the amplification bands 3 days later, demonstrating that telomerase activity further increases in response to injury (Figure 1A). Injury-associated telomerase hyperactivation was accompanied by a 2.2-fold increase in *tert* gene expression 3 days postinjury (dpi), pointing to transcriptional activation as a likely regulation mechanism (Figure 1D).

To determine the relationship between telomerase hyperactivation and cardiac regeneration, we analyzed the regenerative capacity of a recently described zebrafish mutant line that carries a stop codon in the second exon of the *tert* gene (Anchelin et al., 2013; Henriques et al., 2013). This mutant completely lacks telomerase activity in the heart and can be considered a *tert* knockout (Figure 1E). Despite lacking telomerase activity, hearts from 6- to 9-month-old $tert^{-/-}$ fish are of normal size and show normal histology and cardiac function as measured by echocardiography (Figures 1F–1H). The lack of an obvious phenotype in $tert^{-/-}$ hearts at 6–9 months of age is consistent with the lack of phenotypic alterations in low-turnover $tert^{-/-}$ tissues at young ages (Anchelin et al., 2013; Henriques et al., 2013).

We next compared the regeneration response in wild-type (WT) and $tert^{-/-}$ zebrafish siblings subjected to heart cryoinjury. In both genotypes, we observed an obvious wound at the earliest time analyzed (3 dpi) (Figure 2A). The injured region was 20% ± 5% of the total ventricle in WT hearts and 21% ± 6% in $tert^{-/-}$ hearts. In WT hearts, the size of the wound decreased gradually, whereas a large wound persisted in $tert^{-/-}$ hearts at 60 dpi (Figures 2A–2C). Histological analysis in both genotypes confirmed the characteristic scar-like fibrotic tissue deposition triggered by cryoinjury (González-Rosa et al., 2011), but subsequent healing took place only in WT hearts (Figures 2B and 2C). The injured area at 60 dpi represented less than 5% of the ventricular area in WT hearts (2.5% ± 0.8%) but, in $tert^{-/-}$ hearts, was comparable with the injured area at 3 dpi (18% ± 2%; Figure 2C). To further substantiate the impaired regeneration response in $tert^{-/-}$ hearts, we evaluated cardiac function by 2D echocardiography (González-Rosa et al., 2014). Cryoinjury caused a reduction in systolic function at 7 dpi (measured by fractional volume shortening [FVS]) of 47% ± 8% in WT fish and 35% ± 4% in $tert^{-/-}$ fish (Figures 2D and 2E; Movies S1, S2, S3, S4, S5, and S6). FVS recovered gradually during regeneration in WT individuals, indicating reestablished ventricular function. In contrast, ventricular function did not recover in $tert^{-/-}$ animals, even at 60 dpi (Figures 2D and 2E; Movies S1, S2, S3, S4, S5, and S6). These results indicate that telomerase is required for heart regeneration in zebrafish.

Myocardial injury triggers a rapid inflammatory response, leading to the infiltration of the injury site by neutrophils, macrophages, and other circulating cells (Frangogiannis, 2014). This inflammatory response, particularly the infiltration of macrophages, plays a key role in promoting cardiac regeneration in the neonatal mouse heart (Aurora et al., 2014). Given that gene

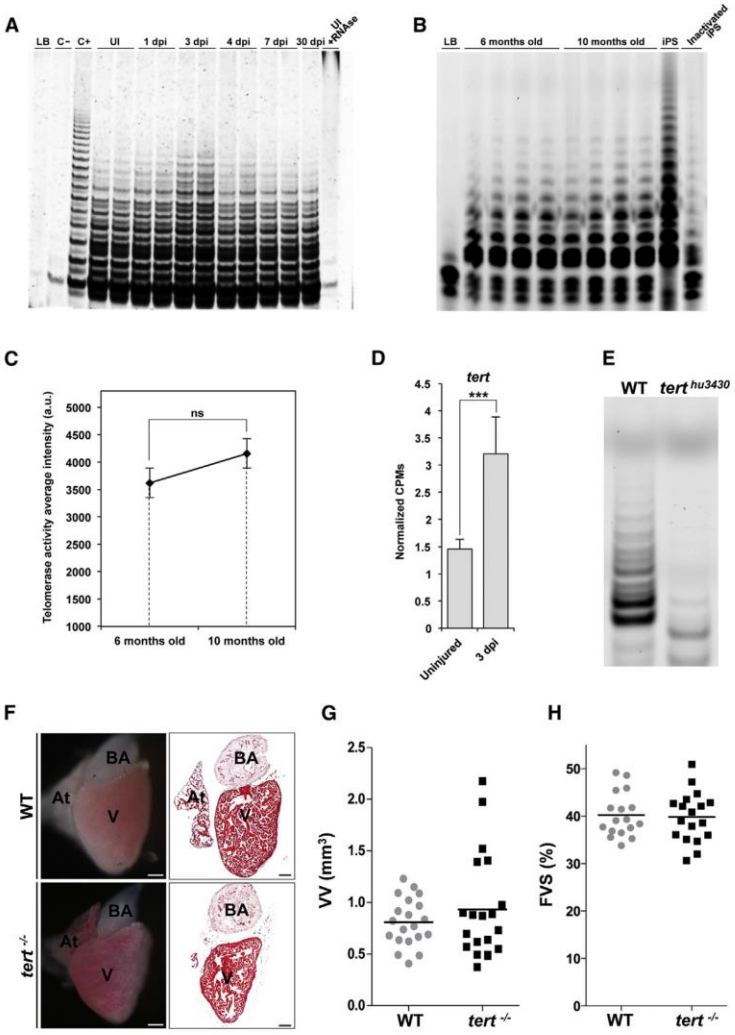

Figure 1. Heart Cryoinjury Augments Telomerase Activity and tert Expression Levels

(A) Representative telomeric repeat amplification protocol (TRAP) activity in uninjured (UI) hearts and hearts at 1, 3, 4, 7, and 30 days post cryoinjury (dpi) (n = 3/condition and time point). Positive control (C+), iPSCs; negative control (C−), *tert*$^{-/-}$ zebrafish heart; reaction specificity control, uninjured + RNase. LB, lysis buffer.

(B and C) Telomerase TRAP activity assay in 6- and 10-month-old zebrafish hearts (n = 4/time point). Data are means ± SEM. ns, not significant (unpaired Student's t test).

(D) Zebrafish *tert* mRNA expression levels in homeostasis and during regeneration (3 dpi) (n = 4 hearts/condition). CPMs, counts per million. Values are means ± SEM. ***p < 0.001 (B–H adjusted p value).

(E) Representative TRAP assay showing the lack of telomerase activity in *tert*$^{-/-}$ hearts (n = 3/genotype).

(F) Lack of telomerase does not affect heart development and function. There is normal anatomy and function in *tert*$^{-/-}$ zebrafish hearts. Shown are whole-mount views of dissected adult WT and *tert*$^{-/-}$ uninjured zebrafish hearts (left) and Masson-Goldner trichrome-stained sagittal sections (center). Five animals were analyzed per genotype. V, ventricle; At, atrium; BA, bulbus arteriosus. Scale bars, 100 μm.

(G and H) Echocardiographic evaluation of heart size (ventricular volume (VV) in diastole) (G) and cardiac function (ventricular FVS) (H) in uninjured WT and *tert*$^{-/-}$ animals. Values for both parameters did not differ between genotypes. Circles and squares show data for individual animals. Horizontal bars represent the mean (unpaired Student's t test). A total of 17–20 animals were analyzed per genotype.

silencing of *tert* has been shown to impair hematopoiesis (Imamura et al., 2008), we assessed whether *tert*$^{-/-}$ zebrafish show alterations in cryoinjury-triggered inflammation. Whole-heart RNA sequencing (RNA-seq) analysis did not detect significant differences between the upregulation of neutrophil, macrophage, and other inflammatory cell markers in *tert*$^{-/-}$ and wild-type hearts at 3 dpi (Figure S1A; Table S1). In addition, L-plastin immunohistochemistry at 3 and 60 dpi revealed no significant differences in macrophage infiltration (Figures S1B–S1G).

The dedifferentiation and proliferation of pre-existing cardiomyocytes during zebrafish heart regeneration is preceded by rapid and organ-wide activation of the endocardium and epicardium (Kikuchi et al., 2011; Lepilina et al., 2006). To determine whether the absence of telomerase activity alters the activation of endocardium and epicardium, we analyzed the expression of *aldh1a2* (*raldh2*) (Kikuchi et al., 2011). WT and *tert*$^{-/-}$ animals showed a similarly strong upregulation of *aldh1a2* RNA and protein in endocardial cells at 6 hr postinjury (hpi) and in endocardial and epicardial cells at 3 dpi (Figure S2A). These results were confirmed by RNA-seq (Figure S2B) and qRT-PCR (data not shown). We also tested the expression of another endocardial gene (*il11a*) and epicardial genes (*wt1b, tbx18*, and *fibronectin)* upregulated upon cardiac injury (Fang et al., 2013; Kikuchi et al., 2011; Lepilina et al., 2006), finding no alterations in their expression in injured *tert*$^{-/-}$ hearts (Figure S2B). The early injury responses of the epicardium and endocardium are therefore not affected in the absence of telomerase.

In response to injury, cardiomyocyte sarcomeres disassemble, mitochondria swell, and cellular attachments loosen (Jopling et al., 2010; Kikuchi et al., 2010). To determine whether these signs of cardiomyocyte dedifferentiation are affected by the loss of telomerase, we analyzed cardiomyocyte ultrastructural

OPEN ACCESS
CellPress

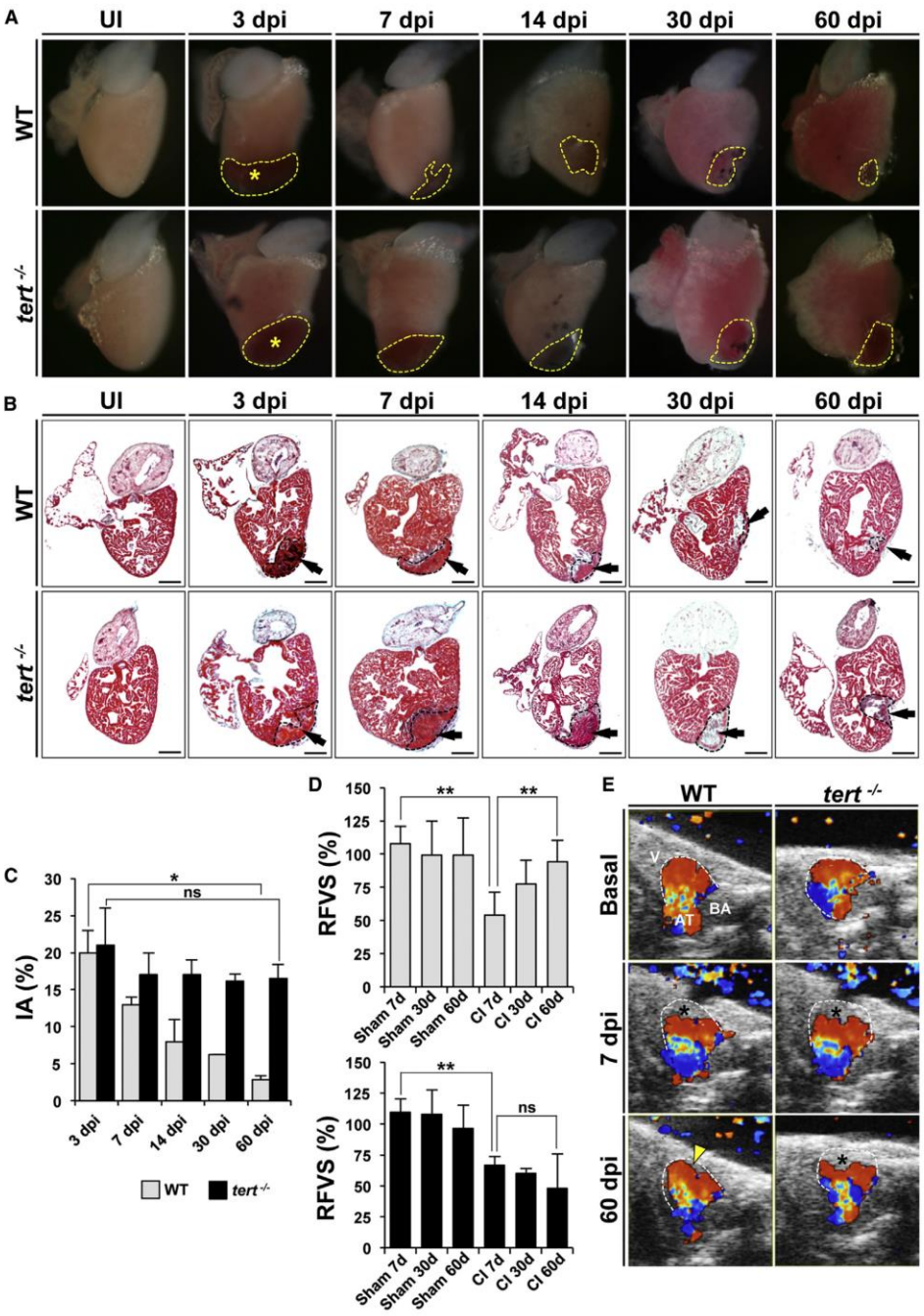

Figure 2. Heart Regeneration Is Inhibited Strongly in tert$^{-/-}$ Animals

(A) Whole-mount views of uninjured and cryoinjured WT and *tert*$^{-/-}$ zebrafish hearts dissected at the indicated times post-injury. Dotted lines outline the injured area. Asterisks mark the initial injury site.

(legend continued on next page)

features at 3 dpi by transmission electron microscopy. A similar extent of sarcomere disassembly and mitochondrial swelling and dysmorphia was detected in WT and *tert*$^{-/-}$ cardiomyocytes close to the injury site (Figure S3), indicating that cardiomyocyte dedifferentiation proceeds normally in the absence of telomerase.

After dedifferentiation, cardiomyocytes proliferate. To study the proliferation response in WT and *tert*$^{-/-}$ animals, we examined the percentage of cardiac cells positive for proliferating cell nuclear antigen (PCNA), a marker of cells in S phase (Figures 3A–3C). A sharp peak in proliferation occurred at 3 dpi in WT hearts, affecting ~11% of total cardiac cells. In *tert*$^{-/-}$ hearts, the proliferation peak was delayed to 14 dpi and affected a maximum of ~6% of cardiac cells (Figure 3A). The impairment in the proliferation response was more pronounced for the cardiomyocyte pool, where the proliferation peak at 7 dpi was 3-fold lower in *tert* $^{-/-}$ hearts (Figure 3B). Proliferating cardiomyocytes in WT hearts were found predominantly at the injury borders but were also detected in peripheral regions (Figure 3C). In *tert*$^{-/-}$ hearts, a weakened proliferation response was evident at all analyzed stages both at the injury border zone and at the periphery (Figure 3C). Interestingly, the few proliferating cardiomyocytes in *tert*$^{-/-}$ hearts were mainly localized close to the epicardium at 60 dpi (Figure 3C). To further characterize the impaired proliferation capacity, we labeled hearts with bromodeoxyuridine (BrdU) to assess DNA synthesis and stained sections with antibodies against BrdU and the mitosis marker phosphorylated histone H3 (pH3). For both markers, we observed large relative reductions in the number of positive cells in *tert*$^{-/-}$ hearts (Figures 3D and 3E; Figure S4A). These results indicate that the failure of cardiac regeneration in the absence of telomerase is due to an impaired proliferation response of cardiomyocytes and other cardiac cells. Gene set enrichment analysis (GSEA) confirmed that cell proliferation-associated pathways were impaired significantly in *tert*$^{-/-}$ hearts compared with the WT (Table S1; Figure S4B).

To dissect the temporal and spatial action of tert during cardiac cell proliferation, we injured hearts ex vivo and examined the effect of tert-targeting vivo antisense Morpholino oligonucleotides (vivoMO). After culture ex vivo for 3 days, untreated injured hearts contained PCNA-positive cardiac cells, including cardiomyocytes, in the peripheral borders of the ventricle. Incubation with *tert* vivoMO during ex vivo culture markedly reduced telomerase activity and the number of PCNA-positive cells (Figures S5A–S5C). Similar results were obtained for the proliferation marker pH3 (data not shown). These data support the conclusion that tert function is necessary for cardiac cell proliferation in the adult heart during cardiac regeneration.

We next investigated how telomerase influences proliferation. Because the canonical function of telomerase is to lengthen telomeres, and long telomeres provide proliferation potential, we conducted telomapping assays to determine whether telomerase hyperactivation leads to changes in telomere length during heart regeneration (Flores et al., 2008). Measurement of average telomere length in each cell on sections of whole WT hearts showed that cardiac telomeres elongate transiently during heart regeneration, with a peak of lengthening at 3 dpi (Figures 4A and 4B). Telomere elongation was detected in cardiomyocytes and other cell types, including endocardial cells (Figure S6). In contrast, telomere length in *tert*$^{-/-}$ hearts decreased after cryoinjury, reaching half the initial length at 60 dpi (Figure 4B).

Given that telomere length is linked to proliferation potential in several organs, we next compared the telomere length of proliferative and non-proliferative cardiac cells. Single-cell profiling of telomere length and analysis of PCNA expression revealed that proliferating WT cardiac cells possess longer telomeres than non-proliferative cells, indicating that, in WT fish, telomere length defines a subclass of cardiac cells with proliferation potential (Figure 5A). During regeneration, telomeres lengthened not only in actively proliferating cells but also in non-proliferating cells, demonstrating that telomere elongation is a general process within the regenerating heart (Figure 5A). To determine the location of proliferative cardiomyocytes and their telomere length, we co-immunostained sections for myosin heavy chain (MHC), PCNA, and telomeres. In uninjured WT hearts, cardiomyocyte telomere length is heterogeneous, with telomeres longer in proliferating cells (Figure 5B; Figure S6). After injury, the number of proliferating cardiomyocytes with long telomeres (>600 a.u.) increased to a peak at 7 dpi but then declined gradually. Therefore, despite telomerase hyperactivation after cryoinjury, telomerase activity levels are insufficient to maintain telomere reserves in cardiomyocytes (Figure 5B). The successive rounds of cell division taking place during regeneration are likely to contribute to telomere erosion. Consistent with this idea, telomeres shortened abruptly in cells close to the injury, the region with the highest proliferation rate (Figure S6). A similar pattern of rapid telomere erosion was observed in regions of the epicardium and endocardium adjacent to the injury site (Figure S6).

Short and dysfunctional telomeres limit cellular proliferative capacity by eliciting a DNA damage response. To assess the levels of DNA damage before and after injury in WT and *tert*$^{-/-}$

(B) Masson-Goldner trichrome staining of sagittal sections of uninjured WT and *tert*$^{-/-}$ hearts at the indicated days after cryoinjury. Dotted black lines outline the injured area. Arrows mark the initial injury site. Scale bars, 100 μm.

(C) Size of the ventricle injury (injured area [IA]) on sagittal heart sections at the indicated times post-injury, presented as the percentage of the total ventricular area. Data are means of at least 4 sections/heart from 3-8 hearts/time point, with the exception of WT 30 dpi, where only one heart was analyzed. Data are means ± SEM. *$p < 0.05$ (Mann-Whitney test).

(D) Relative FVS (RFVS) in WT and *tert*$^{-/-}$ zebrafish hearts under the basal condition (sham-operated animals) and at the indicated times post-injury. WT hearts recover ventricular function over time but *tert*$^{-/-}$ hearts do not. Data are means ± SEM of a pool of 10 animals/condition. **$p < 0.01$ (one-way ANOVA followed by Tukey's honest significant difference test).

(E) Representative Doppler echocardiography images of intracardial blood flow in WT and *tert*$^{-/-}$ hearts in the absence of injury and at the indicated times post-injury. Asterisks mark the initial injury site. See also Movies S1, S2, S3, S4, S5, and S6.

See also Figures S1–S3, and Table S1.

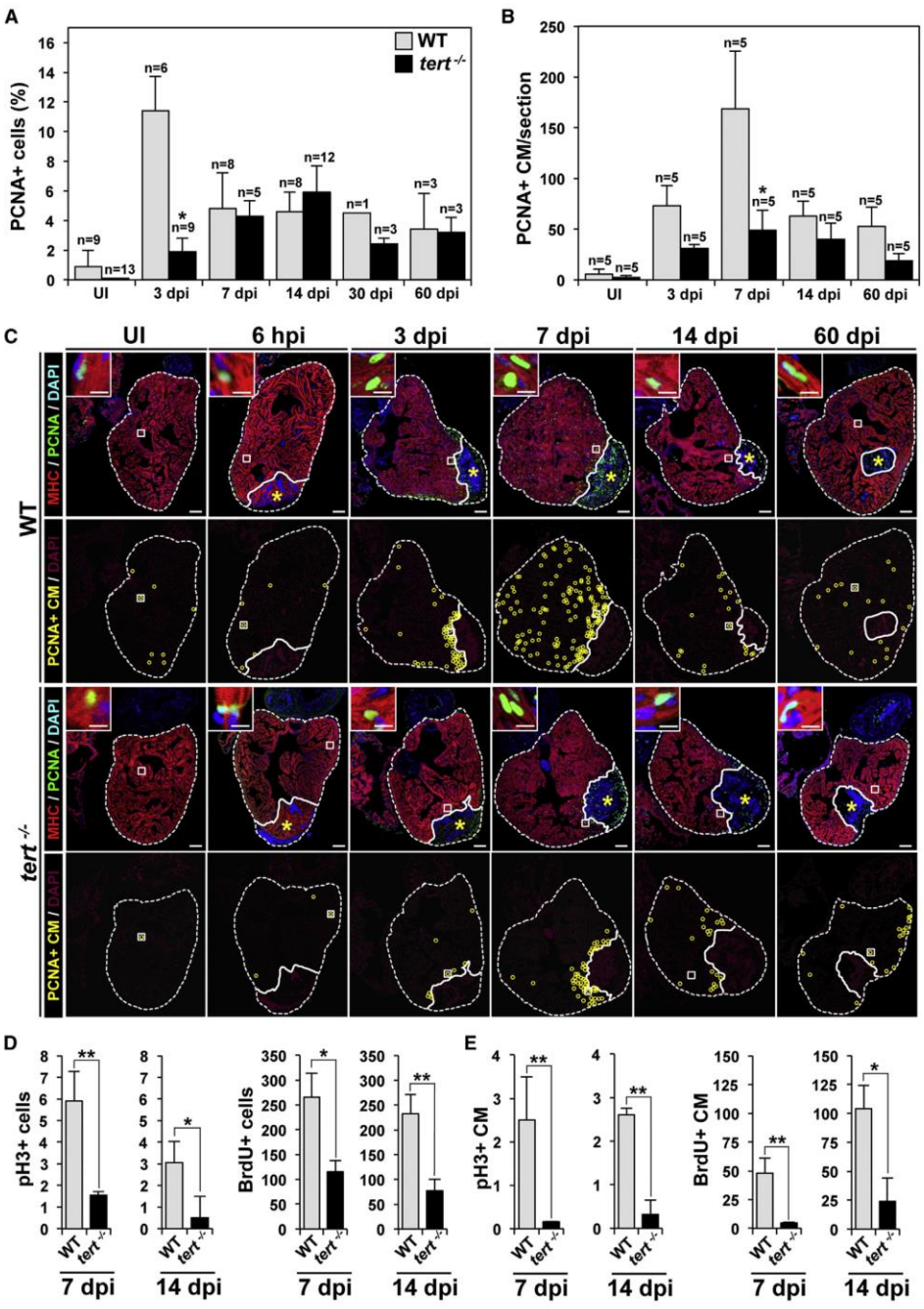

(legend on next page)

hearts, we measured the protein levels of the DNA damage marker phospho-histone H2A.X (γH2AX) (Rogakou et al., 1998; Figure 6). Cryoinjury increased the γH2AX signal in WT and *tert*$^{-/-}$ hearts, but the increase was significant only in *tert*$^{-/-}$ hearts (Figures 6A and 6B). DNA damage in cardiac cells was spread globally in the ventricles of non-injured WT hearts, and the number of damaged cells was not increased significantly after injury (Figures 6C and 6E). In contrast, *tert*$^{-/-}$ hearts contained higher basal numbers of γH2AX-positive cells, and the level of damage increased significantly after injury (Figures 6C and 6E). The same pattern was seen when only cardiomyocytes were examined (Figure 6F). The DNA damage response limits cellular proliferative capacity (Behrens et al., 2014). Consistent with this notion, co-immunostaining of the γH2AX and BrdU labels revealed that the vast majority of BrdU-positive cells were γH2AX-negative in both WT and *tert*$^{-/-}$ hearts (Figure S7). These results indicate that the absence of telomerase is an important contributor to DNA damage, with a likely impact on cardiac regeneration.

Telomere dysfunction-induced DNA damage and cell-cycle blockade can lead to cellular senescence (d'Adda di Fagagna et al., 2003). We therefore used the senescence-associated β-galactosidase assay to detect senescence in *tert*$^{-/-}$ hearts (Figure 7). Uninjured hearts of WT or *tert*$^{-/-}$ animals did not show senescence-specific staining, but a senescence-associated β-galactosidase signal was induced upon cryoinjury. In WT hearts at 3 dpi, senescent cells were almost exclusively limited to the injured region, whereas, in injured *tert*$^{-/-}$ hearts, the signal was distributed more broadly, extending beyond the injured area and border zone to remote regions of the ventricle, consistent with the organ-wide deficit of proliferating *tert*$^{-/-}$ cardiac cells (Figure 7). This tendency was maintained at later stages of regeneration (7 dpi) (Figure 7).

DISCUSSION

Our results indicate that, under the high demands imposed by heart injury, telomere reserves cannot be maintained without telomerase. Absence of telomerase decouples dedifferentiation from proliferation, drastically impairing proliferation and leading to the accumulation of DNA damage. Instead of regenerating myocardium and regressing cardiac fibrosis, *tert*$^{-/-}$ hearts acquire a senescent phenotype. The telomere elongation and DNA protection roles of telomerase might be linked, and senescence could be the final outcome of DNA damage accumulation. The detection of mildly elevated DNA damage in the uninjured *tert*$^{-/-}$ heart might indicate that tert also maintains DNA during homeostasis, perhaps by protecting against oxidative or mechanical stress (Oh et al., 2003). Although this does not seem to impact basal cardiac function, it might contribute to the impaired regeneration observed in *tert*$^{-/-}$ mutant hearts.

In humans, telomerase is downregulated rapidly after birth (Wright et al., 1996). Interestingly, after an ischemic episode, cardiomyocytes can enter a state of hibernation in which viability is maintained but the myocardium is non-functional. This hibernating myocardium has been suggested to represent a partially dedifferentiated state (Heusch, 2004). Given the essential role of telomerase in cardiomyocyte expansion after dedifferentiation, our results highlight the potential of telomere restitution as a strategy to reawaken hibernating myocardium in the post-infarction heart.

EXPERIMENTAL PROCEDURES

Zebrafish Husbandry

All experiments were conducted with adult zebrafish between 6 and 9 months of age, raised at a density of 3 fish/l. Animals were housed and experiments were performed in accordance with Spanish bioethical regulations for the use of laboratory animals. The ethics committee that approved this study was the Community of Madrid "Dirección General de Medio Ambiente." The telomerase *tert*$^{AB/hu3430}$ mutant line used in this study is available from the Zebrafish Model Organism Database (ZFIN) repository (ZFIN: ZDB-GENO-100412-50) at the Zebrafish International Resource Center (ZIRC). The *tert*$^{AB/hu3430}$ mutants have a T→A point mutation in the *tert* gene. Genotyping was performed by PCR of the *tert* gene (*tert* primers were as follows: forward, 5′GACGACCAG TTCGGATCCCTTC 3′; reverse, 5′ CTTTACCCTCCGCCGCTTTACC 3′). Characterization of *tert*$^{-/-}$ zebrafish was performed in F1 and F2 animals produced by *tert*$^{+/-}$ incrossing.

Cryoinjury

Cryoinjury was performed as described previously (González-Rosa and Mercader, 2012). For analysis of regeneration, animals were euthanized at different times post-injury by immersion in 0.16% tricaine (Sigma), and hearts were dissected in medium containing 2 U/ml heparin and 0.1 M KCl. The damaged area was easily identified from the accumulation of blood at the injury site. Damage was also estimated by examination of sections (Poss et al., 2002). The percentage of the ventricular surface area damaged by the procedure was calculated using NIS-Elements AR, 64 bit 3.00, SP7 (Build 547).

Telomerase Assay

Telomerase activity was measured with a modified fluorescence telomere repeat amplification assay (Herbert et al., 2006).

Histological Staining

Hearts were fixed overnight at 4°C in 4% paraformaldehyde (PFA) in PBS. Samples were then washed in PBS + 0.1% Tween 20, dehydrated through

Figure 3. The Absence of Telomerase Severely Affects Cardiomyocyte Proliferation

(A and B) Cardiac cells positive for PCNA in UI WT and *tert*$^{-/-}$ zebrafish hearts and in hearts at the indicated days after cryoinjury. (A) PCNA$^+$ total cardiac cells. (B) PCNA$^+$ cardiomyocytes. Data are means ± SEM of the percentage of PCNA$^+$ cells (A) or number of PCNA$^+$ cardiomyocytes per cardiac ventricle section (at least 3 sections/animal from the indicated number of animals) (B). *$p < 0.05$ compared with WT samples (Mann-Whitney test).

(C) WT and *tert*$^{-/-}$ heart sections immunostained with anti-MHC to mark cardiomyocytes (red) and anti-PCNA to mark cells in S phase (green). Nuclei were counterstained with DAPI (blue). The bottom rows show the location of PCNA$^+$ cardiomyocytes during regeneration (yellow circles). The nuclear area is shown in magenta. Dotted lines outline the ventricle and injured area. Asterisks mark the initial injury site. Insets show high-magnification views of representative PCNA$^+$ cardiomyocytes in the boxed areas. Scale bars, 100 μm (whole-heart views) and 10 μm (magnifications).

(D and E) Quantification of pH3$^+$ and BrdU-labeled cardiac cells (D) and cardiomyocytes (E) at 7 and 14 dpi. Data are means ± SEM. *$p < 0.05$, **$p < 0.01$ (unpaired Student's t test).

See also Figures S4 and S5.

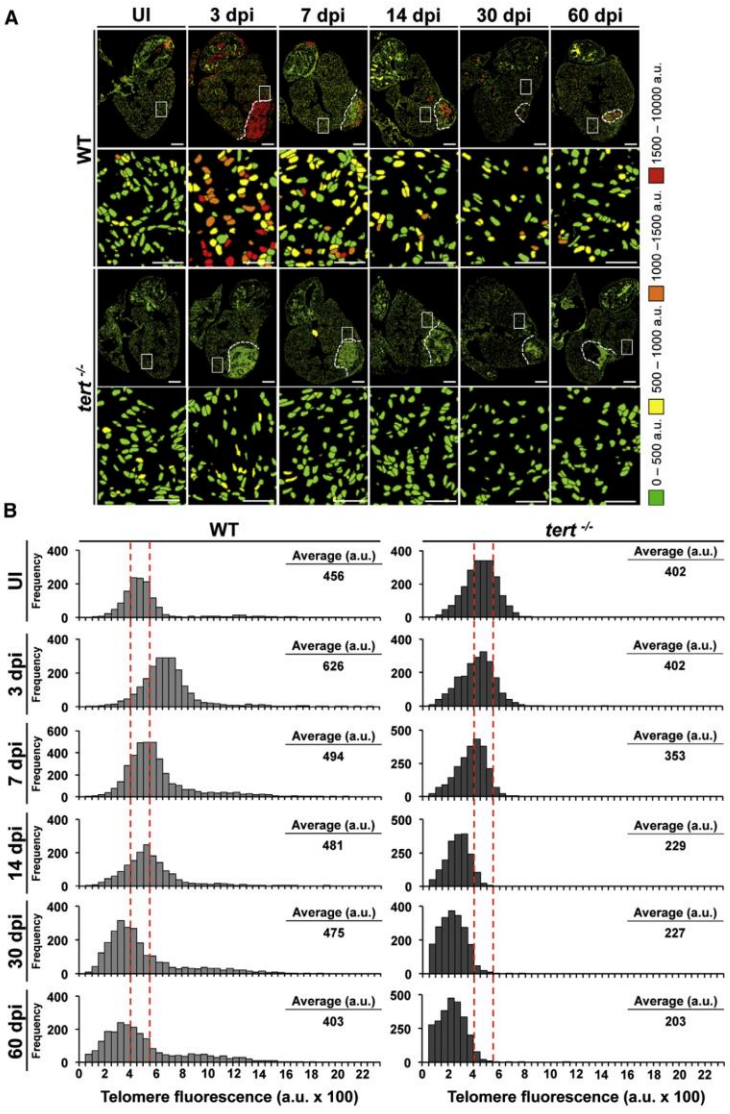

Figure 4. Heart Cryoinjury Induces a Telomerase-Dependent Increase in Telomere Reserves

(A) Representative telomap images of WT and tert$^{-/-}$ heart, uninjured (UI) or fixed at different days postinjury [dpi]. Nuclei are assigned a four-color code according to their average telomere fluorescence in a.u. The cells with the longest telomeres are visualized in red, and the cells with the shortest telomeres are presented in green. Dotted lines mark the injured area. The second and fourth rows show higher magnifications of the boxed areas highlighted in the entire heart section images. Scale bars, 100 μm and 10 μm for magnification images.

(B) Telomere fluorescence frequency histograms of cardiac WT and *tert*$^{-/-}$ cells in uninjured hearts and hearts at 3, 7, 14, 30, and 60 days after cryoinjury. Mean telomere fluorescence is indicated in a.u. The injury site was excluded from the analysis. Note the increase in the number of cells with long telomeres at 3 dpi in WT hearts, followed by reestablishment of the initial profile. This response is lacking in *tert*$^{-/-}$ cells, and, at later stages, cells have shorter telomeres than initially. See also Figure S6.

an ethanol series, and embedded in paraffin wax. All histology was performed on 7-μm paraffin sections cut on a microtome (Leica), mounted on Superfrost slides (Fisher Scientific), and dried overnight at 37°C. Sections were deparaffinized in xylol, rehydrated, and washed in distilled water. Connective tissue was stained using the Masson-Goldner trichrome procedure (Merck).

Cardiac Imaging by Echocardiography

To assess cardiac function in non-injured and post-injury zebrafish, animals were anesthetized with a mixture of tricaine (130 ppm) and isoflurane (200 ppm) diluted in tank water (Huang et al., 2010). Individuals were then placed ventral side up in a custom-made sponge holder in a Petri dish filled with the anesthetic solution. 2D, high-resolution, real-time in vivo images were obtained with the Vevo770 imaging system through an RMV708 (22–83 MHz) scanhead (VisualSonics). Echocardiographic evaluation of heart size was performed by comparing ventricular volume measured in diastole between WT and *tert*$^{-/-}$ animals (González-Rosa et al., 2014).

In Situ Hybridization on Sections

In situ hybridization on paraffin sections was performed according to Mallo et al. (2000) with some modifications.

RNA-Seq Library Production

Index-tagged cDNA libraries were constructed from total RNA (1 μg) with the TruSeq RNA sample preparation v2 kit (Illumina). Four biological replicates consisting of three pooled hearts were used per sample. Quality, quantity, and size distribution of the Illumina libraries were determined using the DNA-1000 kit (Agilent Bioanalyzer). Libraries were sequenced (single-end mode and length of 75 bp) on the Genome Analyzer IIx system using the standard RNA sequencing protocol in the TruSeq SBS kit v5. Fastq files containing reads for each library were extracted and demultiplexed using Casava v1.8.2 pipeline.

RNA-Seq Analysis

Sequencing adaptor contaminations were removed from reads using Cutadapt software (Martin, 2011), and the resulting reads were mapped and quantified on the transcriptome (Ensembl gene-build 66) using RSEM v1.2.3 (Li and Dewey, 2011). Only genes with at least two counts per million in at least four samples were considered for statistical analysis. Data were then normalized, and deferential expression was tested using the bioconductor package EdgeR (Robinson et al., 2010). We considered as differentially expressed genes with a Benjamini-Hochberg-adjusted p value of less than 0.05.

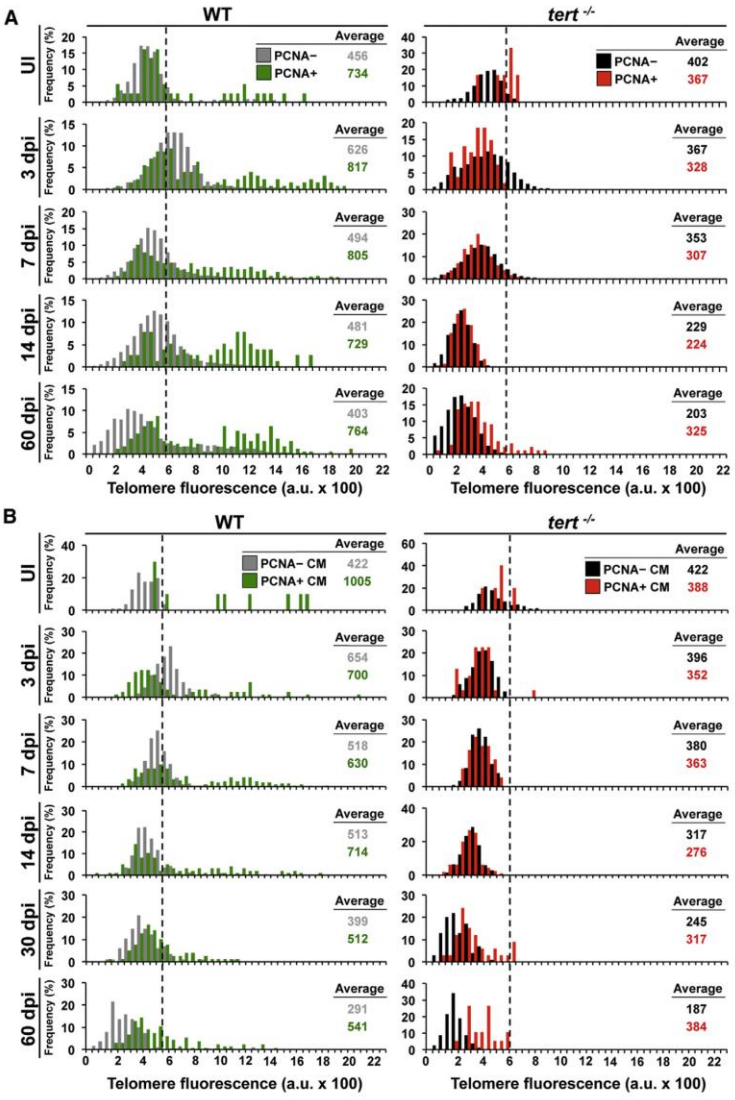

Figure 5. Long Telomeres Mark a Subset of Proliferating Cardiac Cells, Including Proliferating Cardiomyocytes

(A and B) Telomere fluorescence frequency histograms of PCNA$^-$ and PCNA$^+$ WT and *tert*$^{-/-}$ cells in uninjured hearts and hearts at 3, 7, 14, 30, and 60 days after cryoinjury. Histograms show frequencies for (A) total cardiac cells and (B) cardiomyocytes. Telomere fluorescence averages are indicated in a.u. Note that in both cases the subpopulation of proliferating cells with long telomeres is lacking in *tert*$^{-/-}$ hearts. CM, cardiomyocytes. See also Figure S6.

Q-FISH Telomere Length Analysis on Zebrafish Heart Sections

Telomere quantitative fluorescence in situ hybridization (Q-FISH) analysis on paraffin-embedded sections was performed as described previously (Flores et al., 2008). Images were acquired with an A1R-A1 Nikon confocal microscope fitted with a 60× objective. Quantitative image analysis was performed on confocal images using Metamorph version 7 (Molecular Devices) as described previously (Flores et al., 2008). Briefly, the 4′,6-diamidino-2-phenylindole (DAPI) image was used to define the nuclear area and the Cy3 image to quantify telomere fluorescence. Telomere fluorescence intensity was measured as "average gray value" (total gray value per nucleus area). These "average telomere fluorescence" values represent the average Cy3 pixel intensity for the total nuclear area, thereby ruling out any influence of nuclear size on telomere length measurements. Telomere fluorescence values for each sample were exported to Microsoft Excel to generate frequency histograms. A four-color intensity banding was used to generate the map of telomere length. The injury area, determined by the absence of MHC staining, was excluded from the analysis.

Immunofluorescence

Heart sections were deparaffinized, rehydrated, and washed in distilled water. Epitopes were retrieved by heating in citrate buffer (pH 6.0) for 15 min in a microwave at full power. Non-specific binding sites were saturated by incubation for 1 hr in blocking solution (3% BSA, 5% goat serum, and 0.3% Tween 20). Endogenous biotin was blocked with the avidin-biotin blocking kit (Vector Laboratories). Slides were then incubated overnight with primary antibodies at 4°C. The primary antibodies used were anti-myosin heavy chain (MF20, Developmental Studies Hybridoma Bank [DSHB], diluted 1:20), anti-tropomyosin (CH1, DSHB, diluted 1:20), anti-L-plastin (provided by P. Martin, University of Bristol; Evans et al., 2013), anti-erg1 (Abcam, diluted 1:100), anti- PCNA (Santa Cruz Biotechnology, diluted 1:100), anti- BrdU (BD Biosciences, diluted 1:30), anti-pH3 (Millipore, diluted 1:100), and anti-γ-H2AX (GeneTex, diluted 1:300). The primary antibody signal was revealed after incubation for 1 hr at room temperature with biotin- or Alexa 488-, 568-, or 633conjugated secondary antibodies (Invitrogen, each diluted 1:200) and streptavidin-Cy5 (Vector). Nuclei were stained with DAPI (1:1,000), and slides were mounted in Vectashield (Vector). Apoptosis was detected by terminal deoxynucleotidyl transferase dUTP nick end labeling (TUNEL) staining using the in situ cell death detection kit from Roche.

Electron Microscopy

Transmission electron microscopy was performed as described previously (Willett et al., 1999). Briefly, hearts were fixed in 2.5% glutaraldehyde/0.1 M sodium caccodylate at 4°C and post-fixed with 1% osmium tetroxide/0.1 M sodium caccodylate. After washing in 0.1 M sodium caccodylate/5% sucrose, the hearts were dehydrated quickly in increasing concentrations of ethanol to 100%. Hearts were then washed twice with propylene oxide and replaced with a 2:1 mixture of propylene oxide:PB 812 (PolySciences), then a 1:1 mixture of the same components, and, finally, with pure PB 812. Blocks were polymerized at 70°C overnight in fresh PB 812. Ultra-thin sections were double-stained with uranyl acetate and lead citrate, examined, and photographed in a JEOL 10.10 electron microscope.

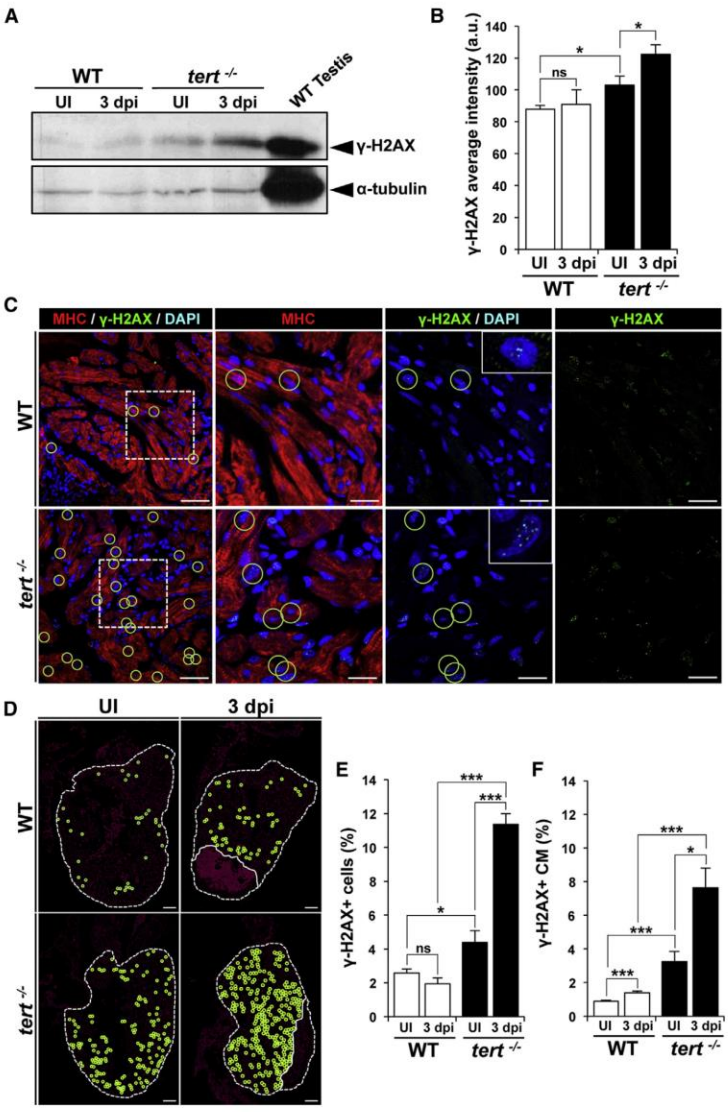

Figure 6. DNA Damage Increases Strongly after Ventricular Cryoinjury in the Absence of Telomerase

(A) Representative western blot of γ-H2AX expression in WT and *tert*$^{-/-}$ hearts without injury and in hearts at 3 dpi.

(B) Quantification of western blot signal intensities (n = 9 hearts/condition). Data are means ± SEM. *p < 0.05 (Mann-Whitney test).

(C) Representative staining of γ-H2AX foci (green) in cardiac cells in uninjured and 3 dpi WT and *tert*$^{-/-}$ hearts. Cardiomyocytes are immunostained with anti-MHC (red), and nuclei are counterstained with DAPI (blue). Examples of γ-H2AX^{+} cardiomyocytes are outlined with green circles. Boxed areas are shown at a higher magnification. Scale bars, 20 μm.

(D) Distribution of γ-H2AX-positive cardiomyocytes (green circles) in uninjured and 3 dpi WT and *tert*$^{-/-}$ hearts. The nuclear area is shown in magenta. The ventricle and injured area are outlined by dotted lines. Scale bars, 100 μm.

(E and F) Percentages of (E) γ-H2AX-positive cardiac cells and (F) γ-H2AX-positive cardiomyocytes in uninjured and 3 dpi WT and *tert*$^{-/-}$ hearts. Data are means ± SEM of cells counted on a minimum of 3 sections/heart in four hearts. *p < 0.05, **p < 0.01, ***p < 0.001 (Student's t test). See also Figure S7.

For combined analysis by Q-FISH and immunostaining for proliferation, we performed an additional step with the Vectastain Elite ABC standard kit (Vector) and the Cy5-conjugated Tyramide Signal Amplification Plus kit (TSA Plus, PerkinElmer). Endogenous peroxidase activities were quenched in 3% H_2O_2 in PBS for 10 min at room temperature. Before applying secondary antibodies, sections were incubated for 30 min with Vectastain Elite ABC reagent at room temperature. After three washes of 5 min each in PBS, slides were incubated for 4 min in tyramide-Cy5 conjugate diluted 1:100 in 1× Plus amplification diluent (PerkinElmer). After three additional 5-min washes, secondary antibodies were applied and slides were processed according to the immunofluorescence and Q-FISH procedure described above.

To quantify cardiomyocyte proliferation, three to six sections showing the largest wounds were selected from each heart, and images were obtained with a 60× objective to generate a tiled composite of the whole heart section. The cells positive for MHC and PCNA were counted manually in all ventricles. The percentages of MHC^{+}PCNA^{+} cells from selected sections were averaged to determine a proliferation index for each heart.

BrdU Labeling

Animals were anesthetized in tricaine, and a single dose of BrdU (Sigma, 0.05 ml of 2.5 mg/ml solution dissolved in PBS) was injected intraperitoneally at 3 or 7 dpi. Animals were then left to continue healing until 7 or 14 dpi, respectively.

Imaging

Whole-heart images were obtained with a Leica MZ16FA fluorescence stereomicroscope fitted with a Leica DFC310FX camera. A Nikon Eclipse 90i microscope was used to examine histological and immunohistochemical staining, and a Nikon A1R confocal microscope was used for immunofluorescence staining.

Western Blot Analysis

Hearts were dissected and lysed in radioimmunoprecipitation assay (RIPA) buffer (50 mM Tris [pH 8], 150 mM NaCl, 0.1% SDS, 1% NP40, and 0.5% sodium deoxycholate) containing protease inhibitor cocktail (Roche). Total proteins (100 μg) were separated by SDS-PAGE and transferred to a polyvinylidene fluoride (PVDF) membrane. Blots were incubated overnight with primary antibodies. Anti-histone γH2AX (GeneTex,

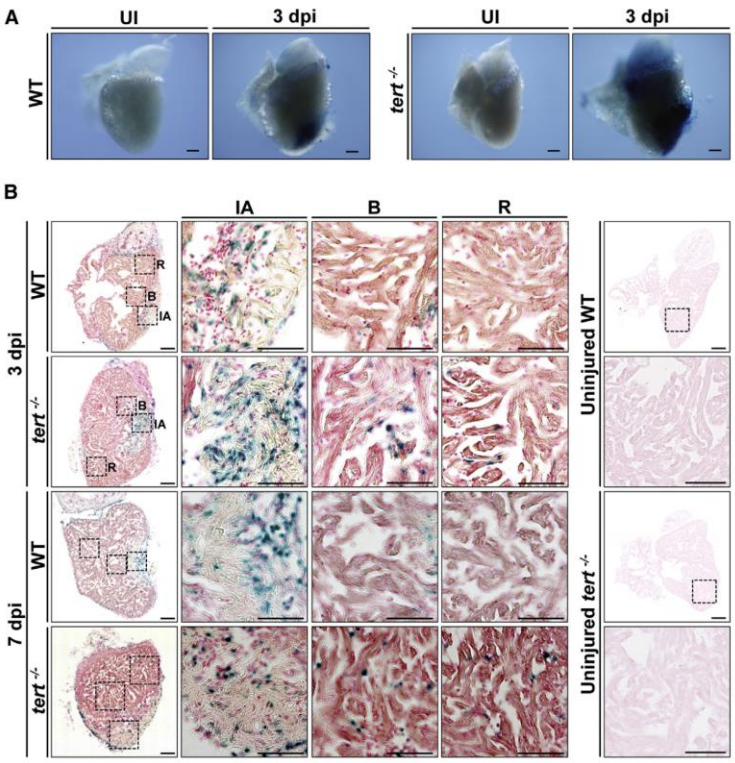

Figure 7. tert$^{-/-}$ Hearts Acquire a Senescence Phenotype after Ventricular Cryoinjury

(A) Whole mounts of uninjured and 3 dpi WT and *tert*$^{-/-}$ hearts stained for SA β-galactosidase. Scale bars, 100 μm.

(B) Cryosections of uninjured, 3 dpi, and 7 dpi WT and *tert*$^{-/-}$ hearts stained for SA β-galactosidase. Magnified views are shown of the injured area, injury border (B), and remote zone (R). Scale bars, 100 μm (whole heart) and 50 μm (magnified views).

catalog no. GTX127342) was used at 1:1,000 dilution and α-tubulin (Sigma, catalog no. T8203) at 1:4,000 dilution. Horseradish peroxidase-coupled secondary antibodies (Dako) were used at 1:5,000 dilution. Band intensities were quantified densitometrically using QuantityOne software (BioRad).

Quantification of Phosphorylated H2AX Foci

Phosphorylated H2AX foci were detected with rabbit polyclonal anti-phospho-histone H2AX antibody (1:300, GeneTex). A cell was considered positive for γ-H2AX when it contained two or more foci. Foci were counted manually.

Senescence-Associated β-Galactosidase Activity

Senescence-associated β-galactosidase (SA β-gal) activity was detected on freshly prepared cryosections and whole-mounts using a senescence β-galactosidase staining kit (Cell Signaling Technology).

Vivo Morpholino Treatment of Ex Vivo-Cultured Hearts

Hearts were dissected from adult WT, Tg(*fli:GFP*) (Lawson and Weinstein, 2002), or Tg(*myl7:GFP*) (Raya et al., 2003) zebrafish in the *AB* genetic background. The apex was injured by stabbing with a tungsten needle. Stabbing was used because this method is less invasive than cryoinjury and, therefore, better supports survival in vitro while being equally well suited to the study of the cardiomyocyte proliferation response to injury (Itou et al., 2014). Hearts were cultured in DMEM supplemented with 10% fetal bovine serum and antibiotics (penicillin and streptomycin) in 96-well plates (Pieperhoff et al., 2014). Two hearts were added per well in 250 μl medium. The vivoMOs used were *tert* vivoMO (5′-CTGTCGAG TACTGTCCAGACATCTG; Imamura et al., 2008) and *gfp* vivoMO (5′-ACAGCTCCTCGCCCTTGCTCACCAT; Huang et al., 2003). All Morpholinos were added at a concentration of 10–15 μM. The medium was changed daily. After 3 days, hearts were either processed for the tert activity assay or fixed for sectioning and immunofluorescence. MO specificity was confirmed by injecting *tert* MOs into *tert*$^{-/-}$ embryos without causing any additional obvious phenotypes (data not shown).

Statistical Analysis

Where normal distribution can be assumed, Student's t test for comparisons between two groups or one-way ANOVA followed by Tukey's honest significance test for comparisons between more than two groups were used. Where the normality assumption could not be verified with a reliable method, Mann-Whitney test was used. Model assumptions of normality and homogeneity were checked with conventional residual plots. To control for the false discovery rate in RNA-seq data, p values were corrected for multiple testing using the Benjamini-Hochberg method (Benjamini and Hochberg, 1995), yielding adjusted p values. The specific test used in each comparison is indicated in the main text or figure legend. Calculations were made with Microsoft Excel version 14.4.9 and Prism version 5.0.

ACCESSION NUMBERS

The accession number for the RNA-seq data reported in this paper is GSE71755.

SUPPLEMENTAL INFORMATION

Supplemental Information includes seven figures, one table, and six movies and can be found with this article online at http://dx.doi.org/10.1016/j.celrep.2015.07.064.

AUTHOR CONTRIBUTIONS

D.B. performed laboratory-based experimental work, image acquisition, data quantification, data analysis, and telomere analysis. J.M.G.R. contributed to the experimental work. G.G. and J.J.B. performed and analyzed the echocardiography study. O.G.G. and T.A. and C.S.F performed the TRAP assay. I.J.M. performed the immunofluorescence analysis and cryoinjuries. M.G. contributed to the experiments with ex vivo cultures. I.D. performed experimental work. M.J.G. R. performed the transcriptome analysis. A.C. and A.Z. performed the TEM study. I.F., N.M., D.B., and J.M.G.R. designed the experiments and wrote the manuscript. I.F. directed the research.

OPEN ACCESS
CellPress

ACKNOWLEDGMENTS

We thank E. Díaz, R. Costa, R. Doohan, and A. de Molina for zebrafish husbandry and technical support; E. Arza and A. M. Santos for help with microscopy acquisition; F. Sánchez-Cabo and C. Torroja for help with statistics; and S. Bartlett for text editing. We are very grateful to M.L. Cayuela (Hospital Virgen de Arritxaca, Murcia, Spain) and M.G. Ferreira (Instituto Gulbenkian de Ciência, Lisbon, Portugal) for sharing unpublished results, fish lines, and insightful discussions. The CNIC is supported by the Ministerio de Economia y Competitividad (MINECO) and the Pro-CNIC Foundation. This work was funded by grants from MINECO (SAF2012-38449 [to I.F.] and BFU2011-25297, Cardiocell, and FIBROTEAM S2010/BMD-2321 [to N.M.]), the Red Temática de Investigación Cooperativa en Enfermedades Cardiovasculares (RD12/0042/0045 [to I.F.]), and the ERC (ERC starting grant 337703–zebraHeart [to N.M]). I.J.M is supported by PIEF-GA-2012-330728. D.B. is supported by FPI fellowship BES2010-033554 from MINECO.

Received: October 2, 2014
Revised: May 27, 2015
Accepted: July 29, 2015
Published: August 27, 2015

REFERENCES

Anchelin, M., Murcia, L., Alcaraz-Pérez, F., García-Navarro, E.M., and Cayuela, M.L. (2011). Behaviour of telomere and telomerase during aging and regeneration in zebrafish. PloS ONE *6*, e16955.

Anchelin, M., Alcaraz-Pérez, F., Martínez, C.M., Bernabé-García, M., Mulero, V., and Cayuela, M.L. (2013). Premature aging in telomerase-deficient zebrafish. Dis. Model Mech *6*, 1101–1112.

Aurora, A.B., Porrello, E.R., Tan, W., Mahmoud, A.I., Hill, J.A., Bassel-Duby, R., Sadek, H.A., and Olson, E.N. (2014). Macrophages are required for neonatal heart regeneration. J. Clin. Invest. *124*, 1382–1392.

Behrens, A., van Deursen, J.M., Rudolph, K.L., and Schumacher, B. (2014). Impact of genomic damage and ageing on stem cell function. Nat. Cell Biol. *16*, 201–207.

Benjamini, Y., and Hochberg, Y. (1995). Controlling the false discovery rate: a practical and powerful approach to multiple testing. J. R. Stat. Soc. Series B Stat. Methodol. *57*, 289–300.

Bergmann, O., Bhardwaj, R.D., Bernard, S., Zdunek, S., Barnabé-Heider, F., Walsh, S., Zupicich, J., Alkass, K., Buchholz, B.A., Druid, H., et al. (2009). Evidence for cardiomyocyte renewal in humans. Science *324*, 98–102.

Chablais, F., Veit, J., Rainer, G., and Jaźwińska, A. (2011). The zebrafish heart regenerates after cryoinjury-induced myocardial infarction. BMC Dev. Biol. *11*, 21.

Couzin-Frankel, J. (2014). The elusive heart fix. Science *345*, 252–257.

d'Adda di Fagagna, F., Reaper, P.M., Clay-Farrace, L., Fiegler, H., Carr, P., Von Zglinicki, T., Saretzki, G., Carter, N.P., and Jackson, S.P. (2003). A DNA damage checkpoint response in telomere-initiated senescence. Nature *426*, 194–198.

Evans, M.A., Smart, N., Dubé, K.N., Bollini, S., Clark, J.E., Evans, H.G., Taams, L.S., Richardson, R., Lévesque, M., Martin, P., et al. (2013). Thymosin β4-sulfoxide attenuates inflammatory cell infiltration and promotes cardiac wound healing. Nat. Commun. *4*, 2081.

Fang, Y., Gupta, V., Karra, R., Holdway, J.E., Kikuchi, K., and Poss, K.D. (2013). Translational profiling of cardiomyocytes identifies an early Jak1/Stat3 injury response required for zebrafish heart regeneration. Proc. Natl. Acad. Sci. U.S.A. *110*, 13416–13421.

Flores, I., and Blasco, M.A. (2010). The role of telomeres and telomerase in stem cell aging. FEBS Lett. *584*, 3826–3830.

Flores, I., Cayuela, M.L., and Blasco, M.A. (2005). Effects of telomerase and telomere length on epidermal stem cell behavior. Science *309*, 1253–1256.

Flores, I., Canela, A., Vera, E., Tejera, A., Cotsarelis, G., and Blasco, M.A. (2008). The longest telomeres: a general signature of adult stem cell compartments. Genes Dev. *22*, 654–667.

Forsyth, N.R., Wright, W.E., and Shay, J.W. (2002). Telomerase and differentiation in multicellular organisms: turn it off, turn it on, and turn it off again. Differentiation *69*, 188–197.

Frangogiannis, N.G. (2014). The inflammatory response in myocardial injury, repair, and remodelling. Nat. Rev. Cardiol. *11*, 255–265.

Gemberling, M., Bailey, T.J., Hyde, D.R., and Poss, K.D. (2013). The zebrafish as a model for complex tissue regeneration. Trends Genet. *29*, 611–620.

González-Rosa, J.M., and Mercader, N. (2012). Cryoinjury as a myocardial infarction model for the study of cardiac regeneration in the zebrafish. Nat. Protoc. *7*, 782–788.

González-Rosa, J.M., Martín, V., Peralta, M., Torres, M., and Mercader, N. (2011). Extensive scar formation and regression during heart regeneration after cryoinjury in zebrafish. Development *138*, 1663–1674.

González-Rosa, J.M., Guzmán-Martínez, G., Marques, I.J., Sánchez-Iranzo, H., Jiménez-Borreguero, L.J., and Mercader, N. (2014). Use of echocardiography reveals reestablishment of ventricular pumping efficiency and partial ventricular wall motion recovery upon ventricular cryoinjury in the zebrafish. PLoS ONE *9*, e115604.

Greider, C.W., and Blackburn, E.H. (1985). Identification of a specific telomere terminal transferase activity in Tetrahymena extracts. Cell *43*, 405–413.

Henriques, C.M., Carneiro, M.C., Tenente, I.M., Jacinto, A., and Ferreira, M.G. (2013). Telomerase is required for zebrafish lifespan. PLoS Genet. *9*, e1003214.

Herbert, B.-S., Hochreiter, A.E., Wright, W.E., and Shay, J.W. (2006). Nonradioactive detection of telomerase activity using the telomeric repeat amplification protocol. Nat. Protoc. *1*, 1583–1590.

Heusch, G. (2004). Myocardial hibernation: a delicate balance. Am. J. Physiol. Heart Circ. Physiol. *288*, H984–H999.

Huang, C.J., Tu, C.T., Hsiao, C.D., Hsieh, F.J., and Tsai, H.J. (2003). Germ-line transmission of a myocardium-specific GFP transgene reveals critical regulatory elements in the cardiac myosin light chain 2 promoter of zebrafish. Dev. Dyn. *228*, 30–40.

Huang, W.C., Hsieh, Y.S., Chen, I.H., Wang, C.H., Chang, H.W., Yang, C.C., Ku, T.H., Yeh, S.R., and Chuang, Y.J. (2010). Combined use of MS-222 (tricaine) and isoflurane extends anesthesia time and minimizes cardiac rhythm side effects in adult zebrafish. Zebrafish *7*, 297–304.

Imamura, S., Uchiyama, J., Koshimizu, E., Hanai, J., Raftopoulou, C., Murphey, R.D., Bayliss, P.E., Imai, Y., Burns, C.E., Masutomi, K., et al. (2008). A non-canonical function of zebrafish telomerase reverse transcriptase is required for developmental hematopoiesis. PLoS ONE *3*, e3364.

Itou, J., Kawakami, H., Burgoyne, T., and Kawakami, Y. (2012). Life-long preservation of the regenerative capacity in the fin and heart in zebrafish. Biol. Open *1*, 739–746.

Itou, J., Akiyama, R., Pehoski, S., Yu, X., Kawakami, H., and Kawakami, Y. (2014). Regenerative responses after mild heart injuries for cardiomyocyte proliferation in zebrafish. Dev. Dyn. *243*, 1477–1486.

Jopling, C., Sleep, E., Raya, M., Martí, M., Raya, A., and Izpisua Belmonte, J.C. (2010). Zebrafish heart regeneration occurs by cardiomyocyte dedifferentiation and proliferation. Nature *464*, 606–609.

Kikuchi, K., and Poss, K.D. (2012). Cardiac regenerative capacity and mechanisms. Annu. Rev. Cell Dev. Biol. *28*, 719–741.

Kikuchi, K., Holdway, J.E., Werdich, A.A., Anderson, R.M., Fang, Y., Egnaczyk, G.F., Evans, T., MacRae, C.A., Stainier, D.Y.R., and Poss, K.D. (2010). Primary contribution to zebrafish heart regeneration by gata4+ cardiomyocytes. Nature *464*, 601–605.

Kikuchi, K., Holdway, J.E., Major, R.J., Blum, N., Dahn, R.D., Begemann, G., and Poss, K.D. (2011). Retinoic acid production by endocardium and epicardium is an injury response essential for zebrafish heart regeneration. Dev. Cell *20*, 397–404.

Lawson, N.D., and Weinstein, B.M. (2002). In vivo imaging of embryonic vascular development using transgenic zebrafish. Dev. Biol. *248*, 307–318.

Lepilina, A., Coon, A.N., Kikuchi, K., Holdway, J.E., Roberts, R.W., Burns, C.G., and Poss, K.D. (2006). A dynamic epicardial injury response supports progenitor cell activity during zebrafish heart regeneration. Cell *127*, 607–619.

Li, B., and Dewey, C.N. (2011). RSEM: accurate transcript quantification from RNA-Seq data with or without a reference genome. BMC Bioinformatics *12*, 323.

Lund, T.C., Glass, T.J., Tolar, J., and Blazar, B.R. (2009). Expression of telomerase and telomere length are unaffected by either age or limb regeneration in Danio rerio. PloS ONE *4*, e7688.

Mallo, M., Schrewe, H., Martin, J.F., Olson, E.N., and Ohnemus, S. (2000). Assembling a functional tympanic membrane: signals from the external acoustic meatus coordinate development of the malleal manubrium. Development *127*, 4127–4136.

Martin, M. (2011). Cutadapt removes adapter sequences from high-throughput sequencing reads. EMBnet J. *17*, 10–12.

Mollova, M., Bersell, K., Walsh, S., Savla, J., Das, L.T., Park, S.-Y., Silberstein, L.E., dos Remedios, C.G., Graham, D., Colan, S., et al. (2013). Cardiomyocyte proliferation contributes to heart growth in young humans. Proc. Natl. Acad. Sci. U.S.A. *110*, 1446–1451.

Mummery, C.L., and Lee, R.T. (2013). Is heart regeneration on the right track? Nat. Med. *19*, 412–413.

Oh, H., Wang, S.C., Prahash, A., Sano, M., Moravec, C.S., Taffet, G.E., Michael, L.H., Youker, K.A., Entman, M.L., and Schneider, M.D. (2003). Telomere attrition and Chk2 activation in human heart failure. Proc. Natl. Acad. Sci. U.S.A. *100*, 5378–5383.

Parente, V., Balasso, S., Pompilio, G., Verduci, L., Colombo, G.I., Milano, G., Guerrini, U., Squadroni, L., Cotelli, F., Pozzoli, O., et al. (2013). Hypoxia/reoxygenation cardiac injury and regeneration in zebrafish adult heart. PloS ONE *8*, e53748.

Pieperhoff, S., Wilson, K.S., Baily, J., de Mora, K., Maqsood, S., Vass, S., Taylor, J., Del-Pozo, J., MacRae, C.A., Mullins, J.J., and Denvir, M.A. (2014). Heart on a plate: histological and functional assessment of isolated adult zebrafish hearts maintained in culture. PLoS ONE *9*, e96771.

Porrello, E.R., Mahmoud, A.I., Simpson, E., Hill, J.A., Richardson, J.A., Olson, E.N., and Sadek, H.A. (2011). Transient regenerative potential of the neonatal mouse heart. Science *331*, 1078–1080.

Porrello, E.R., Mahmoud, A.I., Simpson, E., Johnson, B.A., Grinsfelder, D., Canseco, D., Mammen, P.P., Rothermel, B.A., Olson, E.N., and Sadek, H.A. (2013). Regulation of neonatal and adult mammalian heart regeneration by the miR-15 family. Proc. Natl. Acad. Sci. U.S.A. *110*, 187–192.

Poss, K.D., Wilson, L.G., and Keating, M.T. (2002). Heart regeneration in zebrafish. Science *298*, 2188–2190.

Raya, A., Koth, C.M., Büscher, D., Kawakami, Y., Itoh, T., Raya, R.M., Sternik, G., Tsai, H.-J., Rodríguez-Esteban, C., and Izpisua Belmonte, J.C. (2003). Activation of Notch signaling pathway precedes heart regeneration in zebrafish. Proc. Natl. Acad. Sci. U.S.A. *100*, 11889–11895.

Robinson, M.D., McCarthy, D.J., and Smyth, G.K. (2010). edgeR: a Bioconductor package for differential expression analysis of digital gene expression data. Bioinformatics *26*, 139–140.

Rogakou, E.P., Pilch, D.R., Orr, A.H., Ivanova, V.S., and Bonner, W.M. (1998). DNA double-stranded breaks induce histone H2AX phosphorylation on serine 139. J. Biol. Chem. *273*, 5858–5868.

Saretzki, G., and von Zglinicki, T. (2002). Replicative aging, telomeres, and oxidative stress. Ann. N.Y. Acad. Sci. *959*, 24–29.

Schnabel, K., Wu, C.-C., Kurth, T., and Weidinger, G. (2011). Regeneration of cryoinjury induced necrotic heart lesions in zebrafish is associated with epicardial activation and cardiomyocyte proliferation. PloS ONE *6*, e18503.

Takeuchi, T. (2014). Regulation of cardiomyocyte proliferation during development and regeneration. Dev. Growth Differ. *56*, 402–409.

Tümpel, S., and Rudolph, K.L. (2012). The role of telomere shortening in somatic stem cells and tissue aging: lessons from telomerase model systems. Ann. N.Y. Acad. Sci. *1266*, 28–39.

Wang, J., Panáková, D., Kikuchi, K., Holdway, J.E., Gemberling, M., Burris, J.S., Singh, S.P., Dickson, A.L., Lin, Y.-F., Sabeh, M.K., et al. (2011). The regenerative capacity of zebrafish reverses cardiac failure caused by genetic cardiomyocyte depletion. Development *138*, 3421–3430.

Wang, J., Karra, R., Dickson, A.L., and Poss, K.D. (2013). Fibronectin is deposited by injury-activated epicardial cells and is necessary for zebrafish heart regeneration. Dev. Biol. *382*, 427–435.

Willett, C.E., Cortes, A., Zuasti, A., and Zapata, A.G. (1999). Early hematopoiesis and developing lymphoid organs in the zebrafish. Dev. Dyn. *214*, 323–336.

Wright, W.E., Piatyszek, M.A., Rainey, W.E., Byrd, W., and Shay, J.W. (1996). Telomerase activity in human germline and embryonic tissues and cells. Dev. Genet. *18*, 173–179.